STRUCTURAL BASIS FOR THE FORMATION OF PTPRG•CNTN COMPLEXES IN NEURAL TISSUES

A DISSERTATION IN
Molecular Biology and Biochemistry
And
Cell Biology and Biophysics

Presented to the Faculty of the University
of Missouri-Kansas City in partial fulfillment of
the requirements of the degree

DOCTOR OF PHILOSOPHY

by
ROMAN M. NIKOLAIENKO

B.A., National Technical University of Ukraine "KPI", 2007
M.S., National Technical University of Ukraine "KPI", 2009
M.S. University of Missouri, Kansas City, 2012

Kansas City, Missouri
2016

STRUCTURAL BASIS FOR THE FORMATION OF PTPRG•CNTN COMPLEXES IN NEURAL TISSUES

Roman M. Nikolaienko, Candidate for the Doctor of Philosophy Degree
University of Missouri - Kansas City, 2016

ABSTRACT

Receptor protein tyrosine phosphatase gamma (PTPRG) is a cell surface receptor expressed primarily on neurons. It combines cytoplasmic tyrosine phosphatase domains and an extracellular region that includes a carbonic anhydrase-like (CA) domain. This domain mediates binding to members of a family of neural cell adhesion molecules called contactins (CNTNs) that are expressed on neurons during development and adulthood. The ectodomains of CNTNs are organized into six N-terminal immunoglobulin domains followed by four fibronectin type III repeats (FN) and a glycophosphatidylinositol anchor. Previous work demonstrated that PTPRG interacts specifically with CNTN3-6. Here, we combine biochemical and structural approaches to further characterize the interactions between PTPRG and its cognate CNTN partners. In particular, our work indicates that PTPRG associates with CNTN3-6 with similar binding affinities. This finding is consistent with our structural analyses of PTPRG•CNTN3 and PTPRG•CNTN6 complexes suggesting that CNTN3-6 use a conserved interface to bind the CA domain of PTPRG. As a first step to determine the *in vivo* functions of PTPRG•CNTN complexes, we attempted to localize the sites where these receptors interact. In particular, we identified the PTPRG•CNTN3 complex in the outer segment (OS) of adult mouse retinas. Further investigation of these complexes in the OS revealed

that PTPRG and CNTN3 form complexes when expressed on the same cell (*cis* interactions). However, we also performed cell-aggregation assays indicating that PTPRG and CNTN3 can associate when expressed on distinct cells (*trans* interactions). To explain how the PTPRG•CNTN3 complex could form in these two distinct geometries, we analyzed the conformations taken by the CNTN3 ectodomain. In particular, our work indicates that the FN1-FN3 of CNTN3 adopts a bent conformation suggesting that the CNTN3 ectodomain bends sharply between FN2 and FN3 domains and then extends in parallel to the cell surface. Importantly, this bent conformation is found in all six CNTN family members suggesting that all CNTNs might lie parallel to the cell membrane. This orientation of CNTN ectodomains would accommodate the formation of *cis* and *trans* PTPRG•CNTN complexes. Finally, we discuss the implications of our results in PTPG/CNTN-mediated signaling.

APPROVAL PAGE

The faculty listed below, appointed by the Dean of the School of Graduate Studies, have examined a dissertation titled "Structural Basis for the Formation of PTPRG•CNTN Complexes in Neural Tissues", presented by Roman M. Nikolaienko, candidate for the Doctor of Philosophy degree, and certify that in their opinion it is worth of acceptance.

Supervisory Committee

Samuel Bouyain, DPhil, Committee Chair
Molecular Biology and Biochemistry

Leonard Dobens, Ph.D.
Molecular Biology and Biochemistry

Brian Geisbrecht, Ph.D.
Cell Biology and Biophysics

Erika Geisbrecht, Ph.D.
Cell Biology and Biophysics

Xiaolan Yao, Ph.D.
Molecular Biology and Biochemistry

CONTENTS

LIST OF ILLUSTRATIONS

Figure Page

LIST OF TABLES

Table Page

ABBREVIATIONS

Carbonic anhydrase domain	CA
Cell-adhesion molecule	CAM
Chondroitin sulfate proteoglycans	CSPGs
Contactin	CNTN
Contactin associated protein	CNTNAP
Cyclic nucleotide-gated channel	CNG
Dally-like protein	Dlp
Delta-like protein 4	DLL4
Diacylglycerol	DAG
Epidermal growth factor receptor	EGFR
External granular layer	EGL
Extracellular matrix	ECM
Extracellular signal–regulated kinase	ERK
Fibronectin type III domain	FN
GABAergic interneurons	GABApre
Gamma-Aminobutyric acid	GABA
Ganglion cell layer	GCL
Glycophosphatidylinositol	GPI
Heparan sulfate proteoglycans	HSPGs
Human Embryonic Kidney 293 cells	HEK293
Human growth hormone	hGH
Immunoglobulin superfamily of cell-adhesion molecules	Ig-CAMs
Immunoglobulin-like domain	Ig
Inner nuclear layer	INL
Inner plexiform layer	IPL

Inner segment	IS
Insulin receptor	IR
Insulin-like growth factor 1	IGF-1
Leukocyte antigen-related tyrosine phosphatase	LAR
Lipopolysaccharide	LPS
Neurofascin 155	NF-155
Nuclear magnetic resonance	NMR
Olfactory sensory neurons	OSNs
Oligodendrocyte precursor cells	OPCs
Outer nuclear layer	ONL
Outer plexiform layer	OPL
Outer segment	OS
Phosphodiesterase	PDE
Phosphoinositide-3 kinase	PI3K
Phospholipase C γ	PLCγ
Pleiotrophin	PTN
Protein data bank	PDB
Protein Tyrosine Phosphatases	PTPs
Proximity ligation assay	PLA
Receptor Protein Tyrosine phosphatase alpha	PTPRA
Receptor Protein Tyrosine phosphatase delta	PTPRD
Receptor Protein Tyrosine phosphatase epsilon	PTPRE
Receptor Protein Tyrosine phosphatase eta	PTPRJ
Receptor Protein Tyrosine phosphatase gamma	PTPRG
Receptor Protein Tyrosine phosphatase kappa	PTPRK
Receptor Protein Tyrosine phosphatase mu	PTPRM
Receptor Protein Tyrosine phosphatase sigma	PTPRS

Receptor Protein Tyrosine phosphatase tau	PTPRT
Receptor Protein Tyrosine phosphatase zeta	PTPRZ
Receptor Protein Tyrosine phosphatases	RPTPs
Retinal ganglion cells	RGC
Retinal pigmented epithelium	RPE
Small angle X-ray scattering	SAXS
Southeast Regional Collaborative Access Team	SER-CAT
Syndecan	Sdc
T-cell receptor	TCR
Tyrosine kinase C	TrkC

ACKNOWLEDGMENTS

I would like to thank my mentor and a committee chair Dr. Samuel Bouyain for being an outstanding teacher and an understanding friend during the whole program. This dissertation would not be possible without his guidance, support, and patience. Thank you, Samuel. I would like to express my gratitude to the past and present members of my committee Dr. Leonard Dobens, Dr. Brian Geisbrecht, Dr. Erika Geisbrecht, Dr. Salvatore Stella and Dr. Xiaolan Yao for their advice and help.

Scientific research is a collaborative endeavor and I want to acknowledge all the individuals who contributed data and reagents throughout my time in the laboratory: Dr. Samuel Bouyain, Dr. Salvatore L. Stella, Dr. Michal Hammel, Dr. Véronique Dubreuil, Dr. Sheila Harroch, Rana Zalmai, David R. Hall and Nurjahan Mehzabeen.

Finally, I would like to mention all past and present lab members for their friendship and support: Boadi Agyekum, Jessica Kawakami, Rana Zalmai, David R. Hall, Nurjahan Mehzabeen, Victor Broerman and Brandon Holder.

Support for this research came from National Institute of General Medical Sciences of the National Institutes of Health under award number R01GM088806 (SB). X-ray data were collected at the Southeast Regional Collaborative Access Team beamlines at the Advanced Photon Source, Argonne National Laboratory. X-ray scattering experiments were made at the Lawrence Berkeley National Laboratory SIBYLS beamline of the Advanced Light Source.

DEDICATION

This Dissertation is dedicated to my family, friends, colleagues and all people who helped me throughout my entire life.

CHAPTER 1

INTRODUCTION

Phosphorylation and dephosphorylation in the Nervous system

The development and maintenance of the nervous system requires a robust set of cellular events, such as cell migration, proliferation and maturation, neurite outgrowth and synapse formation. At the molecular level these processes are driven by extra- and intracellular cell signaling. The accuracy of these signaling events is an essential element for the precise regulation of nervous system development and its functionality.

Reversible protein phosphorylation is an essential signaling mechanism, utilized by nearly all living cells in metazoans, including neural cells. Protein phosphorylation is catalyzed by a class of enzymes called protein kinases. A change in phosphorylation state may modulate the activity of a protein and/or create docking sites for specific binding partners. An example of a kinase-mediated activation in the nervous system is the neurotrophic receptor tyrosine kinase A (TrkA), a receptor for nerve growth factor (NGF) discovered in the 1950s (Levi-Montalcini, 1952). Upon ligand binding, TrkA dimerizes and activates itself by tyrosine cross-autophosphorylation. Phosphorylated Y490 and Y785 residues serve as docking sites for several binding partners, such as the Grb2 adaptor protein (ERK signaling pathway), phospholipase C-γ (PLCγ) and phosphoinositide-3 kinase (PI3K); these interactions in turn launch corresponding signaling cascades that result in various cellular events (Arévalo and Wu, 2006). In contrast, the proteins responsible for dephosphorylation are called phosphatases. Kinases and phosphatases work in tandem to maintain the necessary balance between

phosphorylated and dephosphorylated forms of the proteins. Together, they guide the cellular processes necessary for the development and maintenance of all tissues and in particular the nervous system. Protein phosphatases are organized into evolutionarily distant families that include serine/threonine phosphatases, tyrosine phosphatases, and dual-specificity phosphatases (Tonks, 2006). Both kinases and phosphatases may exist as either receptor or non-receptor forms. Receptor forms are particularly interesting because they signal across the membrane and extracellular cues to intracellular enzymatic activity. The work presented in this dissertation is focused on Receptor Protein Tyrosine phosphatases (RPTPs) – the subset of glycoproteins that combine both an extracellular receptor ectodomain and an intracellular phosphatase region.

General properties of RPTPs

RPTPs belong to the family of classical Protein Tyrosine Phosphatases (PTPs), which is defined by the presence of a canonical membrane-proximal phosphatase domain (D1) with the signature (I/V)HCSxGxGR(S/T)G motif (Andersen et al., 2004; Tonks, 2006). All RPTPs are grouped into 8 different subtypes (Fig. 1) based on their structural organization (Nam, 2005). In addition to catalytic D1 domain, more than one half of known RPTPs are characterized by an additional membrane-distal phosphatase domain – D2, which is usually inactive except in the case of PTPRA (Tonks, 2006). Apart from the cytoplasmic phosphatase domains, RPTPs also include an extracellular receptor portion variable in different subtypes of RPTPs. The ectodomains of RPTPs might provide an additional mode of the phosphatase activity regulation through ligand binding. Importantly, the extracellular region of most RPTPs resembles the ectodomains of cell

adhesion molecules, which presumably indicates that RPTPs participate in cell-cell and cell-matrix contact events (Burridge et al., 2006; Sallee et al., 2006).

Whereas the mechanism of regulation of kinase receptors through ligand-induced oligomerization is well described (Schlessinger, 2014), the regulation of RPTPs by the same mechanism remains unclear. Moreover, it appears that distinct receptor phosphatases might utilize different strategies for the regulation of their phosphatase activity through the binding of extracellular ligands, oligomerization, reversible oxidation and phosphorylation (Tonks, 2006). The mode of RPTP regulation by oligomerization was originally proposed in the structural study of CD45 phosphatase (Desai et al., 1993). In this study the intracellular region of CD45 that included tandem phosphatase domains D1 and D2 was attached to the extracellular and transmembrane domains of the EGF receptor (EGFR). EGFR/CD45 chimera restored T-cell receptor (TCR) signaling in CD45-null cells, indicating the autonomy of phosphatase signaling relative to its native extracellular domain. Moreover, EGF stimulation of the chimera leads to the repression of TCR signaling, indicating a mode of regulation through ligand-induced oligomerization similar to what has been described for EGFR. However, recent studies have shown that a long and rigid ectodomain of CD45 is sterically excluded from sites of TCR-ligand engagement that leads to segregation of CD45 and the tyrosine kinase Lck. This shifts an equilibrium towards TCR phosphorylation by Lck and further activation of TCR (Chang et al., 2016). Other findings suggest that Lck should be dephosphorylated by CD45 to be able to activate TCR signaling (Hermiston et al., 2003).

Therefore, the repression of TCR signaling upon EGF stimulation of the EGFR/CD45 chimera might be caused by its failure to activate Lck.

Although the dimer formation for CD45 has been shown to inhibit the phosphatase activity, the structural basis for the RPTPs regulation though the oligomerization was unclear. One of the first structural insights into the oligomerization-induced inactivation of RPTPs comes from PTPRA (Bilwes et al., 1996). The crystal structures of the D1 domain of PTPRA domain revealed a dimer that was observed in three different space groups. The active site of each D1 monomer in the dimer was occluded by the N-terminal helix-turn-helix region of another D1 monomer, named "wedge" based on its shape (Fig. 2). This raised the possibility that the phosphatase activity of RPTPs is inhibited by oligomer formation and subsequent occlusion of the active site by the wedge from the opposing monomer.

However, the proposed wedge model had some limitations. The crystal structure of PTPRA was obtained solely for the D1 domain and did not include the D2 domain (Sonnenburg et al., 2003). Moreover, the model of wedge inhibition was not supported by the structural analyses of the D1-D2 tandem domains for LAR and CD45 phosphatases (H. J. Nam et al. 1999; H. J. Nam 2005). The superimposition of the LAR and CD45 D1-D2 domain crystal structures on the corresponding PTPRA D1 crystal structure revealed steric clashes between the opposite D2 domains so that the model of wedge inhibition cannot apply to either LAR or CD45. In the large-scale structural analyses of tyrosine phosphatase domains (Barr et al., 2009), none of the obtained crystal structures of RPTPs dimerized via the wedge region as is the case for PTPRA D1.

Subsequent analytical ultracentrifugation experiments revealed that the tandem phosphatase domains for most of RPTPs are monomeric in solution. A monomeric state in solution has been confirmed for IA2, IA2β, GLEPP1, DEP1 and STEP single-phosphatase domain RPTPs, as well as for CD45, PTPRE, and PTPRM tandem-phosphatase domain RPTPs. These findings suggest an alternative mechanism to the previously established model of the inhibitory wedge, which may include the binding of an extracellular ligand followed by ectodomain oligomerization, proteolysis, and oligomerization under an oxidative stress conditions (Barr et al., 2009).

Even though the tyrosine phosphatase domains appear monomeric in solution, the intact RPTPs might still be regulated by ligand-induced oligomerization. For example, an association of type IIa RPTPs (LAR, PTPRS, PTPRD) with proteoglycans modulates their activity. The binding of heparan sulfate proteoglycans (HSPGs) induces oligomerization and clustering of PTPRS phosphatase molecules and presumably decreases their activity, creating zones of increased phosphorylation and promoting axon outgrowth. In contrast, the binding of chondroitin sulfate proteoglycans (CSPGs) to PTPRS stabilizes phosphatase molecules in a monomeric state maintaining a constitutive phosphatase activity and inhibiting axonal extensions (Coles et al., 2011).

An oxidative stress regulation model, which has been proposed for PTPRA, suggests an equilibrium between monomeric and dimeric forms of the membrane-bound phosphatase. The treatment of PTPRA by H_2O_2 oxidizes the D2 active site Cys723 residue that triggers a conformational change in the D2 domain. This leads to the stabilization of the catalytically inactive dimeric conformation by the formation of a

disulfide bond between the Cys723 residues of two D2 domains (Blanchetot et al., 2002; Tonks, 2006).

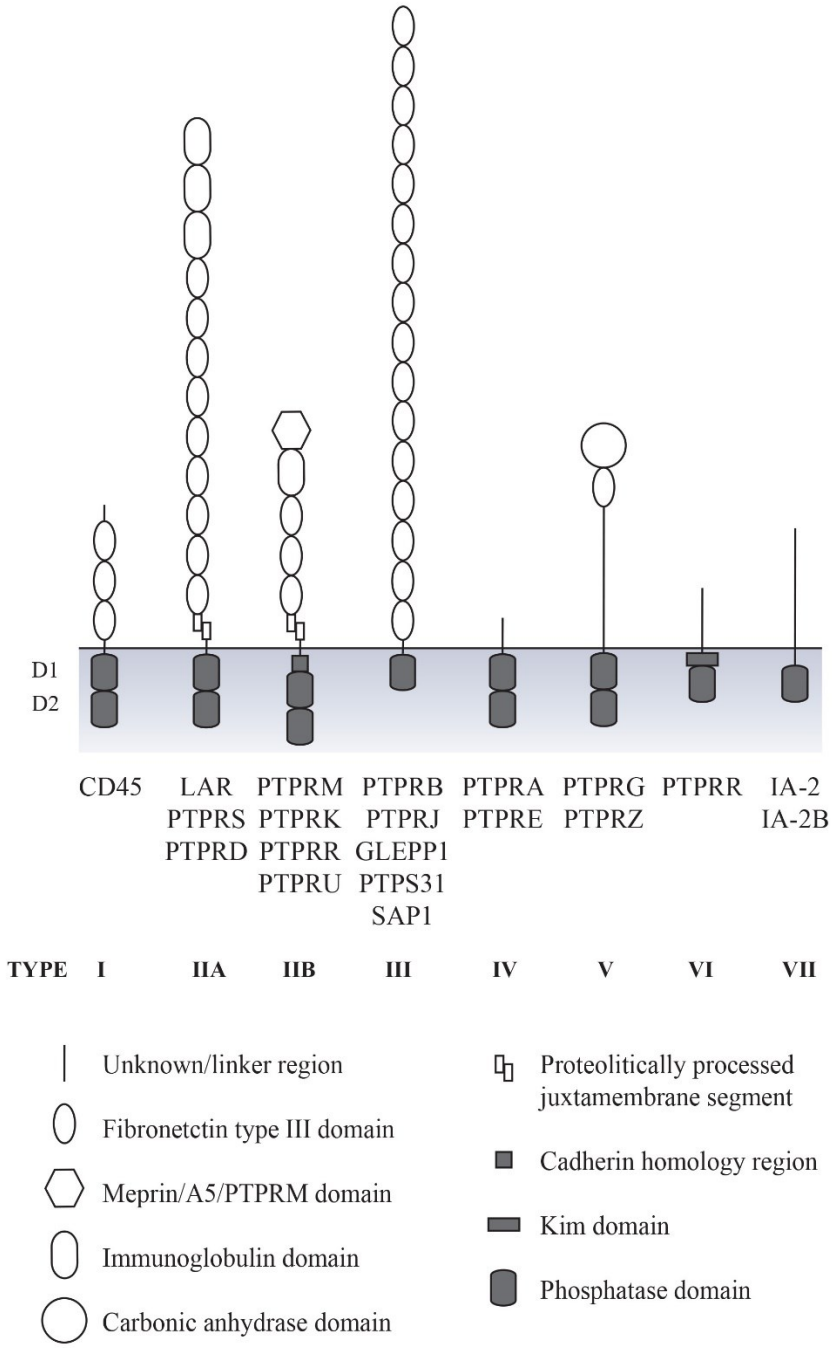

Figure 1. Structural organization of Receptor Protein Tyrosine Phosphatases. Eight families of RPTPs are expressed in nervous system and participate in various cellular events that involve neuronal survival, synapse formation, axon targeting and neurite outgrowth (Mohebiany et al., 2013).

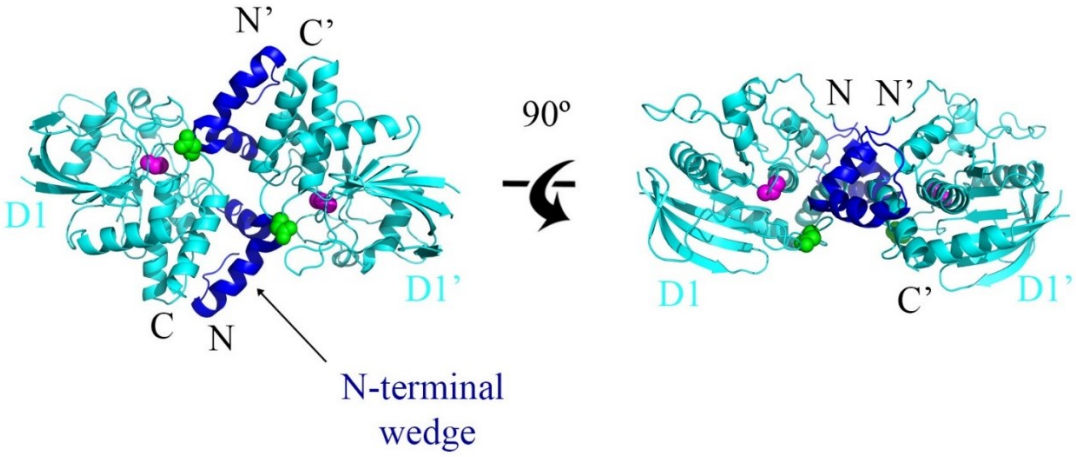

Figure 2. PTPRA D1 domain forms an autoinhibitory dimer. Crystal structure (PDB ID: 1YFO) of the PTPRA D1 domain (Bilwes et al., 1996) is shown in ribbon diagram and colored in cyan. N-terminal loop-helix-loop wedge (blue) occludes the active site of the opposing PTPRA D1'monomer. PTPRA D1 active site is represented by the key catalytic residues shown in spacefill - Cys433 (magenta) and Asp401 (green).

PTPRZ and PTPRG

PTPRG and PTPRZ are two phosphatases that form the type V subfamily of RPTPs. PTPRG and PTPRZ share a common structural organization and consist of a carbonic anhydrase (CA) domain, a fibronectin type III (FN) repeat, a spacer region, a transmembrane domain and tandem intracellular tyrosine phosphatase domains (Fig. 1, 5) (Krueger and Saito, 1992; Barnea et al., 1993; Bouyain and Watkins, 2010). Both phosphatases are highly expressed in the developing and adult nervous system. In the nervous system, PTPRZ is mostly localized to glial cells while PTPRG is predominantly expressed on neurons (Canoll et al., 1996; Lamprianou et al., 2006). However, PTPRZ can also be expressed in subsets of neurons (Hayashi et al., 2005), whereas PTPRG may also be upregulated in certain types of glial cells, including small astrocytes during neuroinflammatory conditions such as lipopolysaccharide (LPS) treatment or in an Alzheimer's disease murine model (Lorenzetto et al., 2013).

PTPRG is the only RPTP whose tandem phosphatase domains have been shown to dimerize in solution (Barr et al., 2009). The crystal structure of PTPRG phosphatase domains revealed that D1-D2 domains are organized in a head-to-toe orientation. In this conformation, the catalytic site of each D1 active phosphatase domain is occluded by the symmetry-related inactive D2 domain (Fig. 3). Structure-based mutations at the PTPRG dimer interface impaired dimer formation as judged by an analytical ultracentrifugation experiments; this indicated that the dimers identified in the crystal structure are identical to those in solution. The dissociation constant (Kd) for the dimer of PTPRG is 3.5 μM suggesting that it exists in a monomer-dimer equilibrium at the cell membrane. It has

been proposed that ligand binding to PTPRG shifts the equilibrium towards the inactive dimeric conformation (Fig. 4) (Barr et al., 2009). Interestingly, in the PTPRG head-to-toe occlusion model each active site of D1 domain is occluded by the loop from the opposing D2 domain that contains a tyrosine residue (Y1307), which in turn has shown to be a site for PTPRG auto-dephosphorylation (Zhang et al., 2012). Therefore, dimer formation of PTPRG and the regulation of its phosphatase activity may also be coupled to increased tyrosine phosphorylation of PTPRG substrates while PTPRG dephosphorylates itself.

It is likely that PTPRZ (RPTPζ), the closest homolog of PTPRG, might be regulated in a manner similar to PTPRG. Although no structural data suggesting the same behavior for PTPRZ have been obtained, sequence alignments of PTPRG and PTPRZ have shown that key residues required for the formation of the D1-D2 phosphatase dimer are conserved (Barr et al., 2009). It has been shown that PTPRZ is inactivated by the heparin-binding growth factor pleiotrophin (PTN) and by the VacA cytotoxin secreted by *Helicobacter pylori* (Fukada et al., 2006; Barr et al., 2009). PTN binding to the extracellular portion of PTPRZ results in increased phosphorylation of PTPRZ downstream substrates Git1 and Magi1, indicating that its phosphatase activity is inhibited. The visualization of PTPRZ distribution upon PTN binding revealed the clustering of phosphatase molecules suggesting that ligand binding induces dimerization as well as inhibition of phosphatase activity. Similar results were obtained in an artificial dimerization system in which the D1-D2 domains of PTPRZ were fused to the intracellular domains of FKBP that forms a dimer upon the stimulation by the AP20187

(ARGENT^{TM} Regulated Homodimerization Kit). Finally, the treatment by polyclonal antibody also inactivated PTPRZ suggesting the inhibitory effect of ligand-induced oligomerization (Fukada et al., 2006). Thus, the potential of PTPRG and PTPRZ to form D1-D2 phosphatase dimers provides an alternative mode of a ligand-dependent RPTP regulation that should be further investigated.

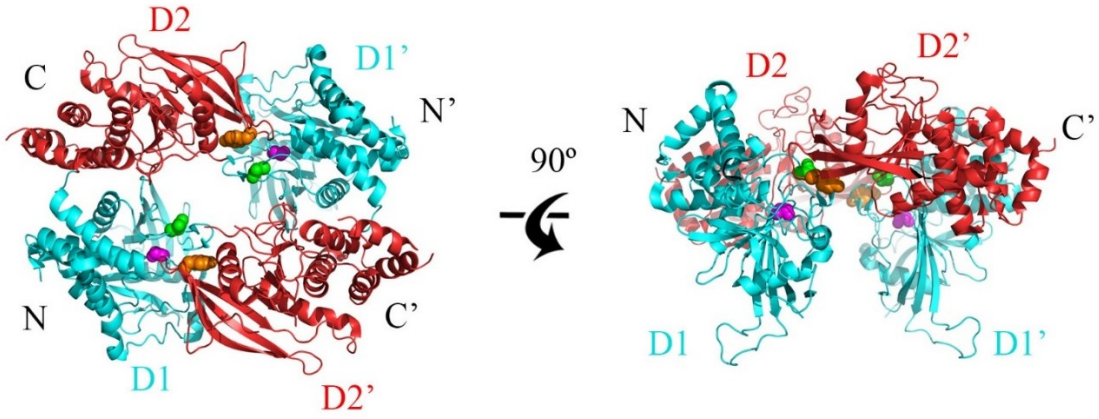

Figure 3. PTPRG D1D2 domains form a dimer on the head-to-toe orientation. Crystal structure **(**PDB ID: 2NLK**)** of PTPRG D1D2 domains (Barr et al., 2009) is shown in ribbon diagram. PTPRG D1 domain is colored in cyan, D2 is colored in red. D1D2 domains form a dimer with a symmetry related mate D1'D2' that results in the occlusion of D1 active site. The PTPRG D1 active site is represented by the key catalytic residues shown in spacefill – Cys1060 (magenta) and Asp1028 (green). The D2 occluding loop is represented by Tyr1307 residue (spacefill, orange), which has shown to be auto-dephosphorylated in PTPRG.

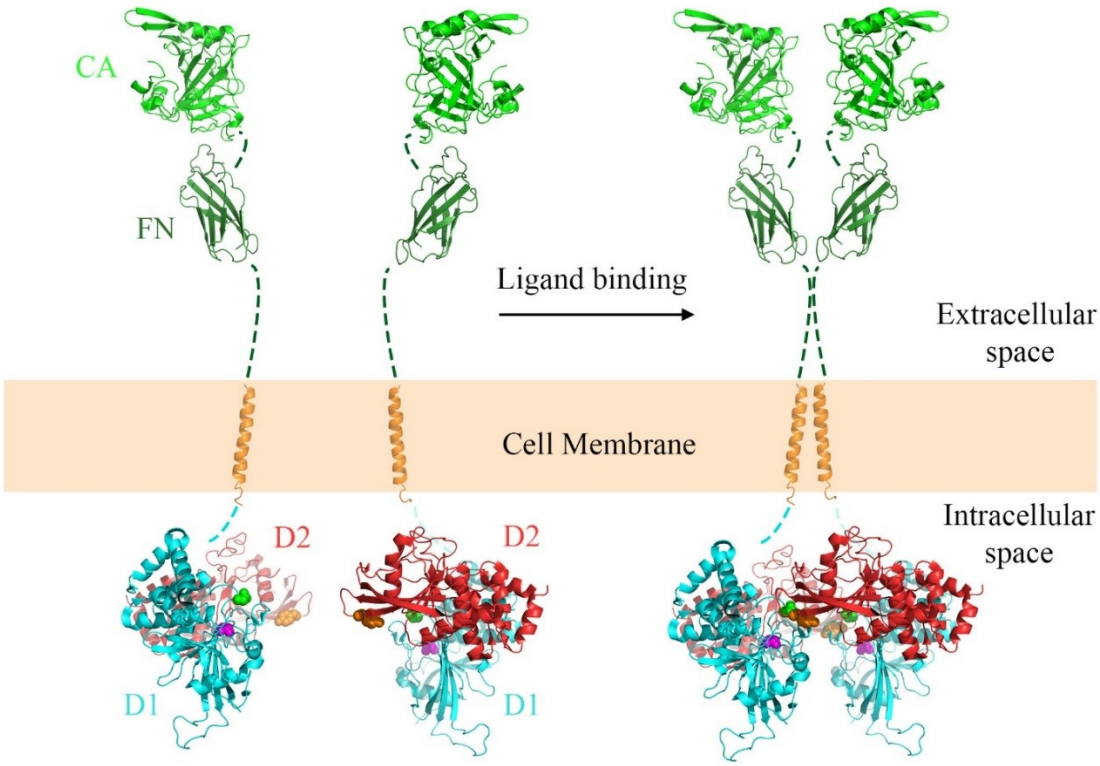

Figure 4. A model for PTPRG ligand-induced dimerization. Hypothetical model of the PTPRG/PTPRZ catalytic inactivation through the ligand-induced oligomerization (Barr et al., 2009). Graphical representations of PTPRG/PTPRZ domains are shown in ribbon diagram. CA domain is colored in green, FN domain – in forest, TM domain – in orange, D1 domain in – cyan, D2 domain in red.

PTPRG and PTPRZ binding partners

Several ligands have been characterized for PTPRZ. In addition to previously mentioned heparin-binding growth factors PTN and VacA cytotoxin, PTPRZ also binds extracellular matrix (ECM) protein tenascin and several members of the immunoglobulin superfamily of CAMs (Ig-CAMs). The first ligand discovered for PTPRZ was Contactin (CNTN1), which was also the first binding partner characterized for any RPTP (Peles et al., 1995). Further studies showed that the PTPRZ•CNTN1 complex is implicated in the maturation of oligodendrocyte precursor cells (OPCs) and the differentiation of oligodendrocytes (Lamprianou et al., 2011). These findings are consistent with data indicating that mice lacking PTPRZ exhibit impaired recovery from demyelinating lesions (Harroch et al., 2002). In contrast to PTPRZ, the binding partners of PTPRG have not been extensively characterized. Based on the interaction of PTPRZ and CNTN1 it was predicted that the CA domain of PTPRG might interact with some members of CNTN family. Indeed, subsequent *in vitro* analyses indicated that the CA domain of PTPRG bound to specifically to CNTN3, 4, 5 and 6, but not CNTN1 (Bouyain and Watkins, 2010).

The six CNTNs belong to the Ig-CAMs superfamily and are composed of 6 N-terminal immunoglobulin-like (Ig) domains, 4 fibronectin type III domains (FN), and a glycophosphatidylinositol (GPI)-anchor, which tethers them to a membrane (Fig. 5). CNTNs are expressed on the surface of neurons at a multitude of sites in the nervous system during development and adulthood. They are involved in various neurodevelopmental processes such as neural cell migration and proliferation, myelin

sheath formation, synaptogenesis and axon guidance (Shimoda and Watanabe, 2009). CNTN3-6, the binding partners of PTPRG, display partially overlapping spatiotemporal expression patterns in the nervous system. CNTN3 is the least studied member of the CNTN family. It is expressed in adult brain in a certain subset of neurons, including Purkinje cells of the cerebellum, granular cells of hippocampus and neurons of the cerebral cortex (Yoshihara et al., 1994; Shimoda and Watanabe, 2009). CNTN4 is best known for its expression in the mouse olfactory system and is found in certain subpopulations of olfactory sensory neurons (OSNs). Despite a normal gross brain anatomy, *CNTN4* deficient mice exhibit abnormalities in axonal projections of OSNs to multiple glomeruli suggesting a role for CNTN4 in the formation of odor maps (Kaneko-Goto et al., 2008). Recently, CNTN4 was discovered in retinal ganglion cells (RGC), where it is crucial for RGC axon targeting to the nucleus of the optic tract, the region responsible for horizontal image stabilization during the processing of a visual signal (Osterhout et al., 2015). CNTN5 expression was characterized in developing glutamatergic synapses of the adult rat auditory pathway. The characterization of *CNTN5* deficient mice mutants did not reveal significant anatomical brain abnormalities. However, mutant mice exhibited impaired processing of acoustic stimuli in the brain (Toyoshima et al., 2009). The sites of *CNTN6* mRNA expression include the olfactory bulb, certain layers of the cerebral cortex, cerebellum and some other regions of the brain (Lee et al., 2000). Similarly to *CNTN4* and *CNTN5* mutants, *CNTN6* deficient mice showed no gross abnormalities in brain development. However, $CNTN6^{-/-}$ animals demonstrated some defects in motor coordination (Takeda et al., 2003). This may be

associated with the role of CNTN6 in forming of glutamatergic synapses between specific subsets of neurons (Purkinje cells and parallel fibers of granule cells) during development of the cerebellum (Sakurai et al., 2009). A broader look at the role of CNTN3-6 in mammalian brain function and development suggests they play a specific role in transmission and processing of sensory signals, motor activity, and higher cognitive function.

Although it is known now that CNTN3-6 bind PTPRG *in vitro*, there is no evidence that the same binding event occurs on the cell surface. Moreover, the physiological roles these complexes might play remain unknown. Interestingly, the expression pattern of PTPRG in the nervous system partially overlaps with the sites of CNTN3-6 expression. It is expressed in pyramidal neurons of the cerebral cortex and hippocampus as well as in RGCs, olfactory bulb glomerulus cells, and ear sensory cells (Lamprianou et al., 2006). Similarly to *CNTN4-6* mutants, tissue analysis did not uncover any visible abnormality for nervous system development in *PTPRG*$^{-/-}$ mice. Comparative behavioral analyses have shown only mild changes in *PTPRG* mutants (Lamprianou et al., 2006). At the same time, both the PTPRG knockdown and the phosphatase-inactive mutant forms of PTPRG (C1060S) have been shown to produce the antidepressive-like phenotype in mice. In addition to antidepressive behavior, the complete loss of PTPRG resulted in increased locomotor activity; this was not detected in mice expressing a catalytically inactive form of PTPRG indicating that PTPRG can be involved in signaling events independent from its primary catalytic activity (Zhang et al., 2012).

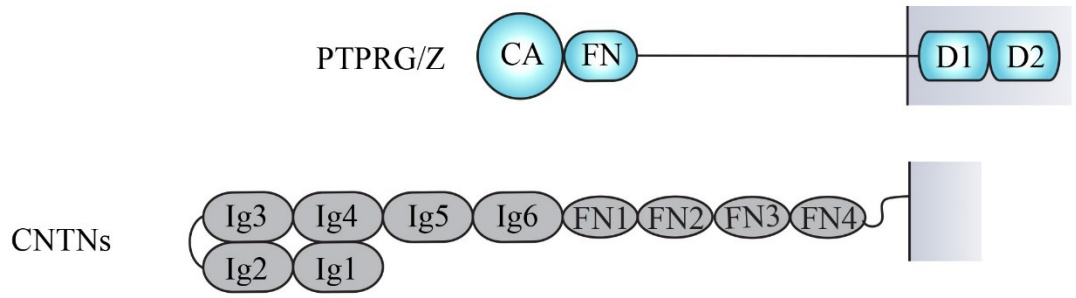

Figure 5. Structural organization of type V RPTPs and their binding partners CNTNs. PTPRG/Z phosphatases include a carbonic anhydrase domain (CA), fibronectin-like type III domain (FN), a spacer region, a transmembrane domain and two phosphatase domains (D1 and D2). PTPRG/Z binds the members of CNTN family that contain 6 immunoglobulin-like domains (Ig) and 4 FN domains. CNTNs do not have an intracellular domain and tethered to a membrane with a glycophosphatidylinositol (GPI) anchor.

Conclusions

RPTPs are unique proteins that combine an intracellular phosphatase activity with an extracellular receptor moiety. PTPRG and PTPRZ are two members of the type V family of RPTPs that bind to CNTN family members *in vitro*. PTPRZ binds CNTN1, whereas PTPRG binds CNTN3-6. The role of the PTPRZ•CNTN1 complex in OPC proliferation and maturation has been extensively studied, but the function for PTPRG binding to CNTN3-6 is poorly understood. Moreover, there is still no data confirming that PTPRG•CNTN binding occurs on the cell surface. It would be very useful to obtain more structural information about the geometry of these complexes to have a better understanding of the possible outcomes from any PTPRG•CNTN binding event. In particular, CNTNs may act as regulators of PTPRG phosphatase activity or co-receptors together with the PTPRG ectodomain. Another question is the reason for the apparent redundancy of having four highly homologous molecules bound to the same PTPRG molecule. This work is intended to obtain more structural and biochemical insights into the interactions between CNTNs and PTPRG, as well as to shed light on the possible functional significance of these complexes.

CHAPTER 2

MATERIAL AND METHODS

Protein expression and purification

Mouse CNTN5(Ig1-Ig4) was transiently expressed using the pSGHP1 vector as a fusion protein with human growth hormone (hGH), an octahistidine tag, and a human rhinovirus 3C protease site. N-acetylglucosaminyltransferase I-negative HEK293S cells were used for protein expression. The resulting protein was cleaved with human rhinovirus 3C protease, deglycosylated using endoglycosidase H, and immobilized by metal affinity and ion exchange chromatography. The purification was completed by size-exclusion chromatography using a Superdex 200 26/60 column (GE Healthcare) equilibrated in 20 mM Tris-HCl, pH 8.0 and 200 mM NaCl (Bouyain and Watkins, 2010). Mouse CNTN3(Ig2-Ig3) and mouse CNTN6(Ig2-Ig3) were expressed in *Escherichia coli* strain T7 Shuffle Express cells (New England Biolabs) using the pT7HMP vector. Proteins were expressed as hexahistidine fusion proteins with a human rhinovirus 3C protease site. After proteolytic cleavage, proteins were purified by metal affinity, ion exchange and size exclusion chromatographies (Bouyain and Watkins, 2010).

Mouse and human PTPRG(CA) were expressed as fusion proteins with a thioredoxin tag, a hexahistidine tag, followed by a human rhinovirus 3C protease site in *Escherichia coli* strain Origami 2 (DE3) using a modified version of the pET32 plasmid (Novagen). The proteins were released from the thioredoxin tag following cleavage by human rhinovirus 3C protease and purified metal affinity, ion exchange, and size exclusion chromatographies (Bouyain and Watkins, 2010).

Complexes of mouse CNTN3(Ig2-Ig3) and human PTPRG(CA) and of mouse CNTN3(Ig2-Ig3) with mouse PTPRG(CA) were prepared by mixing the corresponding purified proteins in equimolar ratios and further purification by gel filtration using a Superdex 200 26/60 column (GE Healthcare) in equilibrated in 20 mM Tris-HCl, pH 8.0 and 200 mM NaCl.

Full-length mouse CNTN3, 4, 5, and 6 fused to a human IgG Fc were expressed transiently in HEK293 cells. Conditioned media was dialyzed against a solution of 200 mM NaCl and 20 mM Tris-HCl pH 8.0, which also served as a binding buffer. Proteins were purified by affinity chromatography using protein A UltraLink resin (Pierce). Bound proteins were eluted with 0.1 M Glycine-HCl pH 2.0 and neutralized immediately with 1 M Tris base (Bouyain and Watkins, 2010).

A mutant form of mouse PTPRG(CA) was engineered with a C-terminal cysteine for the production of biotinylated PTPRG(CA), because free sulfhydryl groups react specifically with maleimide groups at pH 7.0. The protein was expressed in *Escherichia coli* strain Origami 2 (DE3) cells. The expression and purification process was the same as described for the wild type PTPRG(CA), except the buffers were prepared at pH 7.0 to prevent the formation of disulfide dimers. After an ion-exchange purification step, the protein was mixed with EZ-link Maleimide-PEG2k-Biotin reagent according to manufacturer's instructions and then further purified by gel filtration.

Mouse PTPRG(CA) mutants cDNAs were generated by PCR using the megaprimer approach (Sarkar and Sommer, 1990). The mutants included the following mutations: H295A+V296A and H226A+K229A. A cDNA for the β-hairpin deletion

mutant of mouse PTPRG(CA) with the residues $E^{291}QQDHVKSV^{299}$ was replaced by Ala-Ser-Ala (ASA) sequence was generated by overlapping extension PCR. The cDNAs were subcloned into the modified pET32 plasmid mentioned above (Novagen). The proteins were expressed and purified as described for the wild-type PTPRG(CA).

Domains FN1-FN3 for chick CNTN1, human CNTN5 and mouse CNTN2, 3, 4 and 6 were expressed as fusion proteins with a hexahistidine tag and rhinovirus 3C protease site using pT7HMP vector in *E. coli* strain BL21 (DE3). The methionine auxotroph *E. coli* strain B834(DE3) was used for the production of selenomethionine-labeled CNTN2(FN1-FN3). Proteins were proteolytically cleaved and purified using metal-affinity, ion-exchange, and size exclusion chromatographies.

Crystallization and structure determination

All crystals were grown at 20^0C by hanging drop diffusion. Crystallization and cryoprotection conditions for each protein or protein complex are listed in Table 1. X-ray diffraction data were collected at 1.00 Å at Southeast Regional Collaborative Access Team (SER-CAT) beamlines 22-ID and 22-BM at the Advanced Photon source of Argonne National Laboratory. Diffraction data were processed with HKL2000 software (Otwinowski and Minor, 1997). All structures except mouse CNTN2(FN1-FN3) were solved by molecular replacement using PHASER (McCoy et al., 2007) software from the PHENIX suite (Adams et al., 2010). The initial model for the FN1-FN3 fragment of mouse CNTN2 was obtained by single-wavelength anomalous diffraction using data collected from a crystal grown with selenomethionine-labeled protein. The initial solution was obtained using the PHENIX AutoSol and AutoBuild routines. The BAYES

correlation coefficient and figure of merit for the solution were 45.6 ± 20.4 and 0.25, respectively. Models were manually built in COOT software (Emsley and Cowtan, 2004) and refined by PHENIX. Models were validated for Ramachandran statistics and geometry using the RSCB Protein Data Bank validation server. Superimposition of obtained structures was made by the DaliLite server (Hasegawa and Holm, 2009). Interface area and polar interactions were calculated by the PISA server (Krissinel and Henrick, 2007). CCP4 software was used to identify contact residues (Winn et al., 2011). Shape complementarity coefficients were calculated by SC program (Lawrence and Colman, 1993). Graphical representations of structures were generated by PyMol (www.pymol.org).

TABLE 1

CRYSTALLIZATION AND CRYOPROTECTION CONDITIONS

Protein / Protein complexes	**Conc. (μM)**	**Crystallization condition**	**Cryoprotection solution**
Human PTPRG(CA) and mouse CNTN3(Ig2-Ig3)	50	1% (v/v) Tacsimate pH 7.0, 20% (w/v) PEG 3,350, 50mM Imidazole-HCl pH 6.5	1% Tacsimate pH 7.0, 20% PEG (w/v) 3,350, 50mM Imidazole-HCl pH 6.5 15% (w/v) PEG 400
Mouse PTPRG(CA) and mouse CNTN6(Ig2-Ig3)	100	55% (v/v) Tacsimate pH 7.0, 150 mM NDSB 201	55% Tacsimate pH 7.0, 150 mM NDSB 201, 20% (v/v) Glycerol
Mouse CNTN5(Ig1-Ig4)	40	7% (v/v) Tacsimate pH 7.0, 15% (w/v) PEG 3,350, 50 mM Imidazole pH 7.0	50mM Imidazole pH 7.0, 5% (v/v) Tacsimate pH 7.0, 15% (w/v) PEG 3,350, 20% (v/v) Glycerol
Chicken CNTN1(FN1-FN3)	260	1% (v/v) Tacsimate pH 7.0, 20% (w/v) PEG 3,350, 50mM Imidazole pH 6.5	50 mM Imidazole pH 6.5, 9% (w/v) PEG 3,350, 21% Glycerol
Mouse CNTN2(FN1-FN3)	230	50 mM NH_4Cl, 50 mM Tris-HCl pH 8.5, 10% (w/v) PEG 4,000, 2% (v/v) glycerol	50 mM Tris-HCl pH 8.5, 10% (w/v) PEG 4,000, 25% (v/v) glycerol
Mouse CNTN3(FN1-FN3)	200	10% (w/v) PEG 1,500, 50 mM Na-cacodylate pH 6.5	25% (w/v) PEG 1,500, 50 mM Na-cacodylate pH 6.5, 10% (v/v) glycerol

"TABLE 1 -- Continued."

CRYSTALLIZATION AND CRYOPROTECTION CONDITIONS

Protein / Protein complexes	**Conc. (μM)**	**Crystallization condition**	**Cryoprotection solution**
Mouse CNTN4(FN1-FN3)	180	100 mM $(NH_4)_2SO_4$, 50 mM Tris-HCl pH 8.5, 10% (w/v) PEG 4,000	25 mM $(NH_4)_2SO_4$, 50 mM Tris-HCl pH 8.5, 10% (w/v) PEG 4,000, 25% (v/v) glycerol
Human CNTN5(FN1-FN3)	270	1.0 M $NH_4H_2PO_4$, 10% (v/v) Tacsimate pH 5.0	1.0 M $NH_4H_2PO_4$, 10% (v/v) Tacsimate pH 5.5, 38% (w/v) sorbitol
Mouse CNTN6(FN1-FN3)	25	300 mM Na-Malonate pH 7.0, 20% (w/v) PEG 3,350, 50 mM Na-Cacodylate pH 6.5	15% PEG 400, 20% (w/v) PEG 3,350, 250 mM Na-Malonate pH 7.0, 50 mM Na-Cacodylate pH 6.5
Mouse CNTN3(Ig5-FN2)	100	7.5% (w/v) PEG 8,000, 50 mM Imidazole pH 7.5	7.5% (w/v) PEG 8,000, 50 mM Imidazole pH 7.5 15% (v/v) glycerol

AlphaScreen binding assays

The AlphaScreen binding assay (PerkinElmer Life Sciences) is based upon the interaction between a ligand immobilized on donor beads and a second protein bound to acceptor beads (Fig. 6). Upon illumination at 680 nm, phthalocyanine from the donor beads converts ambient oxygen to its singlet form, which travels approximately 200 nm in solution. If there is an acceptor bead within that distance, the singlet oxygen will activate thioxene derivatives within the acceptor bead, and a luminescent signal at 520-620 nm will be emitted. Thus, the signal is produced when donor beads are proximal to acceptor beads, which results from the interaction between proteins immobilized on the bead surfaces.

The assay was designed in 96-well plate format (PerkinElmer Life Sciences semi-opaque microplates) and was based on inhibiting the signal obtained from the interaction of biotinylated PTPRG bound to streptavidin-coated donor beads, and IgG FC fused CNTN3, 4, 5 or 6 bound to protein A-coated acceptor beads. Both types of beads were obtained from an AlphaScreen general IgG (Protein A) detection kit from PerkinElmer Life Sciences. Final reaction volumes were kept at 25 µl for all experiments. Initially, 5 µl of biotinylated mouse PTPRG(CA) (5 nM final concentration) were mixed with 5 µl of human IgG FC-fused CNTN3, 4, 5 or 6 and incubated with 5 µl aliquots of untagged wild-type PTPRG(CA) of varying concentrations. After a 1-hour incubation at room temperature protein A-coated acceptor beads (5 µl, 20 µg/ml final concentration) were added to each well. After another 1-hour incubation, streptavidin-coated donor beads (5 µl, 20 µg/ml final concentration) were added to each well. The reactions were allowed to

stand at room temperature for 30 minutes prior to transferring to 96-well ½ area opaque microplates for detection using an EnSpire multimode plate reader (PerkinElmer Life Sciences). Values for normalized binding were calculated by dividing the signal measured for a reaction without inhibitor. For the control experiment, bovine carbonic anhydrase II was used as an inhibitor in the equivalent assay. Results were fitted to a one-site competition equation, in which the IC_{50} is the concentration of inhibitor that gives 50% inhibition of maximal binding using GraphPad Prism (GraphPad). The values of IC_{50} are reported as averages ± standard deviations of at least three experiments.

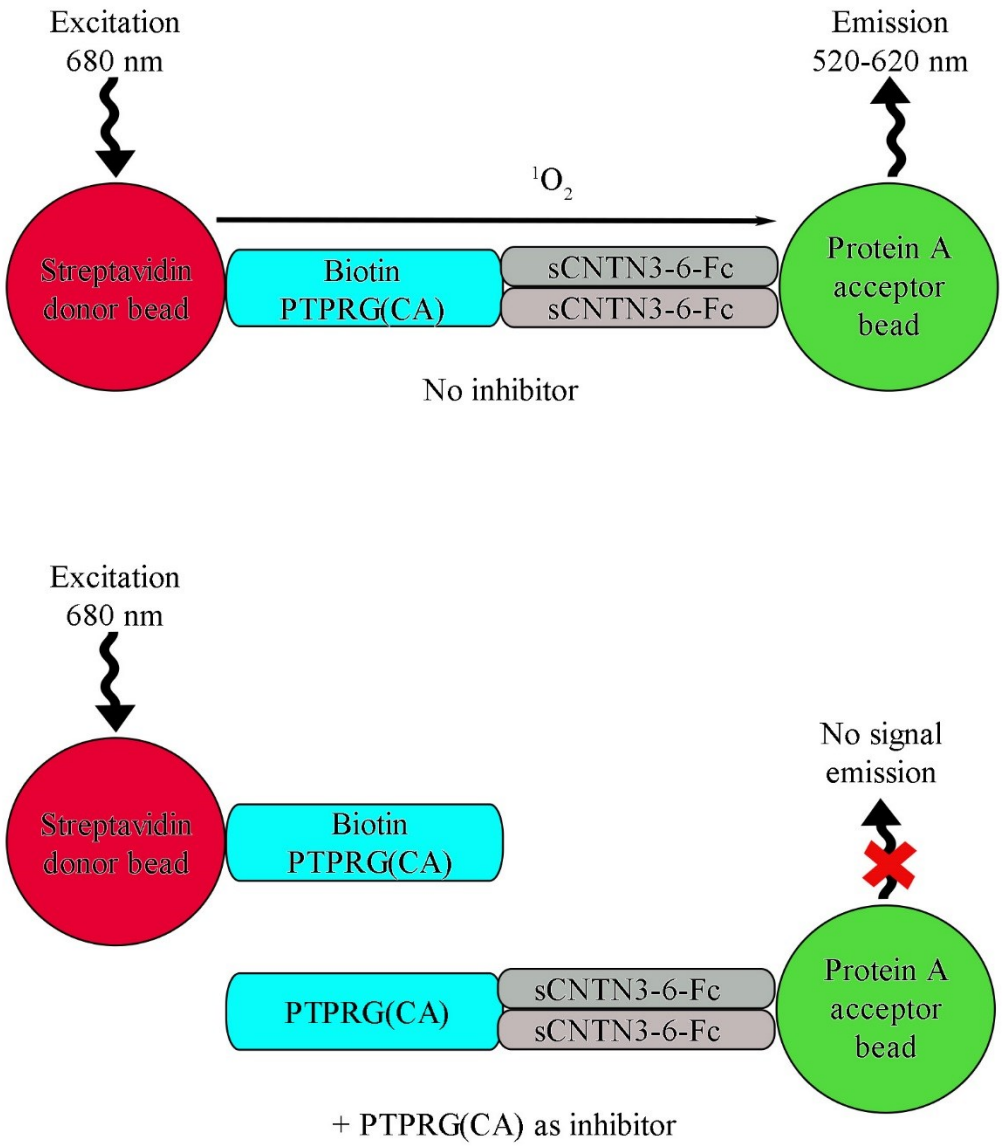

Figure 6. AlphaScreen technology (Perkin Elmer) based competition assay design. Biotinylated PTPRG(CA) protein bound to streptavidin donor bead interacts with the CNTN3 to 6 expressed as fusion proteins with human IgG FC tag, which binds to protein A-coated acceptor bead. Under these conditions, excitation of donor beads at 680 nm triggers the release and migration of singlet oxygen to acceptor beads followed by a signal emission at 520-620 nm. Based on the inhibition of the produced signal by either untagged PTPRG(CA) or control bovine CAII competition curves were obtained and IC_{50} values were determined.

Small angle X-ray scattering (SAXS)

SAXS data were collected at the ALS beamline 12.3.1 LBNL Berkeley, California (Hura et al., 2011). The wavelength λ and the sample-to-detector distances were set to 1.03 Å and 1.5 m, respectively, resulting in scattering vectors q ranging from 0.01 $Å^{-1}$ to 0.32 $Å^{-1}$. The scattering vector is defined as $q = 4\pi \sin\theta/\lambda$, where 2θ is the scattering angle. All experiments were performed at 20 °C and data was processed as described (Hura et al., 2011). Data acquired for 0.5, 1, and 2 M concentrations were merged for calculations using the entire scattering profile. The protein was prepared by size exclusion chromatography on a Superdex 200 10/30 HR column (GE Healthcare) equilibrated in 20 mM Tris-HCl pH8.0, 200 mM NaCl prior to data collection. The experimental SAXS data for different protein concentrations were analyzed for aggregation using Guinier plots (Guinier and Fournet, 1956). The radius of gyration R_G is 30.9 Å and was derived by the Guinier approximation $I(q) = I(0) \exp(-q^2R_G^2/3)$ with the limits $qR_G < 1.6$. The theoretical SAXS profile and the corresponding fit to the experimental data were calculated using the program FoXS (Schneidman-Duhovny et al., 2013). A molecular envelope for CNTN3(FN1-FN3) was calculated from the experimental scattering data using the program DAMMIF and averaged using DAMAVER (Volkov and Svergun, 2003; Franke and Svergun, 2009). The molecular envelope and the crystal structure of CNTN3(FN1-FN3) were superimposed using Chimera (Pettersen et al., 2004).

Cell binding assays

HEK293 cells were maintained in DMEM high glucose supplemented with 10% (v/v) of fetal bovine serum. GPI-anchored mouse CNTNs were transiently expressed in HEK293 cells (Fig. 7) as fusion proteins with hGH as described previously (Bouyain and Watkins, 2010). A fragment of human PTPRG including its CA and FN domains fused to human IgG FC was incubated in the presence of fluorescein isothiocyanate-labeled anti-human Fc antibodies (Jackson) for 30 minutes. The labeled PTPRG was added to the transfected cells for 15 minutes in DMEM/F12 containing 1% N2 supplement at room temperature and then fixed in 4% (w/v) paraformaldehyde (PFA) in PBS for 10 minutes. The presence of transfected proteins was detected by immunostaining against hGH using a rabbit polyclonal antibody (Fitzgerald) (Hamaoka et al., 2004; Bouyain and Watkins, 2010).

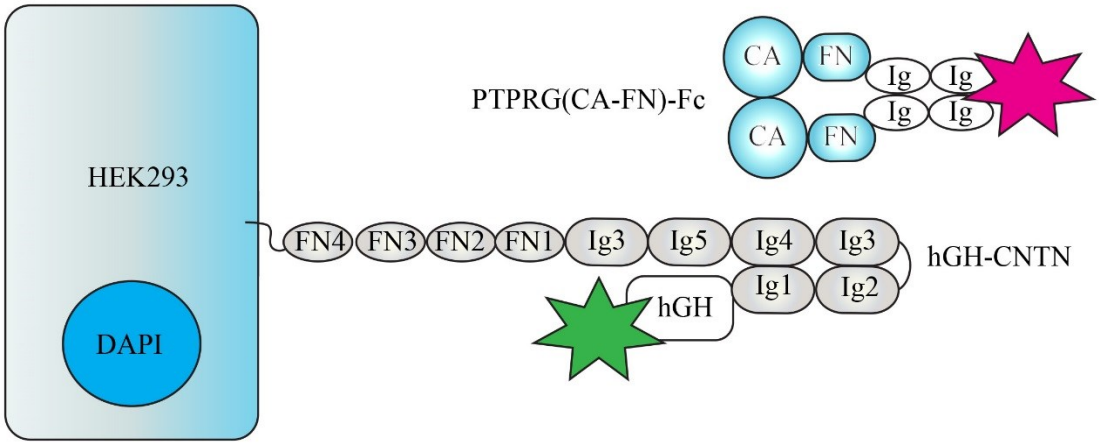

Figure 7. Cell binding assays design. CNTNs fused to hGH were transiently expressed on the surface of HEK293 cells. The expression of CNTNs was detected by the immunostaining against hGH with the rabbit polyclonal antibody (green). A recombinant protein consisting of CA and FN domains of PTPRG was expressed as a fusion with a human IgG Fc fragment and incubated with fluorescein isothiocyanate-labeled anti-human Fc antibodies (magenta). The labeled PTPRG(CA-FN)-Fc protein was applied to the surface of the transfected HEK293 cells. The binding was detected using the immunohistochemistry protocol.

Immunostaining of mouse adult retinas and proximity ligation assays

Retinas were obtained from adult C57BL6 mice (> 8 weeks old) from the Jackson Laboratory. All studies followed the guidelines prescribed by the UMKC IACUC and the U.S. National Institutes of Health/National Eye Institute. Adult mice were deeply anesthetized with CO_2, eyes were enucleated, and the cornea and lens were removed. All eyecups were rapidly fixed for 15 min in 4% (w/v) PFA and processed as previously described for immunohistochemistry (Stella et al., 2012). Solitary rod photoreceptors were dissociated from isolated retina as previously described (Zayas-Santiago and Kang Derwent, 2009) and fixed for 10 minutes in 4% (w/v) PFA, washed in PBS and processed for indirect immunofluorescence or Duolink™ analysis.

All tissue was labeled using the indirect immunofluorescence technique using goat anti-CNTN3 (1:200, R&D systems) and mouse anti-PTPRG (1:80, Novus Biologicals) as described previously (Stella et al., 2012). The primary antibody/antigen complexes were detected using secondary antibodies conjugated to CF488 and CF568 (Biotium). *In situ* proximity ligation assays (PLAs) were performed to detect *in vivo* interactions between PTPRG and CNTN3 using the primary antibodies and dilutions mentioned above. Retinas were labeled using DuoLink™ in situ reagents from Olink Bioscience according to the manufacturer's instructions. A fluorescent signal is obtained when the labeled proteins are within 40 Å of one another. In control experiments, primary antibodies were omitted and only secondary antibodies and Duolink reagents were included in the subsequent steps to rule out spurious non-specific labeling. All images were acquired sequentially using a Nikon C2 confocal microscope with appropriate lasers

for excitation (e.g, 488 and 561 nm) and filters (e.g., 505-530BP and 565-600BP respectively) for emission collection as either 12-bit or 8-bit signals. Images were processed for publication using Fiji (Schindelin J, Arganda-Carreras I, Frise E, Kaynig V, Longair M, Pietzsch T, 2003).

Cell aggregation assays

cDNAs encoding full-length mouse CNTN1, CNTN3 and PTPRG without their signal sequences were cloned into the mammalian expression vectors pSmEmerald (CNTN1, 3) and pSmCherry (PTPRG) designed in the laboratory. These vectors derive from the pLEXm plasmid (Aricescu et al., 2006) and direct the expression of the chicken PTPRS signal sequence followed by a monomeric Emerald or monomeric Cherry fluorescent protein and the protein of interest. HEK293F cells (ThermoFisher Scientific) were grown in suspension in FreeStyle™ 293 expression medium. Cells (10^7 at a density of 10^6 cells/ml) were transfected using a mixture 10 μg of plasmid and 30 μg of Polyethylenimine HCl MAX, Mw 40,000 (Polysciences, Inc) (Longo et al., 2013). Two days after transfection, ~ 5 x 10^6 cells were spun, washed once with Hank's Balanced Salt Solution (HBSS) and resuspended into HBSS supplemented with 1% (v/v) of fetal bovine serum and 10 mM Na-HEPES pH 7.5 to a final density of 5 x 10^5 cells/ml and briefly vortexed. Cell aggregation was initiated by mixing equal amount of cells into a microcentrifuge tube (final volume 1 ml) and incubated at room temperature with constant agitation. After a 45-minute incubation, a 0.5-ml aliquot of the reaction was transferred to a poly-D-lysine coated glass coverslip. Cells were allowed to attach for 20 minutes. The cell suspension was then removed and the coverslip was washed once with

PBS. Cells were fixed with 4% (w/v) PFA, washed with PBS and mounted. Confocal images were acquired sequentially on an Olympus BX61WI with appropriate lasers for excitation (488 and 543 nm) and filters (502-538BP and 604-644BP respectively) using a DP30BW cooled ccd camera. Images were processed for publication using Fiji (Schindelin et al., 2012)

Specific contributions of members of the laboratory and collaborators

Roman M. Nikolaienko: Protein expression, purification, crystallization, and crystal structure determination of CNTN1(FN1-FN3), CNTN6(FN1-FN3), CNTN3(Ig5-FN2), PTPRG(CA)•CNTN3(Ig2-Ig3) and PTPRG(CA)•CNTN3(Ig2-Ig3) complexes. Crystallization and crystal structure determination of CNTN5(Ig1-Ig4). AlphaScreen protein-protein binding assays including protein expression and purification. Protein expression, purification and sample preparation for SAXS experiments for CNTN3(FN1-FN3).

Samuel Bouyain: Protein expression, purification, crystallization, and crystal structure determination of CNTN2, 3, 4, and 5 FN1-FN3 regions. Protein expression of Fc fusion full-length CNTNs for AlphaScreen binding assay. Protein expression and purification of CNTN5(Ig1-Ig4). Cell aggregation assays.

Salvatore L. Stella and Rana Zalmai: Immunostaining of mouse adult retinas and proximity ligation assays.

Michal Hammel: SAXS data collection and analysis of CNTN3(FN1-FN3).

Veronique Dubreil and Sheila Harroch: Cell binding assays.

David R. Hall and Nurjahan Mehzabeen: Protein expression, purification, crystallization and crystal structure determination of CNTN2, 3, 4, and 5 FN1-FN3 regions.

CHAPTER 3

STRUCTURAL BASIS FOR THE CONSERVED INTERACTION OF CNTN3, 4, 5, AND 6 WITH THE CA DOMAIN OF PTPRG

Overview

Interactions between CAMs at the surfaces of neural cells are essential to guide the development and maintenance of the nervous system. Previously, the results of *in vitro* affinity isolation assays have shown that CNTN family members bind to PTPRG and PTPRZ (Bouyain and Watkins, 2010). PTPRZ specifically interacts with CNTN1, whereas PTPRG binds to CNTN3-6. The binding sites encompass the CA domain of PTPRG or PTPRZ and domains Ig2 and Ig3 in CNTNs. The analysis of the crystal structures of the PTPRG(CA)•CNTN4(Ig1-Ig4) and PTPRZ(CA)•CNTN1(Ig2-Ig3) complexes has provided a structural basis for the interactions between PTPRG/Z and CNTNs and confirmed the results of the affinity isolation assays. In particular, these structural data indicate a conserved orientation of the protein molecules within the complexes in which the β-hairpin loop of PTPRG/Z interacts with a horseshoe-like structure formed by repeats Ig2-Ig3 of a CNTN molecule. Despite a similar orientation, binding interfaces in these complexes are not the same, with predominantly hydrophobic interactions in the PTPRZ(CA)•CNTN1(Ig2-Ig3) complex compared to more polar interactions in the PTPRG(CA)•CNTN4(Ig1-Ig4) complex (Bouyain and Watkins, 2010; Lamprianou et al., 2011).

Whereas the binding of CNTN1 and PTPRZ has been demonstrated at the surfaces of neurons and glial cells and has been linked to the maturation and

differentiation of oligodendrocytes, the *in vivo* associations of CNTNs with PTPRG has yet to be confirmed. Here, I present data that confirm the specific interactions of CNTN3-6 and PTPRG at the surfaces of HEK293 cells. These data are complemented with structural and biochemical studies of PTPRG•CNTN complexes that suggest a conserved mode of interactions of PTPRG with CNTN3, 4, 5 and 6 with similar binding affinities.

Specific interaction of CNTN3-6 with PTPRG on cell surfaces

To test that PTPRG interacts with CNTN3-6 on cells surfaces, we used HEK293 cells transfected with full-length hGH-tagged CNTNs and incubated them with the CA and FN domains of PTPRG expressed as fusion proteins with human IgG Fc (Fig. 8). In agreement with previous affinity-isolation assays PTPRG-Fc fusion proteins bound to cells expressing CNTN3-6, but not to cells expressing CNTN1 and 2 (Bouyain and Watkins, 2010). These results demonstrate that the specific interactions of PTPRG with CNTN3-6, which has been shown *in vitro*, also occur at the surface of cells. PTPRG does not interact with CNTN1, the specific binding partner of PTPRZ. It also does not bind to CNTN2, which has been shown to be involved in homophilic interactions. The configuration of this assay suggests a PTPRG/CNTN interaction in *trans*, which mimics interactions of proteins on opposing membranes, similarly to what has been shown for CNTN1 and PTPRZ. However, it does not exclude that the two proteins might interact when expressed on the same cell (*cis*-interactions).

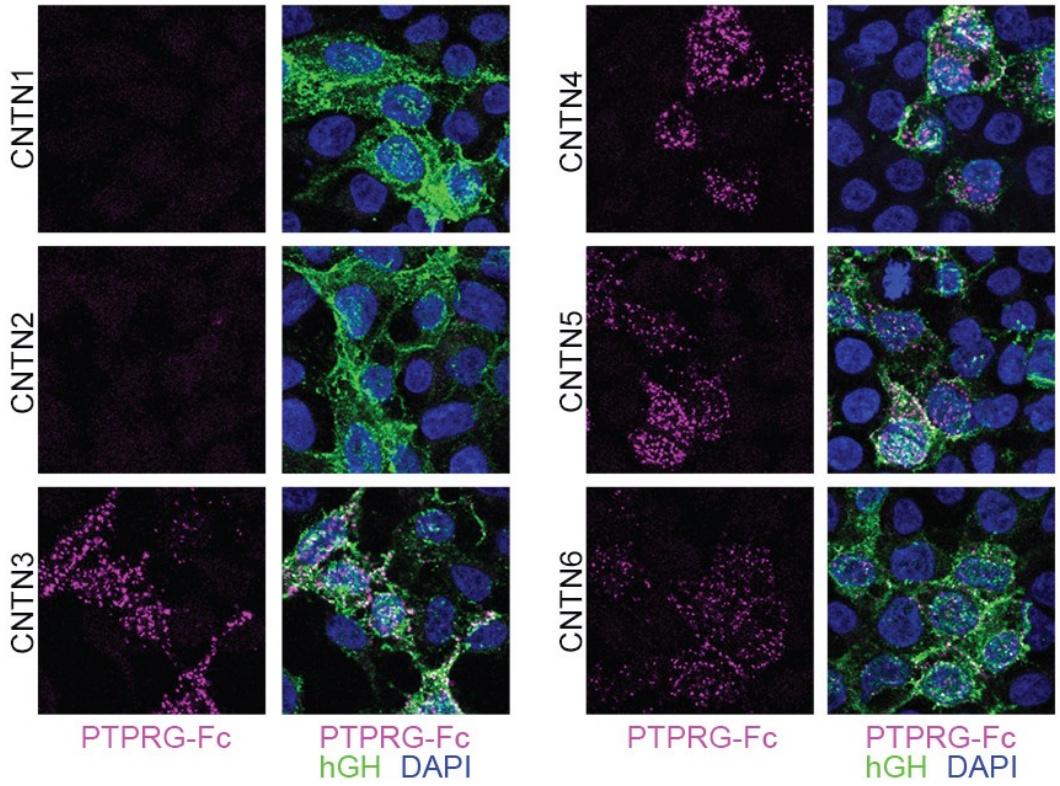

Figure 8. PTPRG interacts with CNTN3-6, but not with CNTN1 or CNTN2. HEK293 cells transfected with full-length CNTNs fused to human growth hormone (hGH) were incubated with an Fc fusion of the CA and FN domains of mouse PTPRG labeled with fluorescein isothiocyanate (magenta). CNTN-expressing cells were labeled with an antibody conjugated to a green fluorophore. The nuclei were visualized using DAPI.

Similar biochemical characteristics of PTPRG•CNTN interactions

Previous data from affinity isolation assays along with the results of cell surface binding assays presented here confirm the interactions of PTPRG with CNTN3-6. However, neither of these techniques can evaluate a difference in binding affinities to PTPRG for each CNTN member. The strict conservation of CNTN3-6 amino acid residues involved in the interaction with PTPRG suggests a similar binding mode for each complex. However, binding affinities may be affected by other factors independent of interactions within a binding site, such as binding geometry, surface potential, glycosylation pattern, and conformations of CNTN ectodomains. To investigate the affinity of interactions within PTPRG•CNTN complexes, we designed a binding assay based on AlphaScreen technology in which a biotinylated form of PTPRG(CA) immobilized on a streptavidin-coated donor bead interacts with a full-length CNTN-Fc fusion protein bound to a protein A acceptor bead via its Fc tag. Protein-protein interactions bring donor and acceptor beads together that allows an emission of a luminescent signal after illumination at 680 nm. Under this condition, we have measured binding affinities indirectly in a competitive-binding assay, using a soluble form of PTPRG(CA) as an inhibitor of interactions between our immobilized proteins.

The calculated IC_{50} values overall suggest that PTPRG binds CNTN3-6 with similar affinities (Fig. 9A). The strongest interaction was detected for the PTPRG•CNTN4 complex (IC_{50} = 235 nM). The IC_{50} values measured for the binding of PTPRG to CNTN3 and 5 are 428 nM and 327 nM, respectively. The association between PTPRG and CNTN6, with an IC_{50} value of 519 nM, appears to be the weakest one. These

IC_{50} values are also similar to the corresponding IC_{50} value of 332 nM for PTPRZ•CNTN1 complex (Fig. 10, Table 2).

The obtained IC_{50} values reflect the binding affinities measured under conditions used in particular binding assays and may not be the most accurate representations of the physiological Kd values in the cellular environment. For example, in our assay, we used a truncated form of PTPRG and artificially dimeric CNTN-Fc fusion proteins. However, we can rely on obtained values to characterize the relative binding affinities within the different members of CNTN family under given conditions. Based on ANOVA and Tukey analysis the differences between CNTN3-CNTN4, CNTN4-CNTN6 and CNTN5-CNTN6 affinities are characterized as statistically significant, whereas the CNTN3-CNTN5, CNTN3-CNTN6, and CNTN4-CNTN5 differences are not (Fig. 9B). It remains unclear, however, whether these differences in binding affinities lead to distinct physiological outcomes.

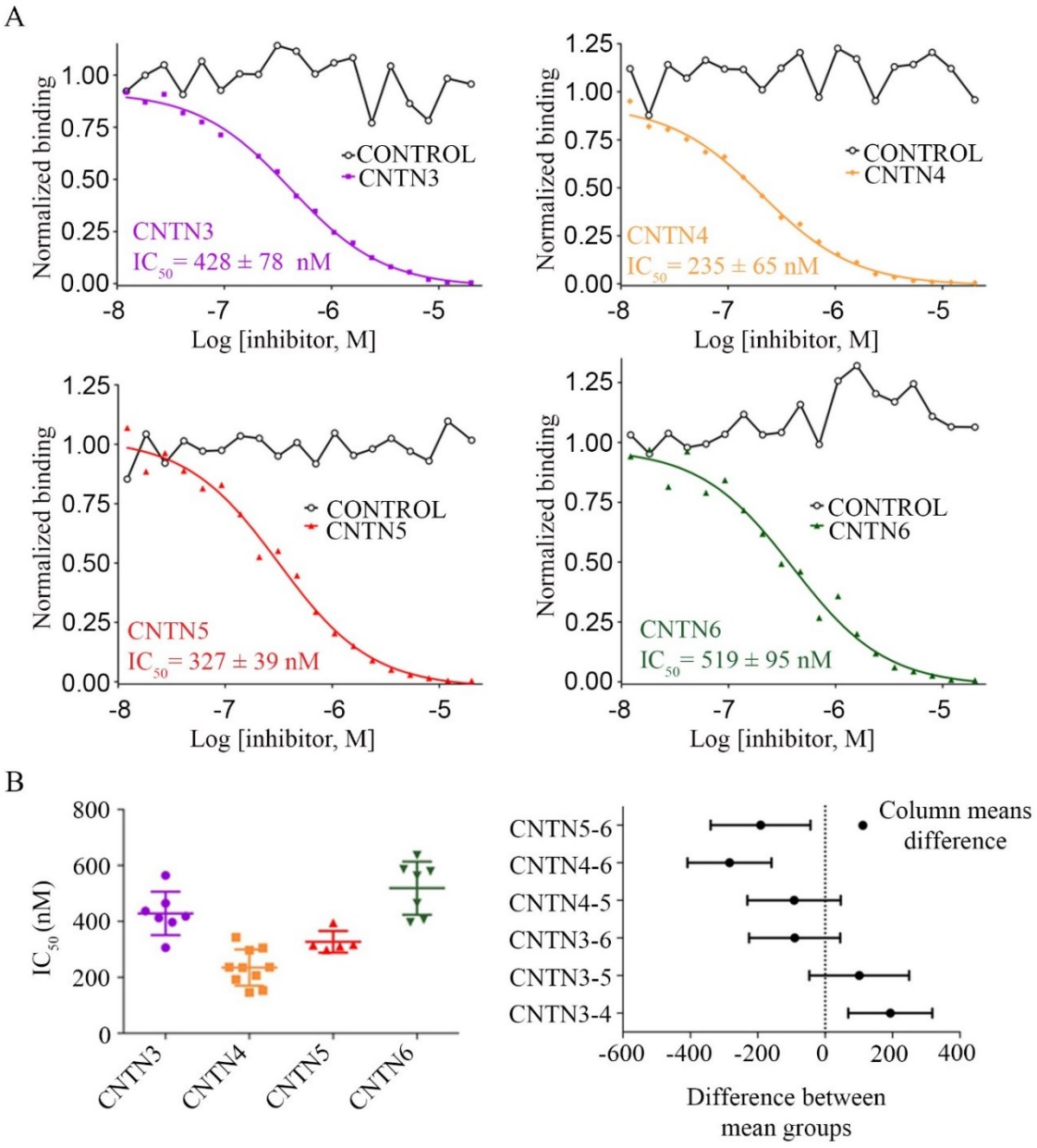

Figure 9. Interactions between the CA domain of PTPRG with CNTN3-6, as determined by an AlphaScreen bead-based competition assay. (A) The ability of mouse PTPRG(CA) or bovine CAII (control) to inhibit binding between an Fc fusion of full length mouse CNTN3-6 and biotin labeled PTPRG(CA) was assessed over a logarithmic dilution series. IC_{50} values are reported as averages ± standard deviations from at least three experiments. One representative experiment for each series is shown. See Table 2 and Appendix for detailed results. (B) One-way ANOVA analysis of the IC_{50} values measured in (A).

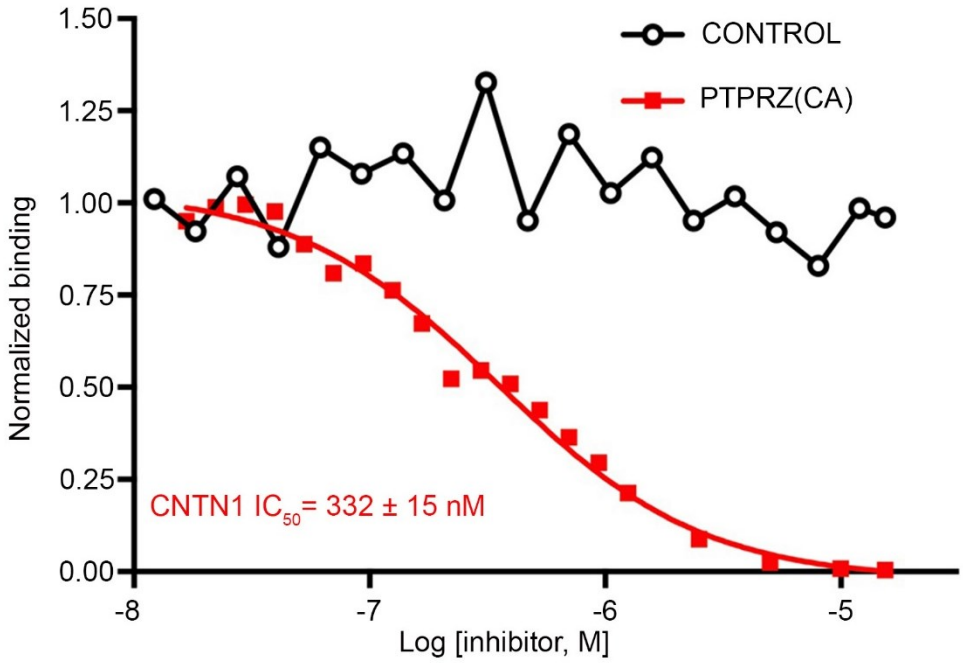

Figure 10. Interactions between the CA domain of PTPRZ with CNTN1, as determined by an AlphaScreen bead-based competition assay. The ability of bovine CAII (control) and human PTPRZ(CA) to inhibit the AlphaScreen signal between an Fc fusion of full length mouse CNTN1 and biotin-labeled PTPRZ(CA) was assessed over a logarithmic dilution series. One representative experiment out of four is shown.

TABLE 2

SUMMARY OF DATA ANALYSIS CURVE-FITTING OF ALPHASCREEN BEAD-BASED COMPETITION ASSAYS

Inhibitor	**Immobilized proteins**	**IC_{50} (nM)**	**Standard deviation (nM)**	**Number of assays**
PTPRZ(CA)	PTPRZ(CA) CNTN1-Fc	332	15	4
PTPRG(CA)	PTPRG(CA) CNTN3-Fc	428	78	7
PTPRG(CA)	PTPRG(CA) CNTN4-Fc	235	65	10
PTPRG(CA)	PTPRG(CA) CNTN5-Fc	327	39	5
PTPRG(CA)	PTPRG(CA) CNTN6-Fc	519	95	7
PTPRG(CA) H295A+V296A	PTPRG(CA) CNTN4-Fc	917	112	4

A conserved binding mode for the PTPRG•CNTN complex formation

Given the strict conservation of PTPRG-interacting residues in CNTN3-6, we wondered if there were distinct structural features that might account for differences in binding affinities. For this reason, we determined co-crystal structures of the Ig2-Ig3 repeats of CNTN3 and CNTN6 bound to the CA domain of PTPRG. The arrangements of the protein molecules in the complexes resembled those determined in the PTPRZ•CNTN1 and PTPRG•CNTN4 crystal structures (Fig. 11, 12). In both crystal structures, the binding interface includes the β-hairpin loop of the CA domain of PTPRG (residues 288-301) that contacts the Ig2-Ig3 repeats of CNTN3 or 6 and the PTPRG(CA) short loop (residues 225-229) that interacts only with the Ig3 domain of CNTN. The interface areas for the PTPRG•CNTN3 and PTPRG•CNTN6 complexes are 1,668 $Å^2$ and 1,446 $Å^2$, respectively, and are comparable to those published for the PTPRZ•CNTN1 (1,658 $Å^2$) and PTPRG•CNTN4 (1,702 $Å^2$) complexes. The values for the shape complementarity coefficients are measured as 0.62 for the PTPRG•CNTN3 complex and 0.68 for the PTPRG•CNTN6 complex. These values are similar to those for the PTPRZ•CNTN1 and PTPRG•CNTN4 complexes (0.68 and 0.67, respectively).

In broad terms, the interfaces for the PTPRG•CNTN complexes can be subdivided into four parts (Fig. 13, 14): (1) a predominantly hydrophobic core site that comprises the residues on the base of the PTPRG β-hairpin loop, (2) a short 5-aa loop region that contacts residues within the Ig3 domain of CNTN3/6, (3) an antiparallel β-sheet formed by the β-hairpin loop interacting with an antiparallel three-strand β-sheet of Ig2 CNTN3/6, and (4) a tip region of the β-hairpin loop formed by residues Q293-V296.

The hydrophobic core site in PTPRG•CNTN3/6 complexes is formed by PTPRG(CA) β-hairpin loop residues F288, T289, T290 and Y301, and CNTN3/6 residues M222 and Y225. Site 2 includes PTPRG residues V225-K229 as well residues E226, P227, K228 and N306 of CNTN3/6. In particular, PTPRG K229 forms a hydrogen bond with N306 and a salt bridge with E226 in CNTN3/6. In site 3, two strands of the PTPRG β-hairpin loop combine with a three strands antiparallel β-sheet in domain Ig2 of CNTN3/6 to form a 5-strand antiparallel β-sheet. It is stabilized by the hydrogen bonds between H295-H300 in PTPRG and G139-L143 in CNTN3/6. In addition, CNTN3/6 Q138 side chain forms two hydrogen bonds with the main chain atoms of V299 and the side chain atoms of E300 in PTPRG. Unlike sites 1-3 that are conserved in all PTPRG•CNTN structures, the tip of the β-hairpin in site 4, which includes Q293-V296 side chains, adopts distinct conformations in the PTPRG•CNTN3 and PTPRG•CNTN6 complexes. The only invariant contact on this site is the packing of H295 from PTPRG against R129 of CNTN3/6. Given the distinct conformations of the β-hairpin loop in PTPRG•CNTN complexes, we suggest that this region is flexible and does not play an essential role in the protein-protein interactions.

Overall, the conservation of molecular contacts in the PTPRG complexes with CNTN3, 4 and 6 (Fig. 15) is consistent with the comparable IC_{50} values determined in protein-protein binding assays. Although it was not possible to obtain co-crystals of the PTPRG•CNTN5 complex, analysis of the crystal structure of unliganded CNTN5(Ig1-Ig4) indicates that the putative PTPRG-binding site is nearly identical to the one discovered in the PTPRG•CNTN4 complex (Fig. 16). Thus, the structural information

and protein-protein binding assays it can be argued that the mode of PTPRG binding to CNTN3, 4, 5 and 6 is conserved.

TABLE 3

DATA COLLECTION AND REFINEMENT STATISTICS FOR PTPRG(CA)•CNTN3/6 (IG2-IG3) COMPLEXES, AND CNTN5(IG1-IG4) CRYSTAL STRUCTURES

	CNTN3(Ig2-Ig3)• PTPRG(CA)	**CNTN6(Ig2-Ig3)• PTPRG(CA)**	**CNTN5(Ig1-Ig4)**
Data Collection			
Beamline	APS 22-ID	APS 22-BM	APS 22-BM
Wavelength (Å)	1	1	1
Unique reflections	31,166	70,482	14,070
Resolution (Å)	50 - 2.6	50 - 2.0	50 - 2.6
Space group	$P2_12_12$	$P2_12_12_1$	C2
Unit cell			
a, b, c (Å)	74.14, 90.53, 147.45	78.64, 113.53, 117.05	179.98, 50.66, 51.02
α, β, γ (º)	90.0, 90.0, 90	90.0, 90.0, 90	90.0, 101.67, 90
R_{sym}[a]	0.134 (0.588)[b]	0.096 (0.593)	0.154 (0.435)
Completeness[b] (%)	99.6 (96.3)	98.7 (89.2)	98.8 (90.7)
Redundancy	11.4 (5.3)	7.1 (5.3)	6.5 (3.5)
I/σI	7.2 (2.3)	19.5 (2.0)	11.4 (2.3)
Refinement			
Molecules in the asymmetric unit	2 x 2	2 x 2	1
Resolution (Å)	49.2 - 2.6	24.9 - 2.0	37.0 - 2.6
R_{work}[c] / R_{free}	0.187/0.249	0.167/0.217	0.195/0.264

"TABLE 3 -- Continued."

DATA COLLECTION AND REFINEMENT STATISTICS FOR PTPRG(CA)•CNTN3/6 (IG2-IG3) COMPLEXES, AND CNTN5(IG1-IG4) CRYSTAL STRUCTURES

	CNTN3(Ig2-Ig3)• PTPRG(CA)	**CNTN6(Ig2-Ig3)• PTPRG(CA)**	**CNTN5 (Ig1-Ig4)**
Refinement			
Number of atoms	7,291	8,039	3,086
Protein	7,205	7,392	2,968
Ligand	27	112	28
Water	59	535	90
R.m.s. deviations			
Ideal bonds (Å)	0.009	0.007	0.003
Ideal angles (°)	1.1	1.05	0.83
Average B factors (Å²)	71.2	40.9	50.1
Protein	71.3	40.4	49.6
Ligand	98.3	71.9	88
Water	49.9	41.6	51.6
Ramachandran statistics			
Favored (%)	94	97	95
Allowed (%)	6	3	5
PDB accession code	5E5R	5E5U	5E4I

[a]$R_{sym} = \Sigma h\, \Sigma_i |I_i(h) - \langle I(h)\rangle| / \Sigma_h\, \Sigma_i\, I_i(h)$, where $I_i(h)$ is the *i*th measurement of reflection h and $\langle I(h)\rangle$ is a weighted mean of all measurements of h.
[b]Values in parentheses apply to the high-resolution shell.
[c]$R = \Sigma_h |F_{obs}(h) - F_{calc}(h)| / \Sigma_h |F_{obs}|$. R_{work} and R_{free} were calculated from the working and test reflection sets, respectively. The test set constituted 5% of the total reflections not used in refinement.

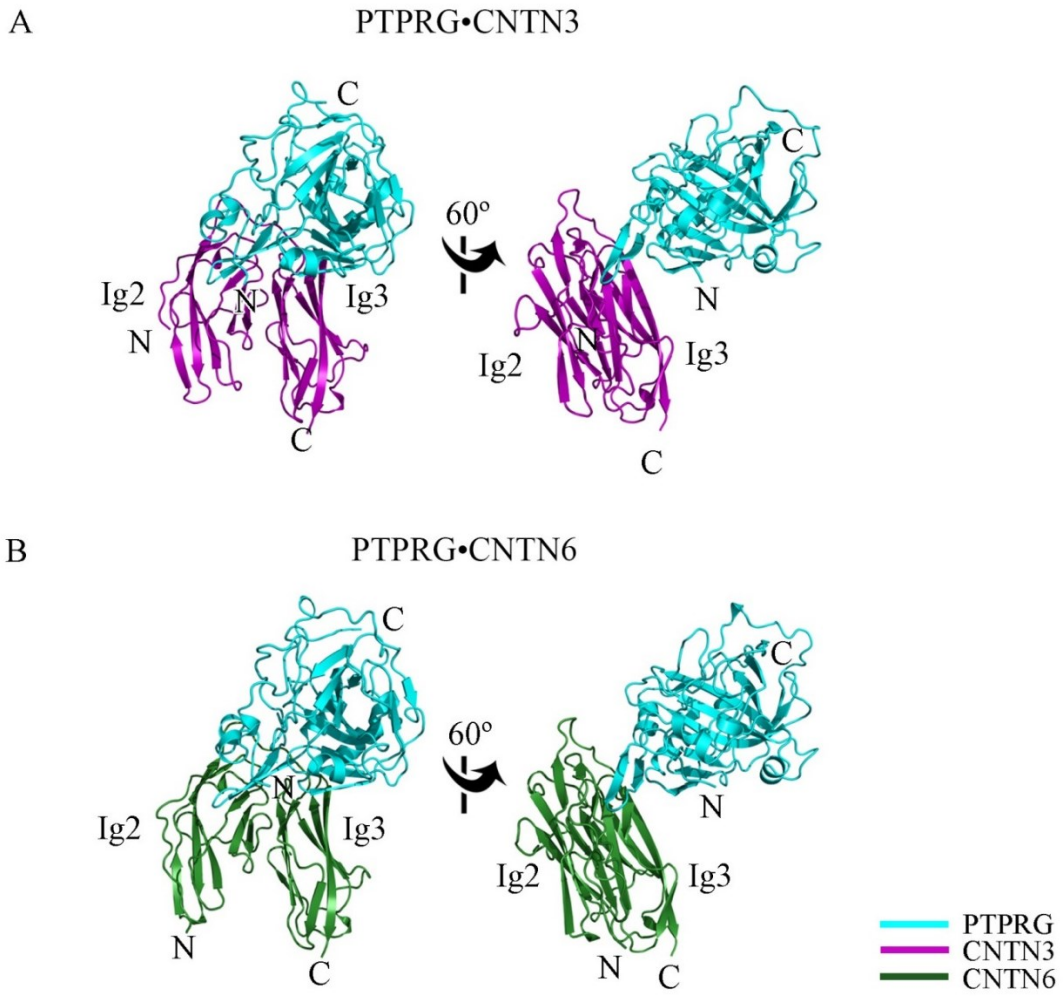

Figure 11. The crystal structures of the PTPRG•CNTN3 and PTPRG•CNTN6 complexes. The PTPRG•CNTN3 (A) and PTPRG•CNTN6 (B) complexes are shown in ribbon diagrams along with an overlay of all the complexes formed by PTPRG, PTPRZ and their CNTN-binding partners. PTPRG and PTPRZ are colored cyan and green, respectively. CNTN3 and CNTN6 are colored in orange and dark green, respectively. The letters N and C indicate the N- and C termini, respectively.

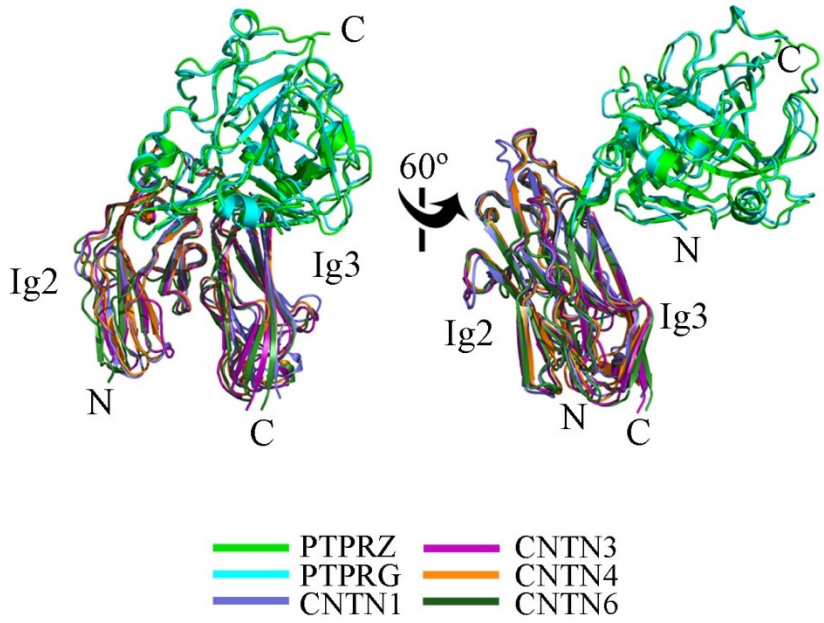

Figure 12. A conserved arrangement of complexes formed by PTPRG/Z and CNTNs. The complexes were superimposed by fitting domains Ig2-Ig3 of CNTN4 with the homologous repeats in CNTN1 (RMSD 1.27 Å over 186 equivalent Cαs), CNTN3 (RMSD 0.97 Å over 180 equivalent Cαs), and CNTN6 (RMSD 1.16 Å over 195 equivalent Cαs). PTPRG and PTPRZ are colored cyan and green, respectively. CNTN1, CNTN3, CNTN4, and CNTN6 are colored slate, magenta, orange and dark green, respectively. The letters N and C indicate the N- and C-termini, respectively.

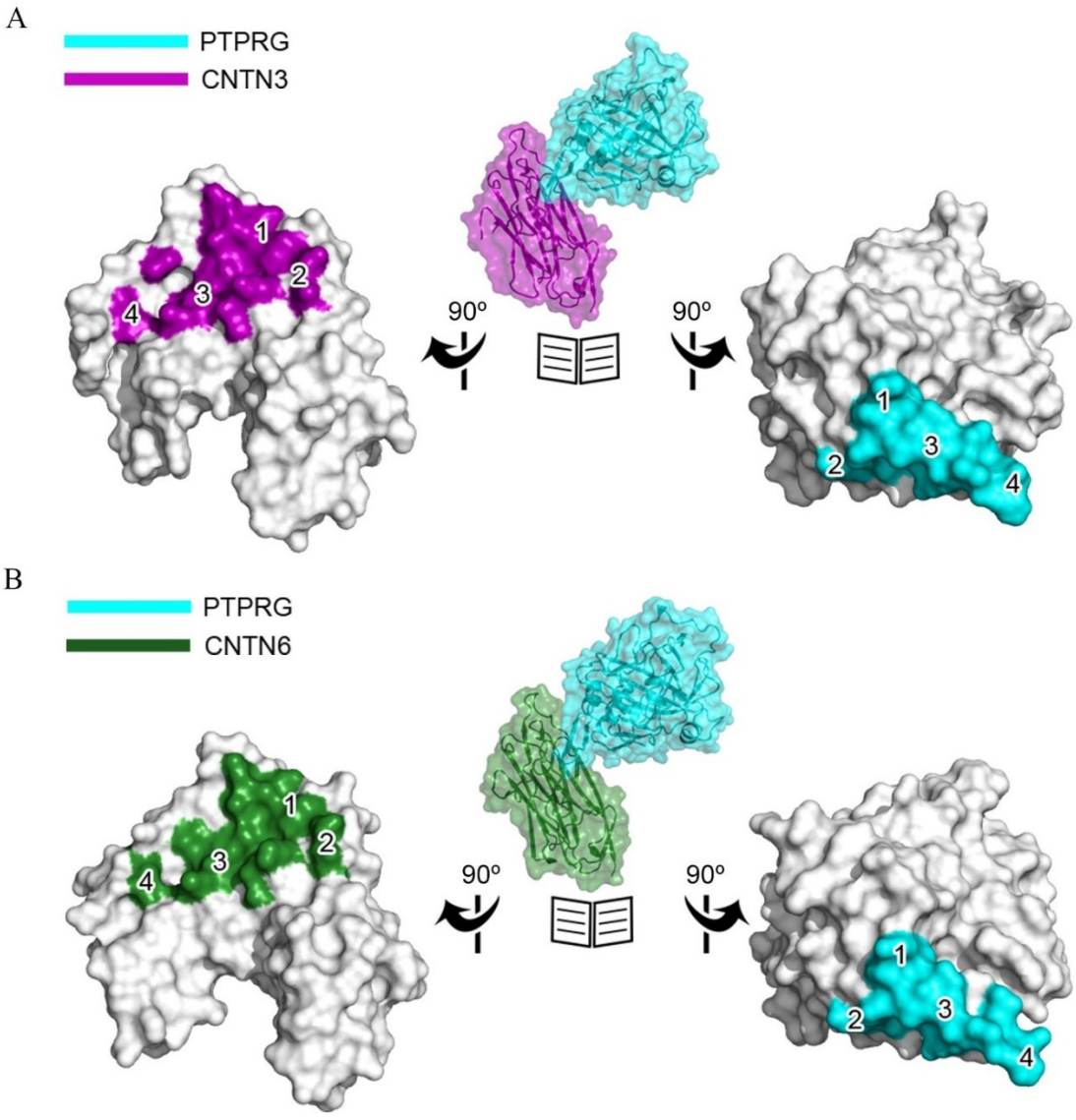

Figure 13. The molecular interfaces in PTPRG•CNTN3 and PTPRG•CNTN6 complexes include four sites of interactions. An "open book" surface representation of the binding interfaces for the PTPRG•CNTN3 (A) and PTPRG•CNTN6 (B) complexes.

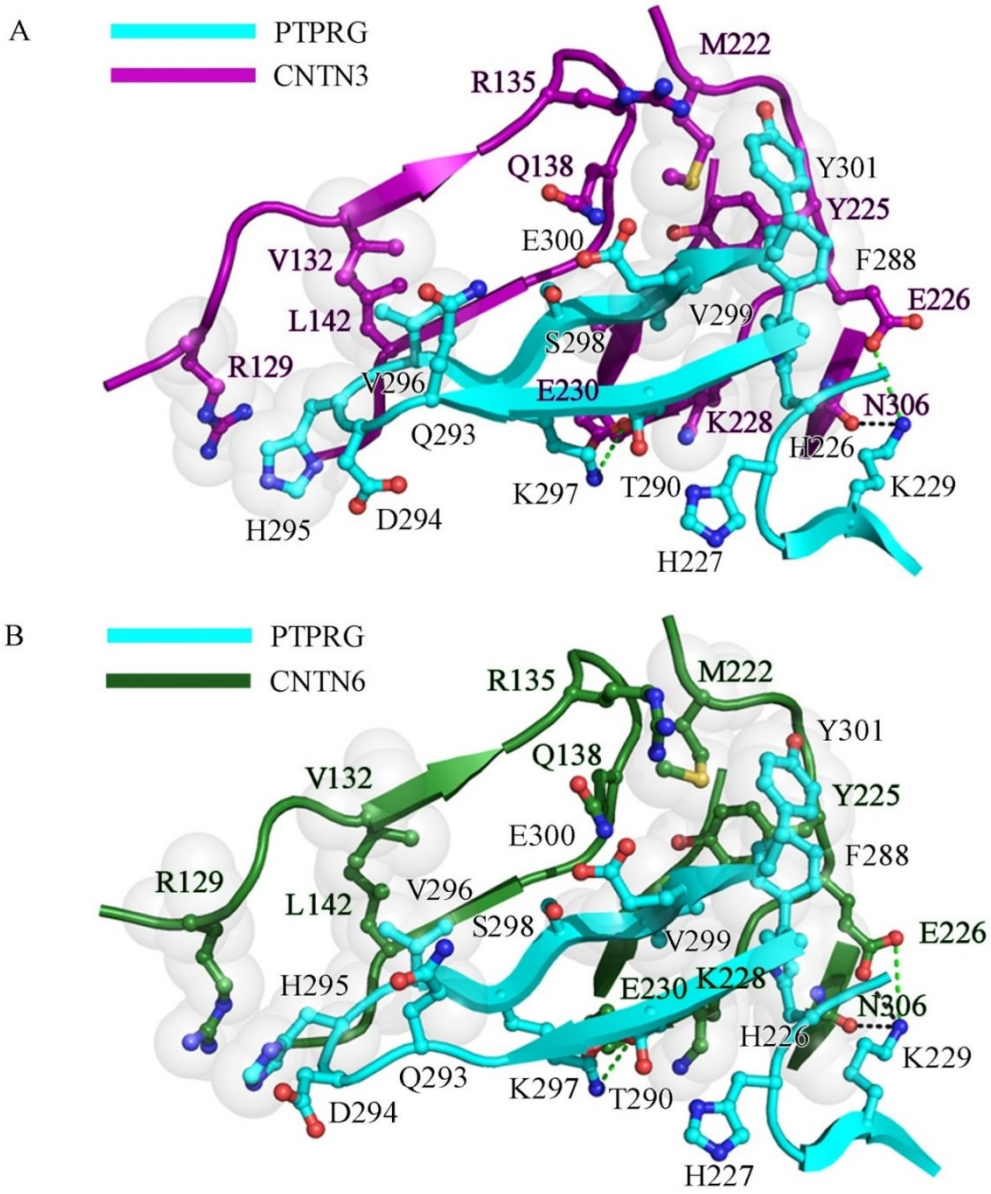

Figure 14. The molecular contacts at PTPRG•CNTN3 and PTPRG•CNTN6 interfaces. Detailed ribbon diagrams of the binding interfaces for PTPRG•CNTN3 (A) and PTPRG•CNTN6 (B) complexes. The contacting residues are shown in ball-and-sticks representation. These views are in the same orientations as the ones shown on the left in Figure 11. Transparent gray spheres highlight residues involved in van der Waals contacts. Dashed lines indicate potential hydrogen bonds (black) and salt bridges (green).

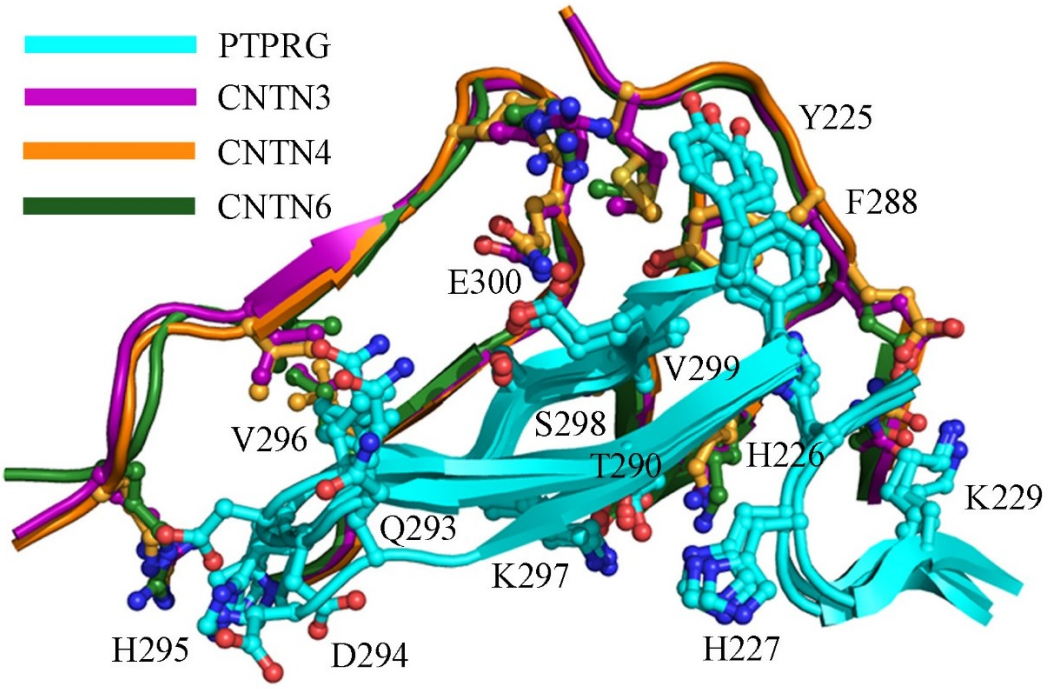

Figure 15. The PTPRG•CNTN interfaces include essentially identical interactions. PTPRG and CNTN3, 4, and 6 are colored cyan, magenta, orange and dark green, respectively. Interfaces are shown as ribbon diagrams with the contacting residues shown in ball-and-sticks representation.

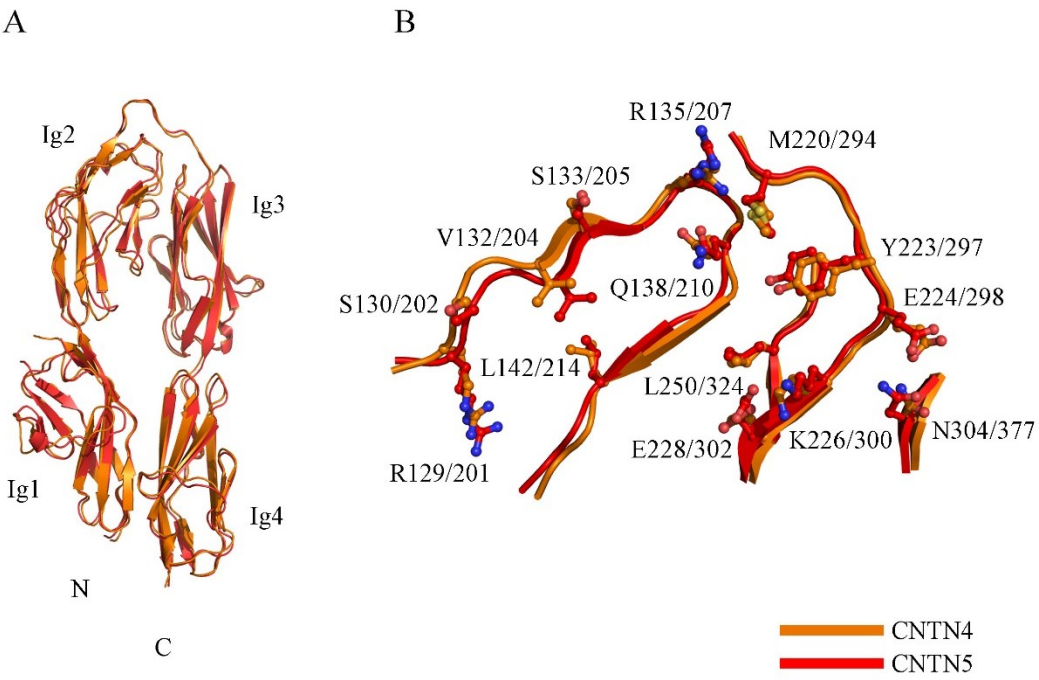

Figure 16. The structure of mouse CNTN5(Ig1-Ig4). (A) The ribbon diagram of mouse CNTN5(Ig1-Ig4) is shown in red overlaid on the crystal structure of mouse CNTN4(Ig1-Ig4). The letters N and C indicate the N- and C-termini, respectively. (B) Overlay of the PTPRG-binding region of mouse CNTN4 (orange) and mouse CNTN5 (red).

Validation of the PTPRG•CNTN interface

Most of the interactions in the PTPRG•CNTN complexes involve residues from the PTPRG β-hairpin loop. However, the conformational flexibility of its tip suggests that this particular region might not be responsible for essential interactions. In order to determine the contribution of the different PTPRG regions to interactions with CNTNs, we designed three mutant forms of the CA domain of mouse PTPRG: (1) a deletion mutant in which residues 290-299 of the β-hairpin loop replaced by the tripeptide ASA, (2) a double mutant form with H295A+V296A mutations at the tip of the β-hairpin, and (3) another double mutant form with the substitution of H226 and K229 in the short loop to alanine (H226A + K229A) (Fig. 17A). These mutant forms were used as inhibitors in a competitive binding assay based on Alpha Technology (Fig. 6). All proteins behaved comparably to wild-type PTPRG(CA) and in particular are monomeric as determined by size exclusion chromatography, which indicates that the mutations did not alter their structures. Because the work accomplished so far indicates that PTPRG and CNTNs share a conserved binding mode, note that the mutants were only tested in the context of the PTPRG•CNTN4 complex.

The β-hairpin deletion mutant, which eliminates sites 3 and 4, does not inhibit interactions between PTPRG and CNTN4, indicating that this region is essential for complex formation. However, the PTPRG double mutant with H295A and V296A mutations at the tip of the β-hairpin loop inhibits the complex formation with a ~ 4-fold increase in IC_{50} compared to the wild type PTPRG inhibitor (Fig. 17B, Table 2). The decrease in the inhibitor binding affinity to CNTN4 may be explained by the disruption

of the interactions between hydrophobic V296 of PTPRG and CNTN L142 and V132. The mutation of the H295 residue to alanine prevents its interaction with CNTN R129 and C144. However, the substitution of H295 and V296 to alanine is not expected to disrupt the formation of the five-strand antiparallel β-sheet in the complex that preserves the most of the mutant's inhibitory effect. Finally, mutation of H226 and K229 to alanine abrogates the CNTN4-binding activity suggesting that these residues in site 2 mediate essential interactions with CNTN4. Indeed, H226 mediates conserved non-polar interactions with Y225, P227 and K228, and a hydrogen bond with the main-chain oxygen atom of E298. In addition, the K229A mutation disrupts the K229-E226 salt bridge and the K229-N306 hydrogen bond. Thus, our interface validation confirms the essential role of the PTPRG β-hairpin loop in the PTPRG interactions with CNTN. Furthermore, it suggests the important contribution of the small loop of the CA domain of PTPRG in complex formation. Although the flexible tip of the PTPRG β-hairpin appears to be less critical for the interaction, it still contributes to the binding of PTPRG to CNTNs.

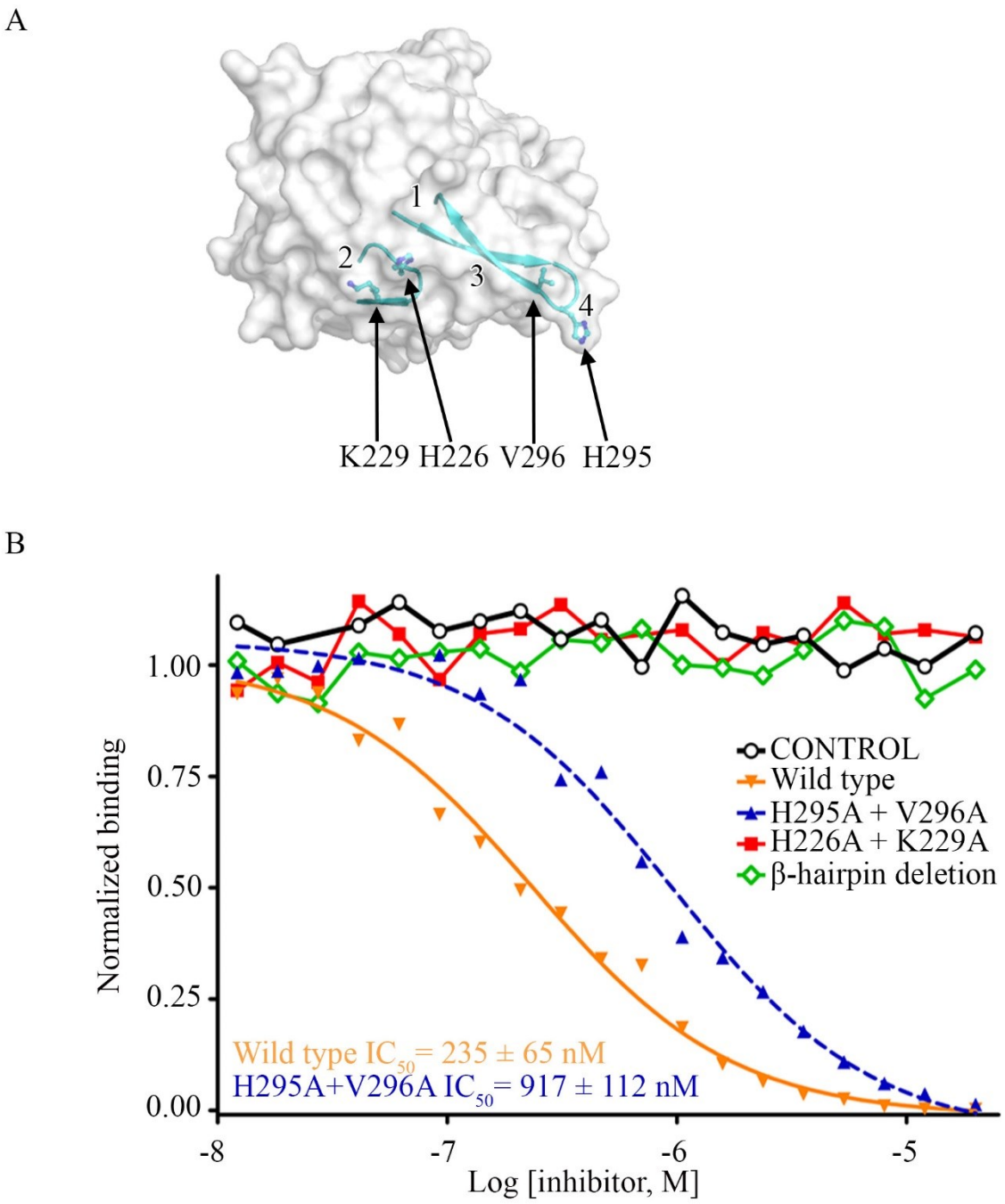

Figure 17. Mutational analysis of interactions between the CA domain of PTPRG with CNTN4. (A) The localization of the introduced mutations against the 4 binding sites on the surface of PTPRG(CA). (B) The ability of bovine CAII (control), mouse PTPRG(CA) or mouse PTPRG(CA) mutants to inhibit binding between an IgG Fc fusion of mouse CNTN4 and a biotin-labeled PTPRG(CA) as it was assessed over a logarithmic dilution series.

Identification of a PTPRG•CNTN complex in adult mouse retina

Although our data strongly suggest that PTPRG interacts specifically with CNTN3-6 *in vitro* and at the surfaces of cells (Fig. 8), the *in vivo* formation of these complexes has not been thoroughly investigated yet and is crucial for the validation of its physiological relevance. According to previous studies, both PTPRG and CNTN3-5 are expressed in specific layers of vertebrate retinas (Horvat-Bröcker et al., 2008; Yamagata and Sanes, 2012) although it unknown whether they form a complex in this tissue. The retina is an extension of the central nervous system (CNS) that combines anatomical and physiological features found in brain and spinal cord (London et al., 2013). It is also convenient for manipulation and imaging, and therefore is a good model for investigation of *in vivo* protein-protein interactions in nervous tissue. Therefore, we focused on the mouse retina to investigate the potential for formation PTPRG•CNTN complex formation and to further examine their physiological roles *in vivo*.

The retina includes three major neuronal layers (Fig. 18A). Light is first detected by photopigments in the outer segments of rod and cone photoreceptor cells spanning the outer segment (OS), inner segment (IS) and outer nuclear layer (ONL). Information is then transmitted to the bipolar cells found in the inner nuclear layer (INL) and then to ganglion cells in the ganglion cell layer (GCL) before being sent to the visual cortex by the optic nerve. The outer plexiform layer (OPL) and inner plexiform layer (IPL) include synapses between the photoreceptors and bipolar cells and between the bipolar cells and ganglion cells, respectively.

As a first step, we decided to characterize the distribution of PTPRG and CNTN3 in an adult mouse retina using immunohistochemistry approach with commercial antibodies that had been previously validated in our laboratory (Fig. 21). We detected a strong signal for PTPRG in the outer segments (OS), inner segments (IS), inner plexiform layer (IPL), and ganglion cell layer (GCL) that is consistent with previous findings (Horvat-Bröcker et al., 2008). In contrast to PTPRG, CNTN3 localizes only to the OS where it overlaps with PTPRG (Fig. 18B). Despite the co-localization of PTPRG and CNTN3 in the OS, it was unclear whether these two proteins form complexes in this layer. To address this question, we used an *in situ* proximity ligation assay (PLA) (Söderberg et al., 2008; Hayashi et al., 2013). This type of assay makes it possible to visualize *in vivo* interactions of endogenous PTPRG and CNTN3 with a signal produced only if these proteins are less than 40 nm apart. The data suggest that PTPRG and CNTN3 associate in the retinal OS, which is in line with the co-localization data in the same region of retina (Fig. 19). No signal could be observed in control experiments that lack the primary antibodies against PTPRG and CNTN3 **(**Fig. 18B). Moreover, a similar PLA signal was observed with a distinct PTPRG antibody raised against its CA domain (Fig. 22). The sum of these experiments strongly suggests that PTPRG and CNTN3 form a complex in the OS of the adult mouse retina.

Although our data have shown that PTPRG and CNTN3 interact on the surfaces of photoreceptors, it was still unclear whether these proteins could form a complex on the same photoreceptor (*cis*-interactions). Previous studies suggest that certain RPTPs are able to form functional *cis*-oriented complexes on the surface of the same cell. For

example, Dlar presynaptically binds the heparan sulfate proteoglycan (HSPG) Syndecan in *cis* to promote the formation of synaptic boutons at neuromuscular junctions in *Drosophila* (Johnson et al., 2006). In a similar fashion, PTPRS (vertebrate homolog of Dlar) interacts with HSPGs on the surface of the same neural cell to promote axon outgrowth (Coles et al., 2011).

To investigate the potential for *cis*-interactions between PTPRG and CNTN3, rod photoreceptor cells were isolated and dissociated for *in situ* PLAs. The PLA signal was observed in the OS of a single rod cell and is thus consistent with a same-cell interaction for PTPRG and CNTN3 in the OS (Fig. 20). Therefore, we can postulate that PTPRG and CNTN3 are capable of forming *cis* complexes in the OS of an adult mouse retina. Given the conserved mode of PTPRG•CNTN interactions and overall high sequence homology of CNTN members, it is likely that PTPRG and CNTN3-6 interact in *cis in vivo*.

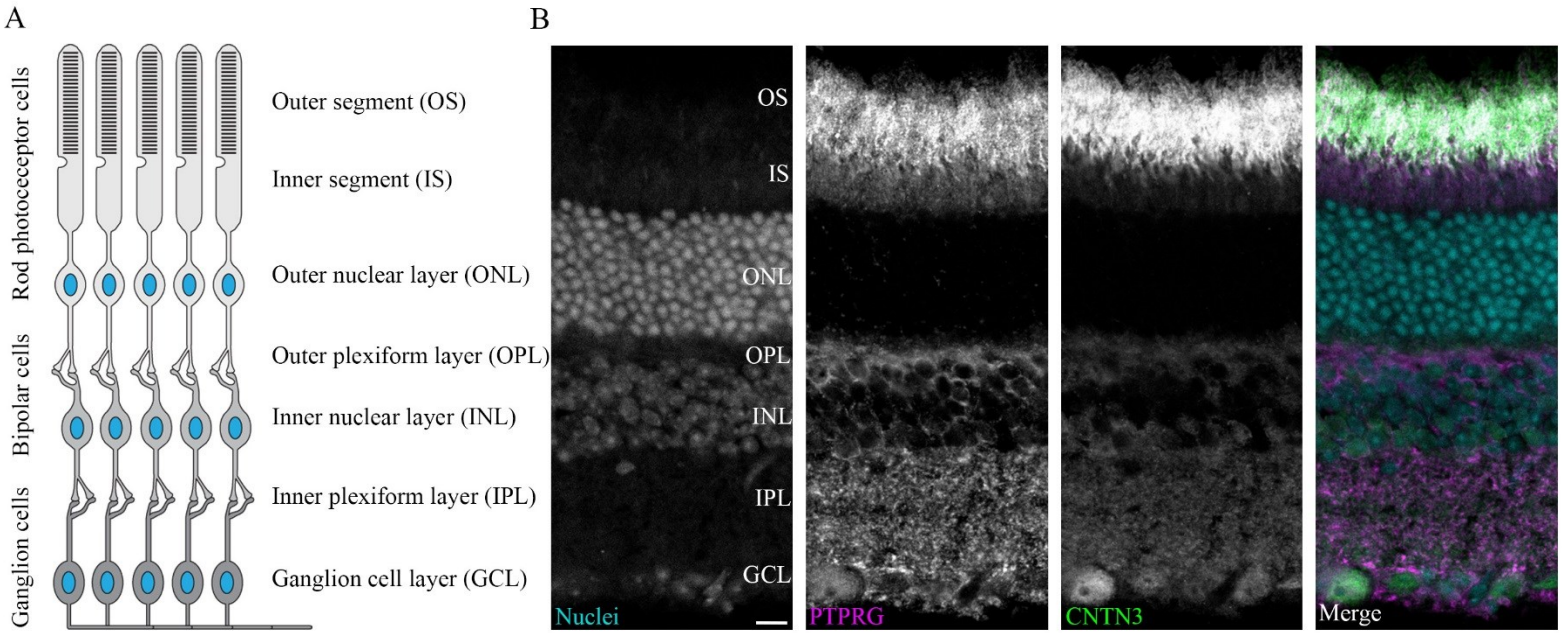

Figure 18. PTPRG and CNTN3 are localized to the outer segment of retina. (A) Schematic representation of the retinal architecture. Light information detected in an outer segment (OS) of a photoreceptor cell is eventually transmitted to cells in the ganglion cell layer (GCL) before being sent to the visual cortex by the optic nerve. (B) PTPRG and CNTN3 both localize to the outer segments of adult mouse retinas. A retinal section was stained with antibodies against PTPRG or CNTN3. RedDot™ 1 staining was used to visualize nuclei. The panel with DIC (differential interference contrast) shows a more detailed view of the retinal organization. Scale bar is 10 μm.

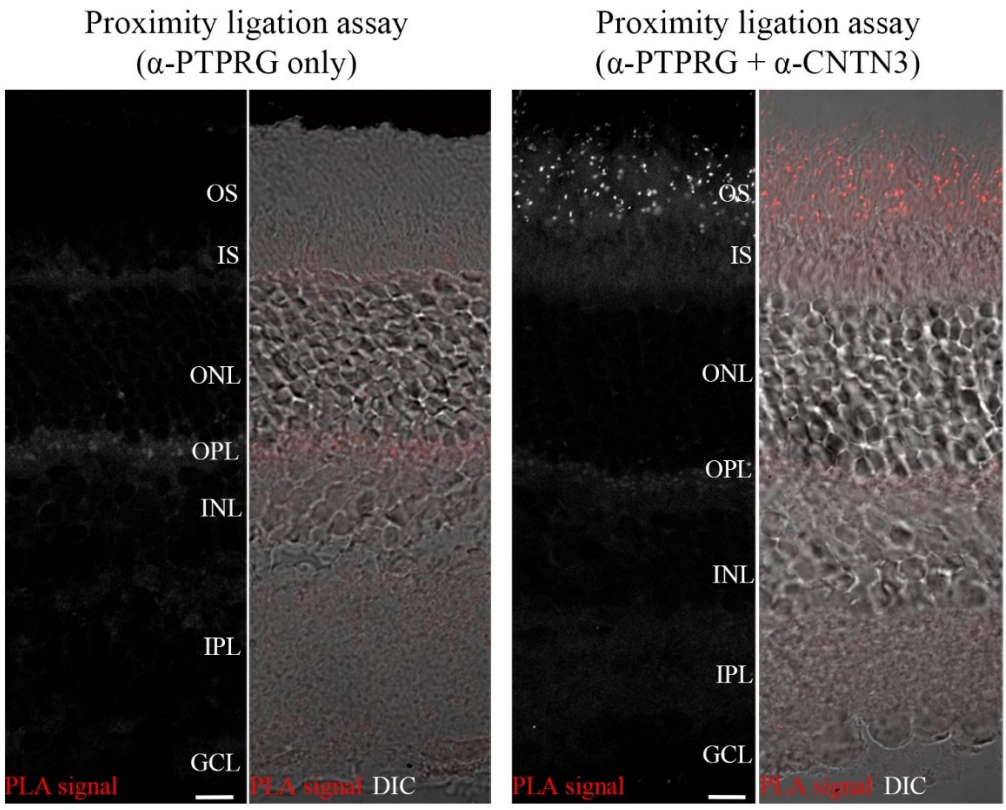

Figure 19. PTPRG and CNTN3 associate in the outer segments of photoreceptors. A proximity ligation assay (PLA) was performed to detect the presence of a PTPRG•CNTN3 complex. Omission of the primary antibodies against PTPRG or CNTN3 did not yield any detectable signal (control, left panels) whereas introducing these antibodies revealed the presence of punctate staining indicative of PTPRG and CNTN3 being in close proximity in the OS. Scale bar is 10 μm.

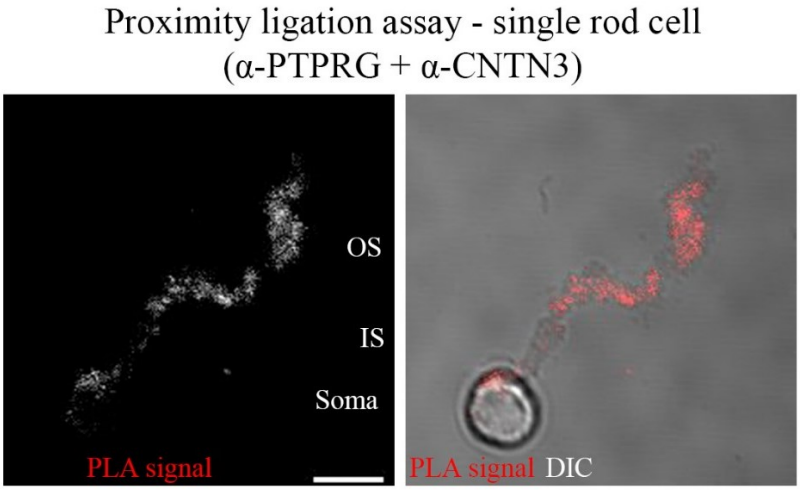

Figure 20. PTPRG and CNTN3 form a *cis* complex on the outer segment of a photoreceptor. An *in situ* PLA performed on a single photoreceptor cell shows the presence of PTPRG•CNTN3 complexes on the same cell. Scale bar is 5 μm.

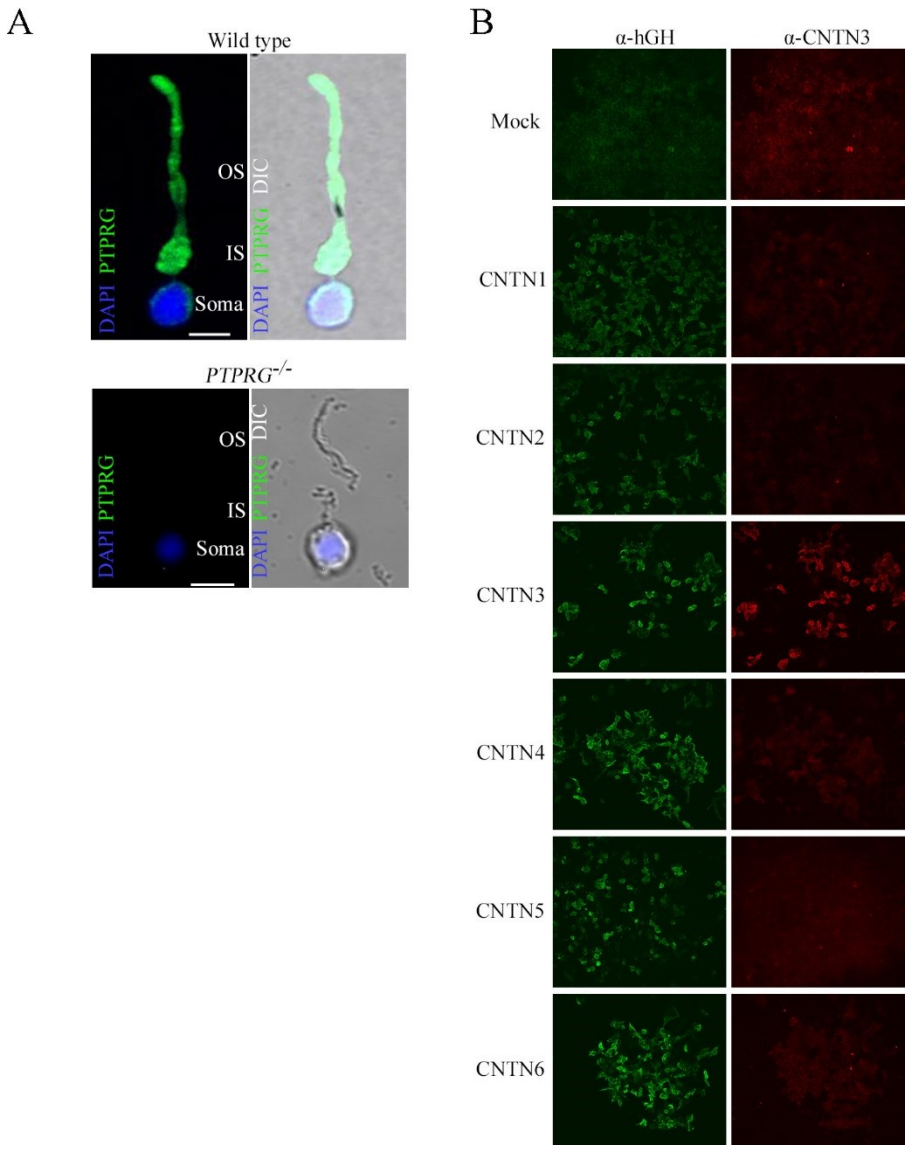

Figure 21. Identification of the PTPRG and CNTN3 complex in the outer segment: antibody validation. (A) The rabbit anti-PTPRG antibody used for the experiments shown in Figures 18-20 stains the outer segment of an isolated mouse rod cell from a wild-type mouse, but not the outer segment of a rod cell from a *PTPRG*-null mouse. Nuclei (blue) were visualized using RedDot™ 1 staining while PTPRG staining is shown in green. Scale bars are 5 μm. (B) Validation of anti-CNTN3 antibody (used in experiments shown in Fig. 18-20) reveals its specificity against CNTN3, but not against other CNTNs.

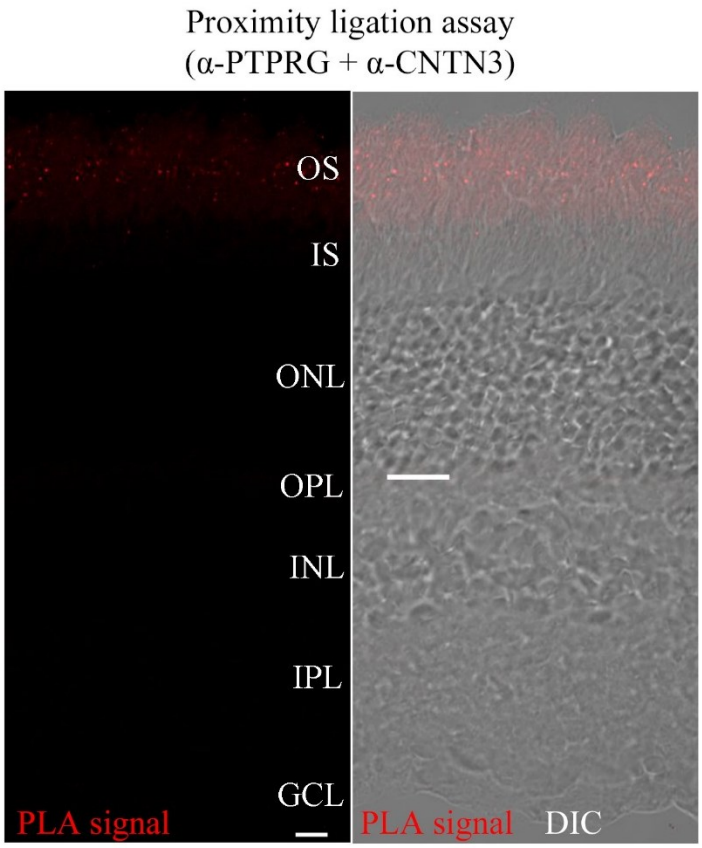

Figure 22. PTPRG•CNTN3 complex formation in the outer segment as reproduced with a different anti-PTPRG antibody. An *in situ* PLA shows that PTPRG and CNTN3 associate in the outer segments. This experiment includes the same goat anti-CNTN3 antibody used for the experiments shown in Figures 18-20, whereas PTPRG is detected with a rabbit polyclonal antibody raised against its CA domain. Scale bar is 10 μm.

PTPRG binds CNTN3 in *trans*

The discovery of *cis* PTPRG•CNTN3 complexes did not exclude the possibility that PTPRG and CNTN3 might interact in *trans*. We decided to investigate this issue by designing a cell aggregation assay in which HEK293F cells were transfected either with mEmerald-CNTN1, mEmerald-CNTN3, or mCherry-PTPRG. Cells were then mixed together and tested for the formation of aggregates. Cells expressing CNTN1, CNTN3 or PTRPG only were not able to form aggregates. However, when mixed together, PTPRG and CNTN3-expressing cells formed clusters composed of red and green colored cells, indicating the presence of the trans cell-adhesion interactions between PTPRG and CNTN3 (Fig. 23). The formation of aggregates did not occur in CNTN1 and PTPRG-expressing cells, consistent with the inability of PTPRG to bind CNTN1, as shown in our previous assays. Thus, our data suggest that *in vivo* interactions of PTPRG with CNTN3 occur in both *cis* and *trans* configurations, which also may be the case for CNTN4, 5 and 6.

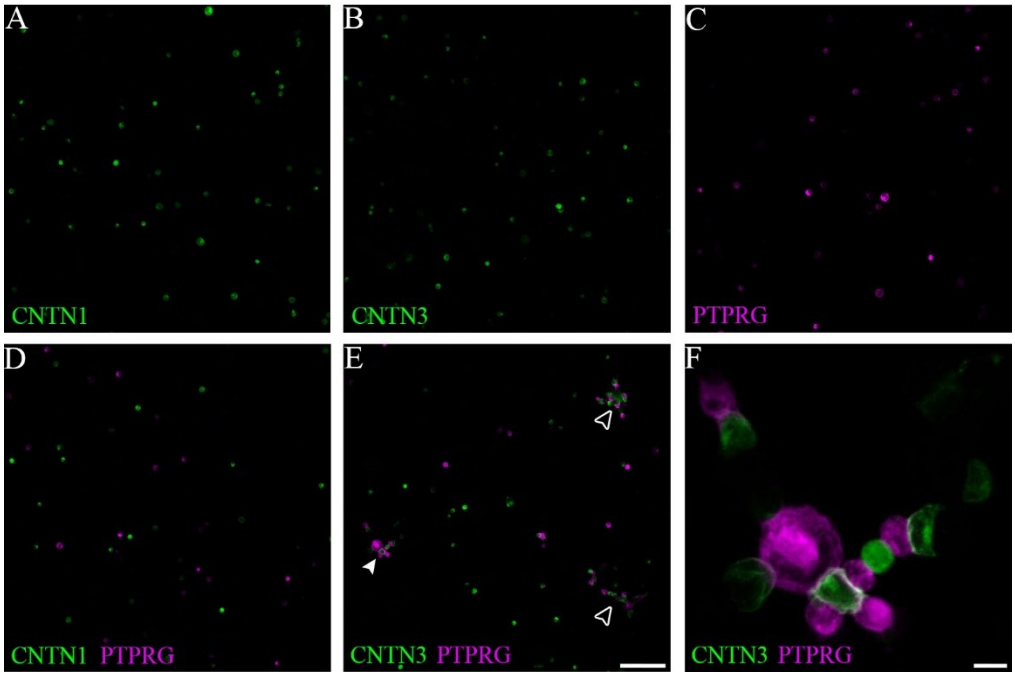

Figure 23. PTPRG and CNTN3 interact in *trans* on the cell surface. The ability of PTPRG and CNTN3 to interact in *trans* was assessed using a cell aggregation assay. (A-C) HEK293F cells grown in suspension were transfected with mEmerald-CNTN1, mEmerald-CNTN3 or mCherry-PTPRG. Cells expressing CNTN1, CNTN3 or PTPRG alone do not form aggregates. Likewise, cellular aggregates do not form when CNTN1 and PTPRG expressing cells are mixed, consistent with the inability of PTPRG and CNTN1 to interact with one another (D). (E) CNTN3 and PTPRG-expressing cells form aggregates (white arrowheads) after the two populations are mixed. Scale bar is 100 μm. (F) Close-up view of the PTPRG-CNTN3 cell aggregate designated by a filled arrowhead in panel E. Scale bar is 10 μm.

Conclusions

In this chapter we have combined cell biology, biochemical and structural approaches to characterize PTPRG•CNTN complexes. We have demonstrated the binding of PTPRG to the HEK293 cells transfected with CNTN3, 4, 5 and 6, but not to cells transfected with CNTN1 or 2, confirming the specific PTPRG•CNTN complex formation on cell surfaces. In the protein-protein binding assays, we have discovered that PTPRG binds to CNTN3-6 with similar affinities. According to our structural analyses, the close IC_{50} values are consistent with the conserved arrangement observed in complexes of PTPRG with CNTN3, 4, and 6. Validation of the binding interface confirmed that both the β-hairpin loop and a small loop region are critical for the interaction of PTPRG with CNTN. Finally, we present data that identify for the first time a complex between PTPRG and CNTN family member *in vivo*. Our PLA analysis suggests that the PTPRG•CNTN3 complex forms on the surface of the OS of a single photoreceptor, whereas our cell aggregation experiments suggest that PTPRG and CNTN3 can interact in trans. Taken together, our data suggest that PTPRG and CNTN3-6 might interact in both *cis* and *trans* configurations through a conserved binding interface.

CHAPTER 4
STRUCTURAL ANALYSES OF CNTN ECTODOMAINS REVEAL AN UNEXPECTED BENT CONFORMATION

Overview

In the previous chapter, we have shown that CNTN3, and presumably other CNTN members, are likely to associate with PTPRG (PTPRZ in the case of CNTN1) in both the *cis* and *trans* conformations. However, it is unclear how the conformations of the CNTN ectodomains would accommodate such distinct binding modes. PTPRG appears to include a ~ 300 amino acid stalk region in between its CA-FN moiety and TM region. This stalk does not include any recognizable structural motifs other than N- and O-linked glycosylation sites and therefore may be flexible enough to engage CNTNs in both *cis* and *trans* conformations (Barnea et al., 1993). Although the ectodomains of CNTNs do not include such a flexible region, they might still be able to bend easily because of the linkers between the Ig and FN domains. For example, structural analyses of the extracellular region of PTPRS indicate that it adopts several distinct conformations. This extent of this conformational mobility is such that PTPRS forms both *cis* and *trans* interactions with its cognate ligands during the formation of synapses (Coles et al., 2014). On the other hand, another model to explain how CNTN3-6 could bind PTPRG in both *cis* and *trans* conformations would be that the ectodomains lie parallel to the cell surface (Fig. 24). Such a conformation has already been described for the neural cell adhesion molecule NCAM2, which features a sharp bend between two membrane proximal domains so that the majority of the receptor lies parallel to the cell surface (Kulahin et al., 2011). Therefore, in this chapter, I present crystallographic data

that provide a rationale for the formation of PTPRG•CNTN complexes in both *cis* and *trans* orientations. These data are confirmed by solution scattering experiments performed on an FN1-FN3 region of CNTN3. Overall, our data indicate that CNTNs lie parallel to the cell membrane to associate with their ligands in both *cis* and *trans* conformations.

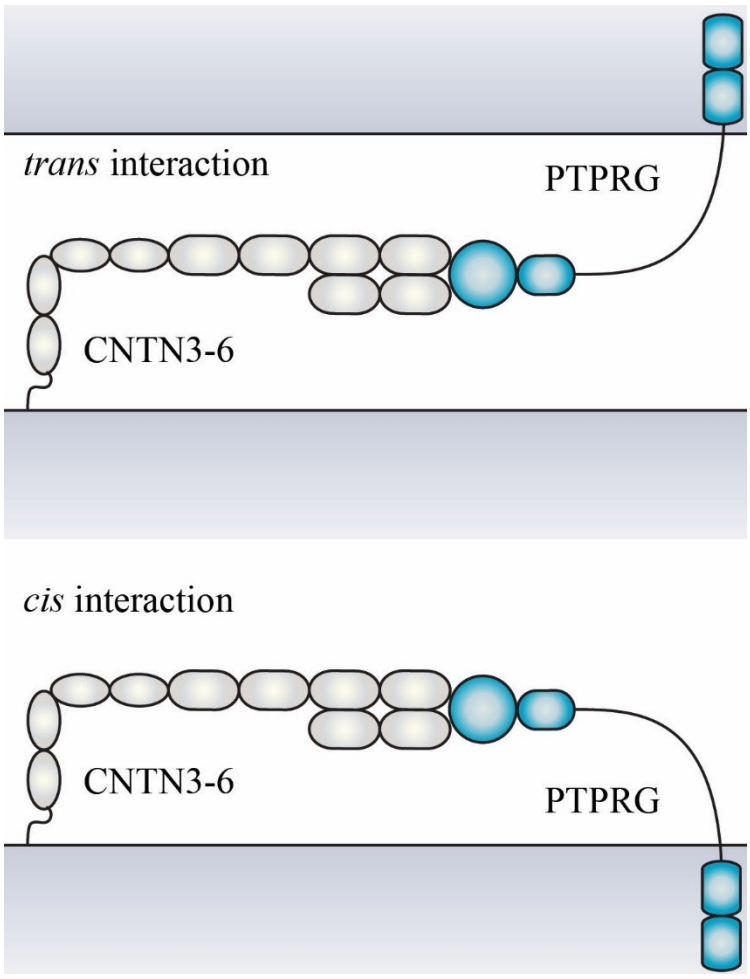

Figure 24. A possible model for the co-existence of *cis* and *trans* interactions between PTPRG and CNTN3-6. A hypothetical model showing how the conformations of PTPRG and CNTN3-6 could accommodate the formation of *cis* or *trans* complexes without altering the interactions between Ig2-Ig3 of CNTNs and the CA domain of PTPRG.

The Ig5-FN2 region of CNTN3 adopts an extended conformation

The results from chapter 3 suggested that CNTN3 forms complexes with PTPRG in both *cis* and *trans* conformations (Fig. 20, 23). Therefore, to gain insights into the geometry of a CNTN3 ectodomain, we undertook structural studies of the region excluding the first four Ig domains. Our unpublished data have shown that fragments of CNTNs that include the FN4 repeat are either unstable or readily form aggregates. Therefore, we limited our investigations to the Ig5-FN3 region of CNTN3. Although we were able to crystallize this protein, the crystals failed to diffract (Fig. 25). We thus further truncated our protein to only the Ig5-FN2 domains of CNTN3 and were able to determine the crystal structure of this region, which adopts an extended conformation (Fig. 26).

The detailed analysis of the molecular contacts between consecutive Ig and FN domains did not reveal a significant interface, suggesting a certain degree of flexibility in this region. For example, the interface between Ig5 and Ig6 domain includes a salt bridge between K471 and D526. D526 is conserved in other CNTNs while K471 is either a lysine or an arginine (the residue conservation was assessed throughout human, mouse and chicken CNTN1-6). Thus, this salt bridge is likely to occur all CNTNs. This interaction is complemented with non-polar interactions between Q420, Q422 in Ig5 and L529, P499, respectively, in Ig6. These residues are not conserved in all CNTNs, which might indicate the transient nature of these interactions. Two contacts occur at the Ig6-FN1 interface. A hydrogen bond is formed between the conserved R595 residue and the carbonyl oxygen of H625. Another contact includes a hydrophobic residue V513 (V, L or I in other CNTNs) that forms a non-polar interaction with the conserved G596. In

contrast to the Ig5-Ig6 and Ig6-FN1 interfaces, the FN1-FN2 interface is more substantial. It includes the non-polar contacts of conserved P667 and W668 residues on FN1 with N731 (conserved in CNTN2-6; replaced by Y in CNTN1) and the conserved G732 on FN2. The conservation of the molecular contacts between the interfaces implies that the Ig5-FN2 fragments of all CNTNs might adopt an extended conformation similar to that observed in the CNTN3(Ig5-FN2) region. It is, however, difficult to predict the conformation of this region in solution. Our attempts to obtain solution scattering data for the Ig5-FN2 region of CNTN3 were ultimately unsuccessful because of protein aggregation. The short interdomain linkers indicate that the extended conformation for CNTN3(Ig5-FN2) might persist in solution. However, further experiments need to be done to characterize the rigidity of this region.

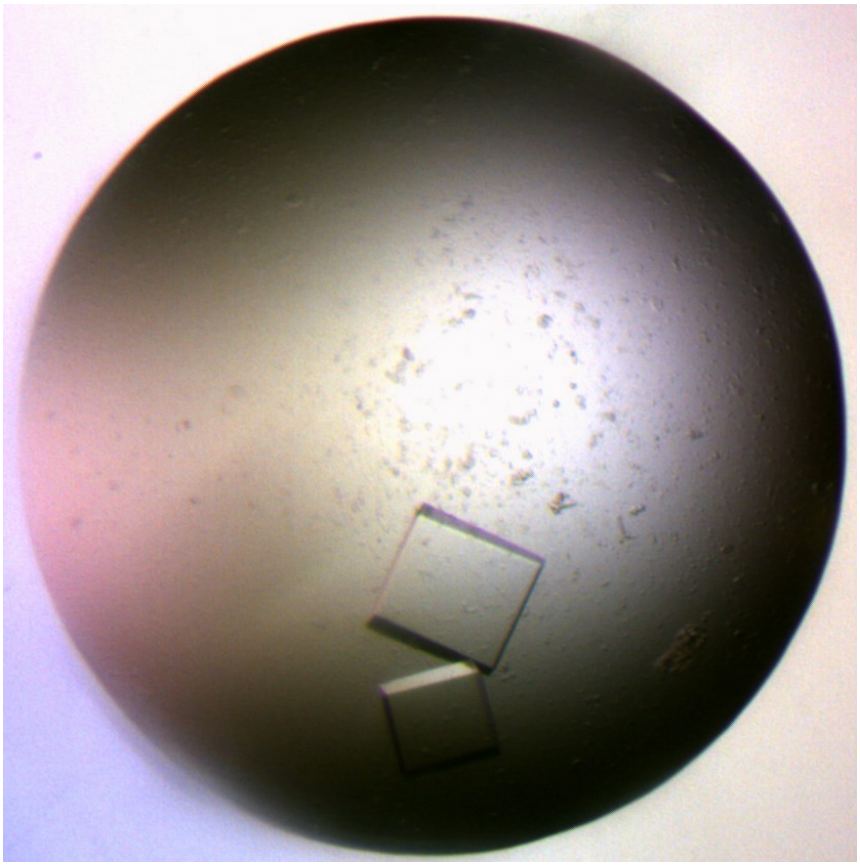

Figure 25. Crystals of mouse CNTN3(Ig5-FN3). Protein crystals were obtained in 2.9 M NaCl, 0.1 Bis-Tris-HCl pH 5.5 but failed to diffract.

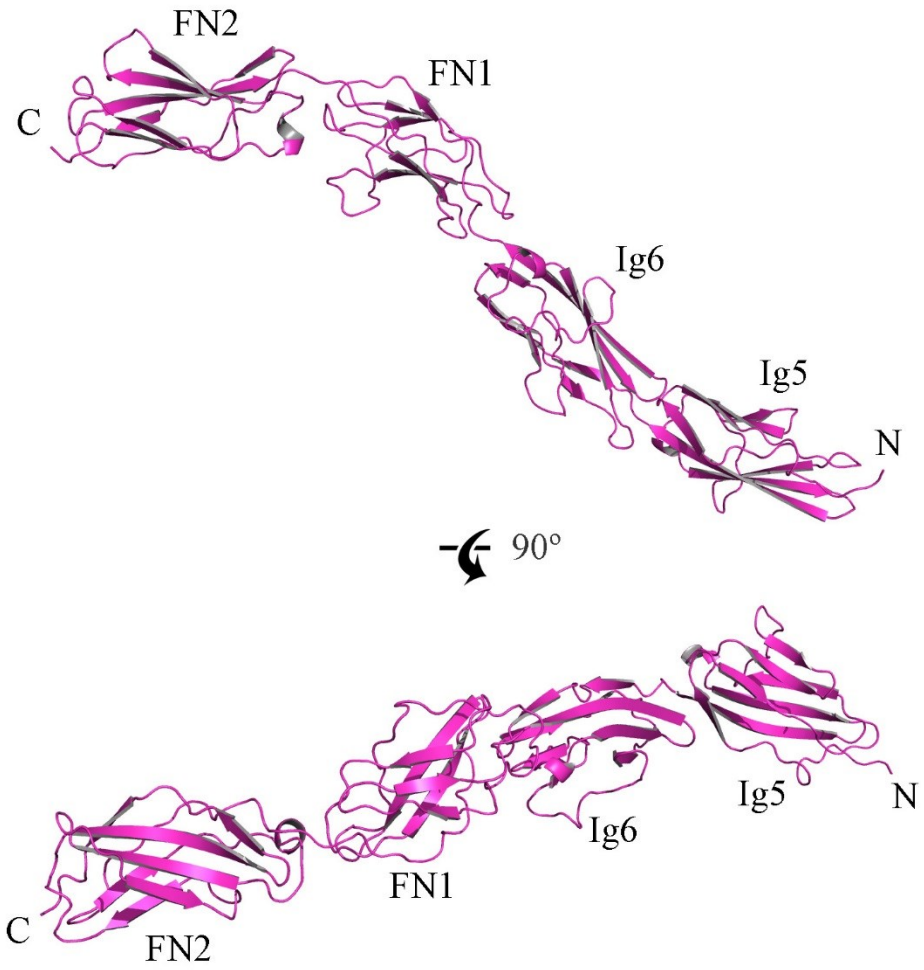

Figure 26. The extended conformation of Ig5-FN2 domains of mouse CNTN3. Two Ig domains (Ig5 and Ig6) and two FN domains (FN1 and FN2) adopt a linear conformation in crystals of mouse CNTN3(Ig5-FN2).

The FN1-FN3 domains of CNTNs adopt a conserved bent conformation

The extended conformation found for the Ig5-FN2 region of CNTN3 was not sufficient to explain the co-existence of *cis* and *trans* interactions of the CNTN3 ectodomain with PTPRG. Therefore, we determined the crystal structure of the FN1-FN3 region for CNTN3. Strikingly, this region adopts an L-shaped conformation with a sharp bend between its FN2 and FN3 domains (Fig. 27). This bent arrangement is not an artifact of crystallization because it is observed in the crystal structures of the FN1-FN3 fragments of CNTN1, 2, 4, 5, and 6. These proteins obtained from different species (mouse, human and chicken) were crystallized in distinct crystal lattices and all feature a sharp bend between domains FN2 and FN3. The superposition performed on FN1-FN2 domains of FN1-FN3 crystal structures for CNTN1-6 reveals a similar conformation in CNTN1-4 and some domain flexibility in the case of CNTN5 and CNTN6 (Fig. 28). These fluctuations likely result from the interactions with a symmetry related protein chain for the CNTN5 structure, or with another protomer in the same asymmetric unit for the CNTN6 structure. The sequence analysis of the FN2-FN3 linker indicates that it is fully conserved in CNTN2-4, but reveals some sequence variations in CNTN1, 5 and 6 (Fig. 29B).

The analysis of the interface between the FN2 and FN3 domains reveals a similar, yet variable mode of interactions for CNTN1-6. Here, one or two negatively charged amino acid residues from the linker region on the FN2 side forms hydrogen bonds with a conserved NXA (X = S, T, G, R) region on the FN3 domain (Fig. 29). Other regions that contact the FN2-FN3 linker include a glycine-rich stretch on the FN2 domain and a positively charged amino-acid residue on the FN3 domain, but these interactions vary

among the six CNTNs (Fig. 30). Although not being fully conserved, the linker arrangements and FN2-FN3 molecular contacts form similar L-shaped conformations for all CNTN members (Fig. 27). The analysis of the FN1-FN2 interface in the FN1-FN3 crystal structures of CNTNs recapitulates our findings from the CNTN3(Ig5-FN2) crystal structure. The non-polar FN1-FN2 interface contacts discovered in CNTN3 are conserved in CNTN1, 2, 4, 5 and 6. Given the conservation of the FN1-FN2 interface throughout CNTN1-6 in FN1-FN3 structures, we suggest that this region is relatively rigid and does not significantly contribute to the flexibility of CNTN ectodomains.

.

TABLE 4

DATA COLLECTION AND REFINEMENT STATISTICS FOR FN1-FN3 DOMAINS OF CNTN1-6 AND IG5-FN2 DOMAINS OF CNTN3

	CNTN1 (FN1-FN3)	**CNTN2 (FN1-FN3)**	**CNTN3 (FN1-FN3)**	**CNTN4 (FN1-FN3)**	**CNTN5 (FN1-FN3)**	**CNTN6 (FN1-FN3)**	**CNTN3 (Ig5-FN2)**
Data Collection							
Beamline	APS 22-ID	APS 22-ID	APS 22-ID	APS 22-BM	APS 22-ID	APS 22-ID	APS 22-BM
Wavelength (Å)	1	1	1	0.97933	1	1	1
Unique reflections	48,701	28,357	8,976	13,387	14,285	21,656	20,578
Resolution (Å)	50 - 2.5	30 - 2.0	50 - 2.8	50 - 2.5	50-2.7	50 - 2.7	50 - 2.4
Space group	$P2_1$	$P2_12_12$	C2	$C222_1$	$C222_1$	$P2_12_12_1$	$P2_12_12_1$
Unit cell							
	87.48	124.39	185.10	94.79	83.77	86.74	58.22
a, b, c (Å)	49.87	40.67	39.03	144.3	154.52	90.85	76.93
	163.3	82.6	52.4	55.4	90.42	99.35	115.82
	90.0	90.0	90.0	90.0	90.0	90.0	90.0
α, β, γ (º)	97.12	90.0	96.9	90.0	90.0	90.0	90.0
	90.0	90.0	90.0	90.0	90.0	90.0	90.0

"TABLE 4 -- Continued."

DATA COLLECTION AND REFINEMENT STATISTICS FOR FN1-FN3 DOMAINS OF CNTN1-6 AND IG5-FN2 DOMAINS OF CNTN3

	CNTN1 (FN1-FN3)	**CNTN2 (FN1-FN3)**	**CNTN3 (FN1-FN3)**	**CNTN4 (FN1-FN3)**	**CNTN5 (FN1-FN3)**	**CNTN6 (FN1-FN3)**	**CNTN3 (Ig5-FN2)**
R_{sym}[a]	0.075 (0.380)	0.110 (0.508)	0.139 (0.377)	0.08 (0.460)	0.112 (0.418)	0.155 (0.515)	0.165 (0.548)
Completeness[b] (%)	99.2 (92.3)	97.8 (89.3)	97.7 (90.0)	98.3 (87.4)	85.7 (56.3)	97.9 (92.5)	98.2 (87.5)
Redundancy	6.9 (4.7)	5.9 (3.2)	8.9 (5.8)	6.1 (4.2)	12 (5.9)	7.4 (4.8)	11.9 (7.9)
I/σI	20.4 (3.3)	12.5 (1.6)	15.0 (4)	20.7 (2.3)	17.35 (3.6)	8.4 (2.1)	14.8 (2.4)
Refinement							
Molecules in asymmetric unit	4	1	1	1	1	2	1
Resolution (Å)	43.51 - 2.5	29.1 - 2.0	47.8 - 2.8	28.7 - 2.5	38.6 - 2.7	43.4 - 2.7	43.1 – 2.4
R_{work}[c] / R_{free}	0.204/0.247	0.190/0.226	0.183/0.244	0.19/0.255	0.194/0.231	0.200/0.241	0.203/0.253
Number of atoms	9,572	2,491	2,135	2,394	2,282	4,715	3,190
Protein	9,267	2,301	2,110	2,325	2,258	4,672	3,032
Ligand	75	-	-	-	5	-	6
Water	230	190	25	69	19	43	152

"TABLE 4 -- Continued."

DATA COLLECTION AND REFINEMENT STATISTICS FOR FN1-FN3 DOMAINS OF CNTN1-6 AND IG5-FN2 DOMAINS OF CNTN3

	CNTN1 (FN1-FN3)	**CNTN2 (FN1-FN3)**	**CNTN3 (FN1-FN3)**	**CNTN4 (FN1-FN3)**	**CNTN5 (FN1-FN3)**	**CNTN6 (FN1-FN3)**	**CNTN3 (Ig5-FN2)**
R.m.s. deviations							
Ideal bonds (Å)	0.004	0.007	0.01	0.009	0.009	0.004	0.009
Ideal angles (°)	0.84	1.06	1.21	1.12	1.13	0.92	1.28
Average B factors (Å^2)	63.7	39.2	57	61.6	93.7	42.8	41.2
Protein	63.9	39.1	57.2	61.8	93.8	42.9	41.3
Ligand	85.5	-	-	-	121.1	-	62.9
Water	50.2	40.5	38.9	53.5	69.7	34.9	36.9
Ramachandran statistics							
Favored (%)	96	98	95	97	94	97	96
Allowed (%)	4	2	5	3	6	3	4
PDB accesion code	5E53	5E7L	5E4Q	5E4S	5E52	5E55	5I99

[a]$R_{sym} = \Sigma h\, \Sigma_i |I_i(h) - \langle I(h)\rangle| / \Sigma_h\, \Sigma_i\, I_i(h)$, where $I_i(h)$ is the *i*th measurement of reflection h and $\langle I(h)\rangle$ is a weighted mean of all measurements of h. [b]Values in parentheses apply to the high-resolution shell.[c]$R = \Sigma_h |F_{obs}(h) - F_{calc}(h)| / \Sigma_h |F_{obs}|$. R_{work} and R_{free} were calculated from the working and test reflection sets, respectively. The test set constituted 5% of the total reflections not used in refinement.

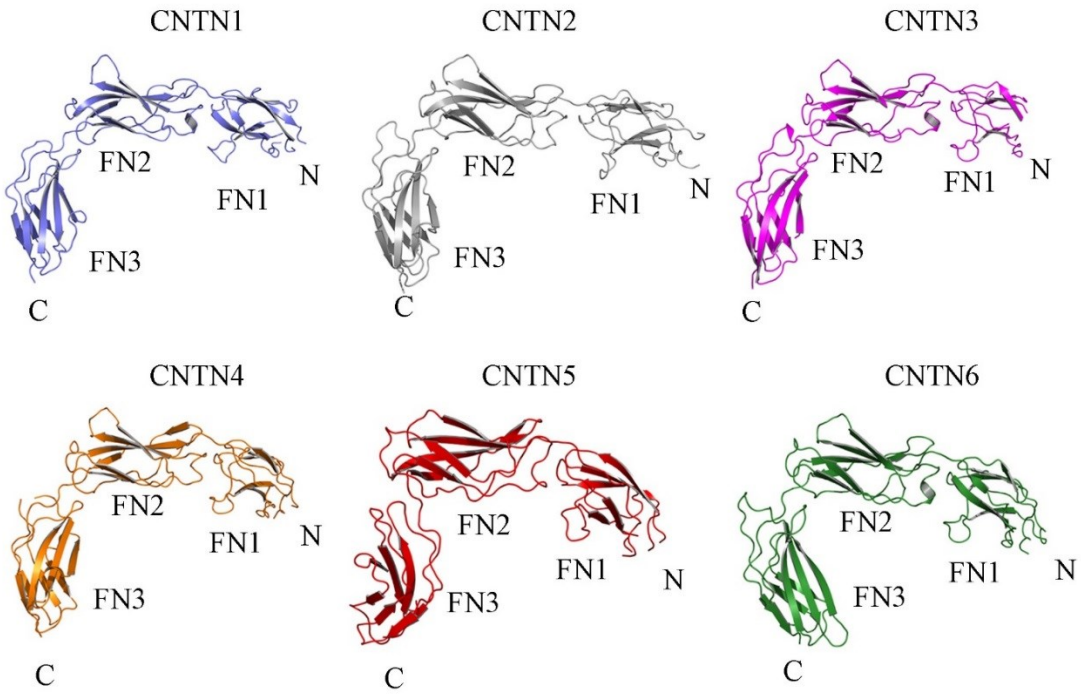

Figure 27. The FN1-FN3 regions of CNTN family members adopt similar bent conformations. Ribbon diagrams of CNTN1-6(FN1-FN3) crystal structures. Residues from CNTN1 are colored in slate, from CNTN2 are colored in gray, from CNTN3 are colored in magenta, from CNTN4 are colored in orange, from CNTN5 are colored in red and from CNTN6 are colored in dark green.

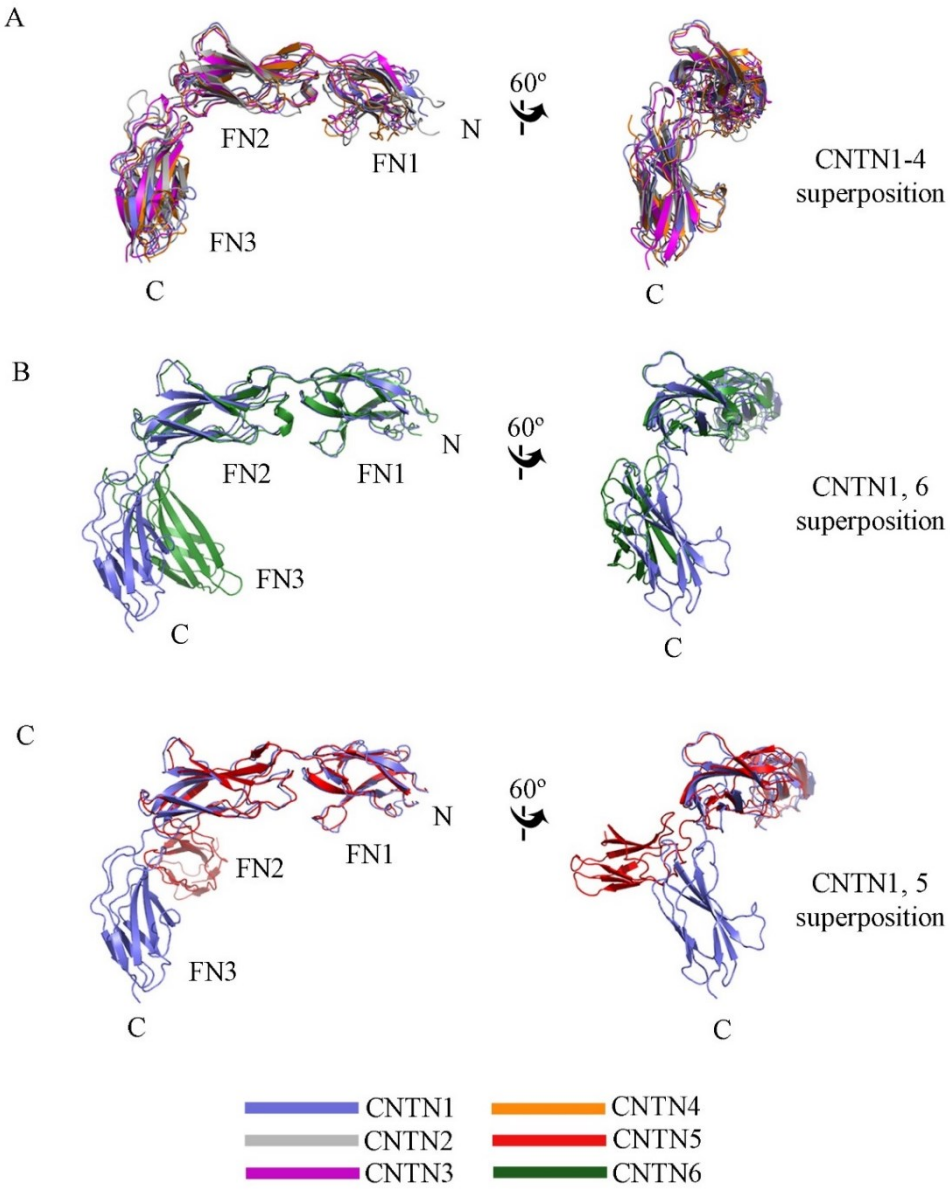

Figure 28. Flexibility in the FN3 domain orientation in CNTN1-6
The FN1-FN2 domains of mouse CNTN2, 3, 4 (A), human CNTN5 (B) and mouse CNTN6 (C) were overlaid on the corresponding region of CNTN1.
Superposition details:
CNTN1(FN1-FN2)/CNTN2(FN1-FN2) – RMSD: 2.36Å over 188 positions;
CNTN1(FN1-FN2)/CNTN3(FN1-FN2) – RMSD: 1.15Å over 175 positions;
CNTN1(FN1-FN2)/CNTN4(FN1-FN2) – RMSD: 2.62Å over 190 positions;
CNTN1(FN1-FN2)/CNTN5(FN1-FN2) – RMSD: 1.91Å over 189 positions;
CNTN1(FN1-FN2)/CNTN6(FN1-FN2) – RMSD: 2.00Å over 190 positions.

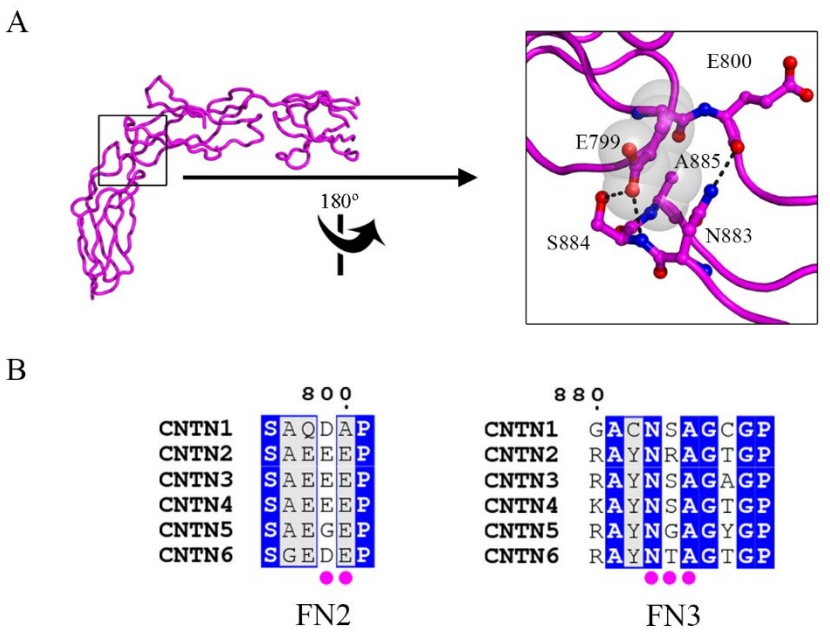

Figure 29. Sequence conservation at the FN2-FN3 interface of CNTNs. (A) Conserved amino acid contacts at the FN2-FN3 interface. The structure of CNTN3(FN1-FN3) is shown as a tube along with a detailed view of the conserved non-covalent interactions at the FN2-FN3 interface. Residues at the interface are shown as ball-and-sticks. Transparent gray spheres and black-dotted lines denote residues involved in van der Waals contacts and potential hydrogen bonds, respectively. A more detailed view of the FN2-FN3 interface for each CNTN is shown in Figure 30.
(B) An alignment of mouse CNTN sequences indicates that the contact amino acids at the FN2-FN3 interface shown in panel A are conserved in CNTN family members. Identical amino acids are shaded in blue while similar residues are colored light gray. The numbering corresponds to the mouse CNTN3 sequence. Magenta dots below the alignments denote residues at the FN2-FN3 interface.

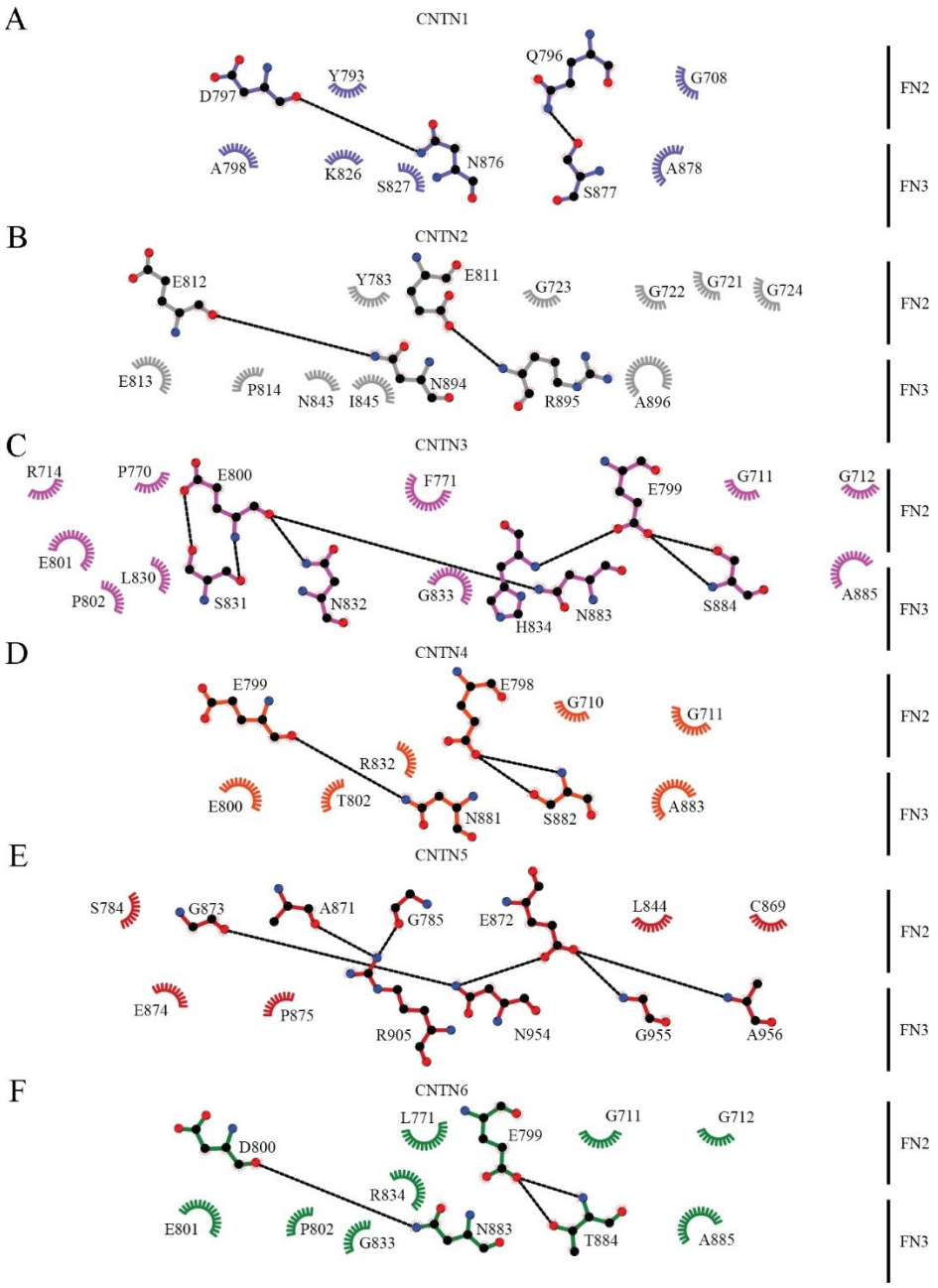

Figure 30. Conserved and specific interactions at the FN2-FN3 interfaces of CNTNs. Two-dimensional representations of the contacts at the FN2-FN3 interfaces of CNTNs were drawn using LigPlot^{+} (Laskowski and Swindells, 2011). Dashed lines indicate potential hydrogen bonds while spine curves indicate residues involved in hydrophobic contacts. Although interactions mediated by the NXA residues found in a loop in FN3 are conserved in all CNTNs, most contacts at the FN2-FN3 interface are unique to each CNTN family member.

The bent conformation is conserved in solution

The results from the previous section indicate that all CNTN FN1-FN3 regions adopt a conserved bent arrangement in crystals. Therefore, we surmised that this conformation would persist in solution. To test this hypothesis, we analyzed the solution conformation of FN1-FN3 of CNTN3 by small angle X-ray scattering. We limited our analysis to CNTN3 because our *in vivo* findings indicate that it forms a *cis*-complex with PTPRG. Data sets were acquired at both different concentrations and exposure times and were merged to obtain an experimental scattering profile for CNTN3(FN1-FN3) (Fig. 31A), which matches closely to the theoretical scattering profile calculated using the crystal structure of CNTN3(FN1-FN3) ($\chi^2 = 1.77$). Furthermore, the crystal structure of CNTN3(FN1-FN3) corresponds a molecular envelope calculated using the experimental scattering profile (Fig. 31B). Overall, this analysis demonstrates that the L-shaped conformation adopted by this fragment of CNTN3 mirrors its conformation in solution. Taken together, these findings indicate that the FN regions of CNTNs all adopt a bent conformation reminiscent of the one adopted by NCAM2 (Kulahin et al., 2011).

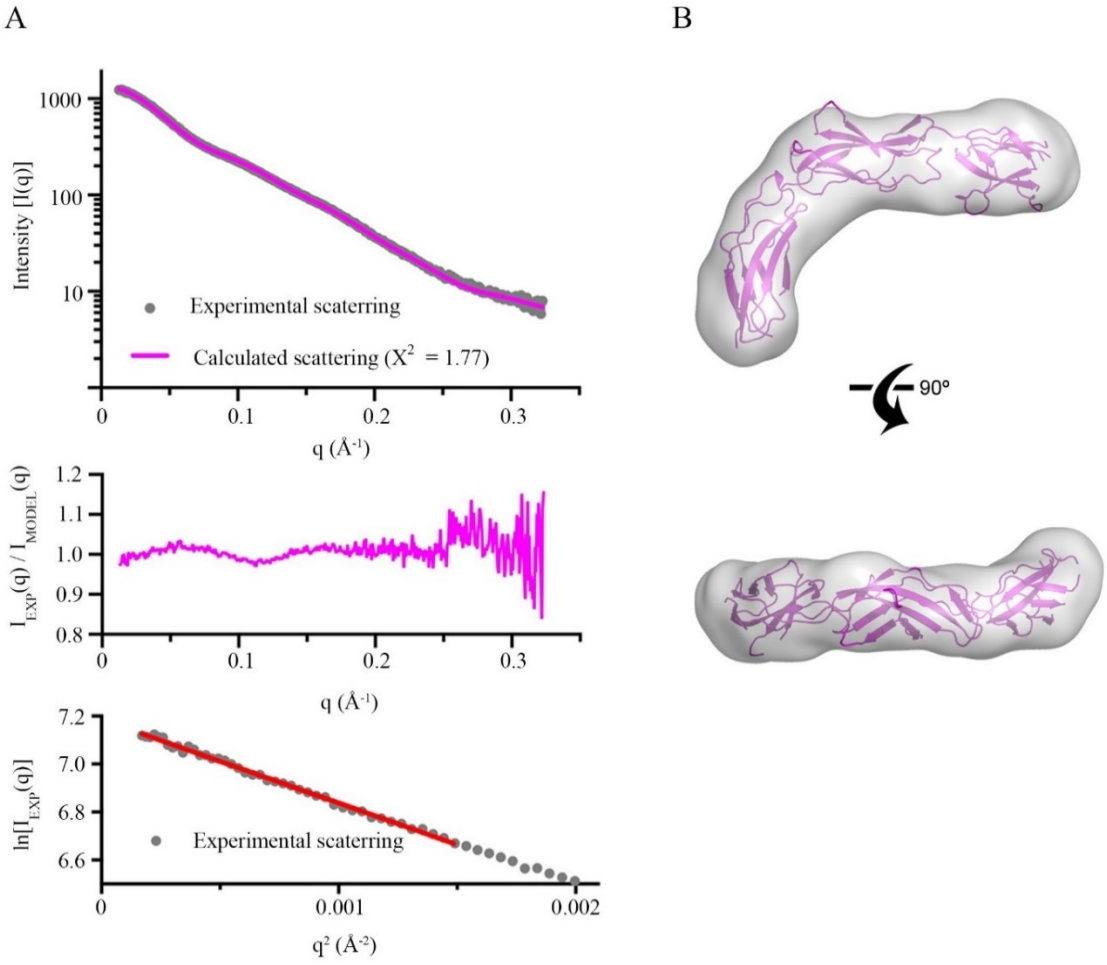

Figure 31. Small-angle X-ray scattering analysis of CNTN3(FN1-FN3). (A) The experimental scattering profile (gray) and the theoretical scattering (magenta line, χ^2 = 1.77) calculated from the CNTN3(FN1-FN3) crystal structure. Residuals from the fitting of the experimental and scattering profiles are shown below. The lower panel shows the Guinier plot with linear fit in red. (B) The crystal structure of CNTN3(FN1-FN3) corresponds to a molecular envelope calculated from the experimental solution scattering profile CNTN3(FN1-FN3) shown in (A).

A model of the PTPRG•CNTN interaction

Based on the available crystallographic information, we have built a model for the conformation of the CNTN ectodomain. First, we superposed the crystal structures of CNTN3(Ig5-FN2) and CNTN3(FN1-FN3) to obtain a model for the Ig5-FN3 region (Fig. 32). The structure of CNTN3 FN4 has been solved by NMR (PDB ID: 1WJ3) by another group. However, we were missing the information about the conformation of the linker between the FN3 and FN4 area. Therefore, we have used Modeller 9.15 software (Sali and Blundell, 1993) to model this region based on the crystal structure of CNTN3(FN1-FN3) and NMR structure of CNTN3FN4. Stereochemical restraints for modeling were obtained from the CHARMM-22 molecular mechanics force field (Mackerell et al., 1998). The structure with the lowest Modeller 9.15 molpdf score was picked. Given the high sequence similarity of CNTNs, we suggest that the conformation of four N-terminal Ig domains of CNTN3 is similar to the one found for the CNTN4(Ig1-Ig4) structure (PDB ID: 3JXA) (Bouyain and Watkins, 2010). Because we were missing the conformation of the CNTN Ig4-Ig5 linker, we hypothesized that Ig3-Ig5 domains of CNTN adopt an extended conformation similar to what has been found in the N-terminal regions of NCAM2 (PDB ID: 2WIM) and SYG1 (PDB ID: 4OFY) crystal structures (Özkan et al., 2014). Therefore, to orient the N-terminal horseshoe-like region of CNTN, we used the crystal structure of mouse CNTN4(Ig1-Ig4) (PDB ID: 3JXA) as a template, and a structure of NCAM2(Ig1-Ig3) to orient the horseshoe-like region against the CNTN3(Ig5-FN2) structure. Immunoglobulin domains 3 and 4 of the CNTN4(Ig1-Ig4) crystal structure were superposed to Ig1 and Ig2 of NCAM2, and the Ig5 domain of the CNTN3(Ig5-FN2) structure was superposed to Ig3 of NCAM2. The modeled structures

of Ig5-FN3, FN1-FN4 and Ig1-FN2 fragments of CNTN3 were then combined to yield a hypothetical model of the full-length CNTN3. Given the missing structural information for the FN3-FN4 and Ig4-Ig5 linkers, our model can only partially predict the conformation of a CNTN ectodomain and we assume that our model might represent only a single structure from an array of possible CNTN conformations. We next superposed the PTPRG(CA)•CNTN3(Ig2-Ig3) crystal structure on our CNTN3 ectodomain model to assess the orientation of PTPRG against CNTN. In this case, the binding interface of PTPRG and CNTN is oriented in perpendicular to a cell surface (Fig. 33). Given the flexible spacer region of PTPRG, we suspect that this orientation allows both *cis* and *trans* interactions without significant conformational changes of both molecules.

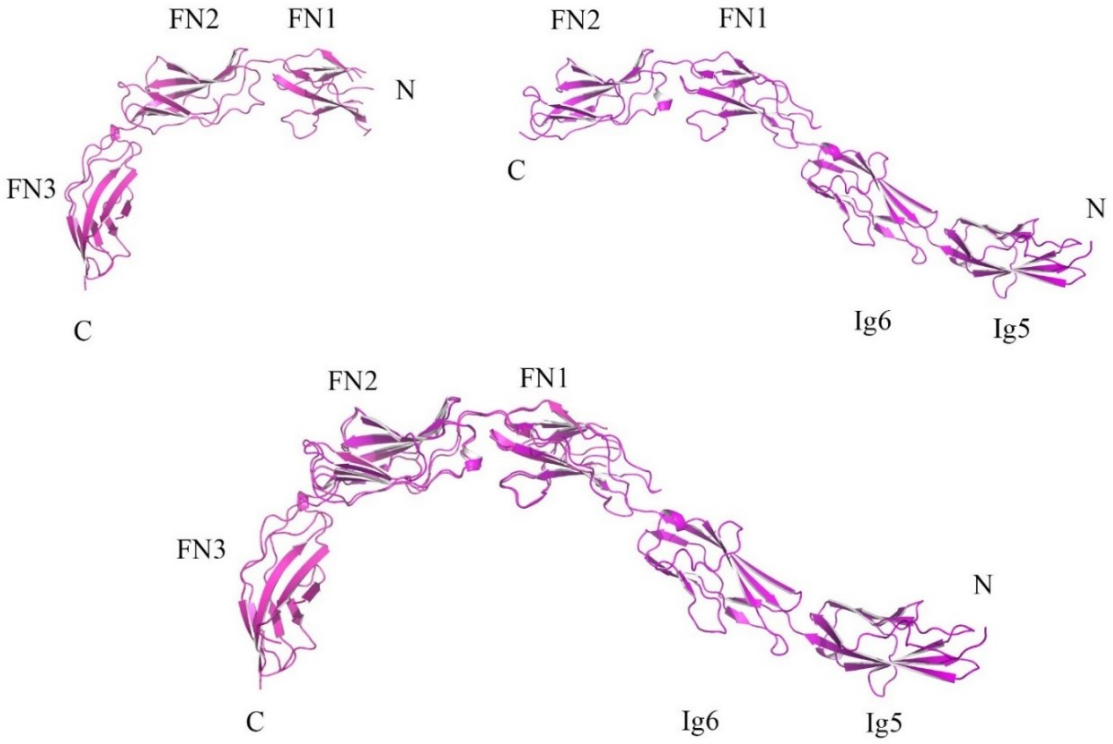

Figure 32. **The model of CNTN3(Ig5-FN3) ectodomain.** The model was created by the superposition of CNTN3(FN1-FN3) and CNTN3(Ig5-FN2) crystal structures (RMSD:1.28 Å, over 176 residues).

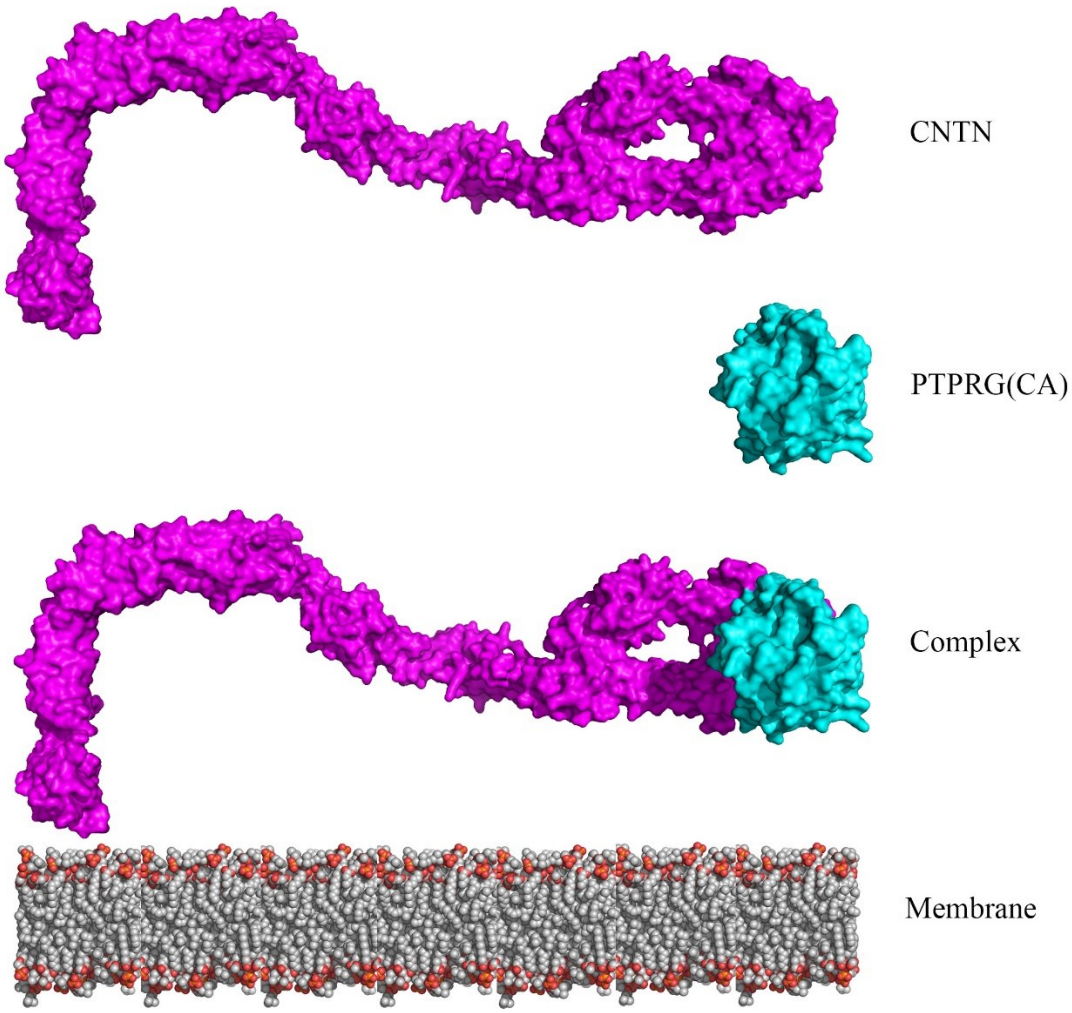

Figure 33. A hypothetical model of the CNTN ectodomain in complex with the CA domain of PTPRG. The full-length model of CNTN was built using the CNTN3(Ig5-FN3) model (Fig. 32), CNTN3FN4 domain (PDB ID: 1WJ3), and a model of CNTN4(Ig1-4) domains. The NCAM2(Ig1-Ig3) (PDB ID: 2WIM) model was used to orient CNTN4(Ig1-4) structure against the rest of the ectodomain. Modeller was used to orient CNTN3FN4 domain. The superposition of the PTPRG(CA)•CNTN3(Ig2-Ig3) complex structure was used to model binding of PTPRG(CA) to our CNTN ectodomain model.

Conclusions

The data presented in this chapter complement the results described in Chapter 3 and provide a structural basis for the *cis* and *trans* interactions between PTPRG and CNTNs. Our results demonstrate that the FN1-FN3 regions of all CNTN family members adopt an L-shaped conformation for the FN1-FN3 region with a sharp bend between FN2 and FN3. This conformation identified in crystals of CNTNs was further confirmed by solution scattering experiments performed on CNTN3(FN1-FN3). The crystal structure of the CNTN3(Ig5-FN2) region suggests an extended conformation for the portion of CNTN ectodomain that follows the FN2-FN3 bend. The modeling of the CNTN ectodomain structure suggests that the CNTN ectodomain undergoes sharp bending at FN2-FN3 and then extends in parallel to the cell surface. In our model, the binding interface of PTPRG•CNTN is oriented perpendicular to the cell surface allowing both a *cis* and *trans* orientation of the complex.

CHAPTER 5

FINAL DISCUSSION

A conserved mode of interactions for PTPRG•CNTNs complexes

In this work, we have used structural, biochemical and cell biological approaches to gain insights into the interactions between the receptor protein tyrosine phosphatase PTPRG and the neural CAMs CNTN3-6. We have demonstrated that PTPRG specifically associates with CNTN3-6 on the cell surface (Fig. 8). It is not uncommon for homologous proteins to interact with the same cell surface receptor in the nervous system. However, these molecules typically do not bind to the receptor with similar binding affinities. For instance, a short splice variant of neurexin – β-neurexin 1 (Nrx1β) specifically binds to neuroligins (NL) 1, 2 and 4 during the maturation of glutamatergic and GABAergic synapses (Leone et al., 2010). In this case, there is a ~500-fold difference between the dissociation constants for these complexes: 16 nM, 8.8 μM, and 115 nM for the complexes of β-neurexin 1 with neuroligins-1, 2, and 4, respectively. However, the binding affinities measured for the interactions between CNTN3-6 and PTPRG are very similar (Fig. 9, Table 2). Moreover, the sum of our structural analyses demonstrates that PTPRG binds to CNTN3, 4, 6 – and most likely 5 – in essentially identical fashion. Thus, it remains unclear why four CAMs would bind the same receptor with the same affinity. This does not mean, however, that all PTPRG•CNTN complexes are identical. There are several ways by which these complexes may be involved in distinct cell signaling events. Those possibilities might include: a difference in the localization and timing of protein expression; the formation of different multipartite signaling receptors through the recruitment of additional binding partners, distinct effects of CNTN binding on the

phosphatase activity of PTPRG, or distinct properties of PTPRG•CNTN complexes depending on their *cis* or *trans* orientation.

In vivo localization of PTPRG•CNTN complexes

In broad terms, the expression pattern of CNTN3-6 and PTPRG might look similar in the cortical layers and hippocampal cell groups of an adult mouse brain (Lein et al., 2007). However, a closer inspection reveals only a partial overlap with some differences at the level of specific layers within particular brain structures (Zuko et al., 2011). The expression patterns of CNTNs are even more complex when observed throughout brain development. For example, analysis of the CNTN expression pattern in developing mouse cerebellum revealed contacting, but not overlapping zones of CNTN2 and CNTN6 expression in the deep external granular layer (EGL). The expression of CNTN6 starts during the P0 stage of postnatal cerebellum development and replaces CNTN2 by stage P15 (Sakurai et al., 2009). Therefore, the expression of PTPRG and CNTN within the same brain structure does not necessarily imply that they will associate in an active signaling unit. To address this problem, we decided to investigate the formation of PTPRG•CNTN complexes by immunofluorescence microscopy of mouse tissues. In particular, we focused on the retina because PTPRG, CNTN3, 4, and 5 are expressed in this tissue during development (Yamagata and Sanes, 2012). During the course of these investigations, we discovered that PTPRG forms a complex with CNTN3 *in vivo* in the outer segment (OS) of adult mouse retinas. We were not able to observe similar results for CNTN4 or 5. In the case of CNTN5, a lack of suitable antibodies thwarted our efforts. In contrast, PTPRG and CNTN4 were not found in similar layers of adult retinas and consequently could not associate.

Cis-orientation of the PTPRG•CNTN3 complexes

Our *in vivo* analysis of the PTPRG•CNTN3 complex has also revealed that these two receptors associate on the surface of a single photoreceptor in a *cis* configuration. Given that CNTNs are GPI-anchored proteins and thus lack intracellular regions to transmit signals inside the cell, a possible role of their *cis* interaction with PTPRG could be the formation of a co-receptor that interacts with other binding partners. There are in fact multiple examples of CNTNs associating in *cis* with other cell surface receptors (see Table 5).

CNTN1 interacts with a contactin-associated protein 1 (CNTNAP1) in *cis*, to form a co-receptor complex that interacts with neurofascin 155 (NF-155) in paranodal junctions (Boyle et al., 2001). These interactions are crucial for paranodal junction integrity, proper nerve conduction velocity and distribution of potassium Shaker-type ion channels. In another example, CNTN2 binds CNTNAP2 in *cis* and forms homophilic interactions with another CNTN2 molecule in *trans* at juxtaparanodal junctions (Traka et al., 2003). Here, the disruption of the CNTN2/CNTNAP2 tertiary complex in the CNTN2 mouse mutant also results in the aberrant localization of CNTNAP2 and Shaker-type potassium channels but does not significantly affect the functionality of the nerve. Recently, CNTN5 has been shown to act as a part of *cis* CNTN5/CNTNAP4 co-receptor complex on the surface of sensory neurons that interacts with Nr-CAM/CHL1 complex expressed at the GABAergic interneurons (GABApre) in the mouse spinal cord. The disruption of these interactions results in a partial decrease in the high-density accumulation of GABApre boutons on sensory terminals (Ashrafi et al., 2014).

Cell adhesion molecules from the the Ig-CAM superfamily are often involved in the formation of a co-receptor complex with CNTNs. Neuronal CNTN1 forms a co-receptor with Nr-CAM, which binds PTPRZ on opposing glial cells (Sakurai et al., 1997). These interactions are essential for the promotion of neurite outgrowth and neuronal differentiation. CHL1, the member of L1-CAM family, interacts with CNTN6 in *cis* to promote the oriented growth of apical dendrites in the neocortex (Ye et al., 2008). It is suggested that the effect of CHL1 and CNTN6 on dendrite outgrowth is mediated through PTPRA.

Another possibility for the formation of *cis* complexes with CNTNs might involve APP/APP-like proteins (Osterfield et al., 2008). The formation of the complex in a *cis* orientation has been shown for CNTN5 and APLP1 at the presynaptic membrane of hippocampal neurons (Shimoda et al., 2012). It has been recently demonstrated that the interaction of CNTN4 and APP, presumably in a *cis* orientation, targets axons of retinal ganglion cells to the nucleus of the optic tract (Osterhout et al., 2015). Thus, it is not unusual for the members of CNTN family to form co-receptors in a *cis* orientation, as it has been shown for the PTPRG•CNTN3 complex.

TABLE 5

PROTEIN-PROTEIN INTERACTIONS OF CONTACTINS

CNTN	***Cis*-partner**	***Trans*-partner**	**Localization**	**Physiological role**	**Reference**
CNTN1	CNTNAP1, Kv1	NF-155	Paranodal junctions	Paranodal junction integrity, distribution of potassium shaker-type ion channels	(Boyle et al., 2001)
CNTN1	NrCAM	PTPRZ	Neuron-glial contacts	Neuronal outgrowth and differentiation	(Sakurai et al., 1997)
CNTN1		PTPRZ, tenascin	Neuron-glial contacts at sites of myelination	Differentiation of OPCs into mature oligodendro-cytes	(Lamprianou et al., 2011)
CNTN2	CNTNAP2, Kv1	CNTN2	Juxta-paranodal junctions	Localization of CNTNAP2 and shaker-type potassium channels	(Traka et al., 2003)
CNTN4	APP		RGCs axons in accessory optic system	Targeting of RGCs axons to the nucleus of the optic tract	(Osterhout et al., 2015)
CNTN5	CNTNAP4	Nr-CAM CHL1	Axoaxonic synapses between sensory neurons and GABA interneurons in mouse spinal cord	Accumulation of GABApre boutons on sensory terminals	(Ashrafi et al., 2014)
CNTN6	PTPRA, CHL1		Pyramidal neurons of neocortex	Oriented growth of apical dendrites	(Ye et al., 2008)

A possible mode of the phosphatase activity regulation

The discovery of a *cis*-interaction between PTPRG and CNTN3 suggests a possible regulatory effect on the phosphatase activity of PTPRG. It has been mentioned previously that tandem phosphatase domains of PTPRG exist in a dimeric conformation, which is thought to be inactive in solution (Barr et al., 2009). Therefore, a *cis*-interaction with CNTN3 might modulate the oligomeric state of PTPRG favoring either a catalytically active or inactive conformation. For example, the PTN-induced clustering of PTPRZ, the close homolog of PTPRG, results in decreased phosphatase activity that might be associated with stabilization of the naturally occurring inactive dimeric conformation of intracellular phosphatase domains (Fukada et al., 2006). The binding of HSPGs to PTPRS stabilizes the phosphatase in an inactive conformation and creates zones of increased phosphorylation, whereas the binding of CSPGs has an opposite effect on PTPRS activity (Coles et al., 2011). The clustering of PTPRA mediated either by CNTN6 or CHL1 leads to increased dephosphorylation of the PTPRA substrate, $p59^{fyn}$ kinase, indicating an increase in phosphatase activity (Ye et al., 2008).

Ligand-induced clustering might also regulate the activity of a receptor phosphatase in a concentration-dependent manner. It has been mentioned before that the CD45 ectodomain is sterically excluded from the receptor-ligand "close-contact" zones during TCR signaling that decreases the effective phosphatase concentration available for substrate dephosphorylation (Chang et al., 2016). It can be speculated that a *cis* interaction with CNTN3 might create specific zones with either increased or decreased PTPRG phosphatase activity.

The model for the *cis* and *trans*-interactions in PTPRG•CNTN complexes

The ability of two cell surface receptors expressed on distinct cells (*trans* interactions) to associate with one another is often a critical event triggering signaling events that determine cellular fates. Whereas *cis* interactions between cell surface receptors often function to dampen the receptor signaling formed in *trans*. In addition to uncovering cis-interactions between PTPRG and CNTN3, we demonstrated that PTPRG and CNTN3 also associate in *trans*. This is consistent with the *trans* interaction found in PTPRZ•CNTN1 complex (Table 4), which has a similar domain orientation to PTPRG•CNTN complexes (Lamprianou et al., 2011). Because of the homology between CNTN3-6, we surmise that these four CNTNs are able to associate in *cis*/*trans* with PTPRG. It was unclear, however, how PTPRG and CNTN3 could form a complex in both the *cis* and *trans* orientation using the same binding interface. Our structural analyses indicate that the CNTN3 ectodomain, and presumably all CNTN ectodomains, is oriented parallel to the cell surface to allow both *cis* and *trans* orientations. On the other hand, our insights into the conformation of the CNTN3 extracellular domain provide an explanation of how long CNTN molecules such as CNTNs could be accommodated within a narrow space between two opposing cells. As mentioned before, CNTN1 is involved in myelination process and localizes at paranodal axon membranes, where it acts as an organizer molecule during the formation of axoglial septate-like paranodal junctions (Boyle et al., 2001; Çolakoğlu et al., 2014). The intermembrane spacing in septate-like paranodal junctions was measured by electron tomography as ~ 75 Å (Nans et al., 2011). Given an approximate length of a single Ig or FN domain of

CNTN measured along the domain axis as ~ 40 Å, the total length of an extended CNTN extracellular moiety would be around 320 Å. Indeed, to pack within a narrow space such as this one, a long CNTN molecule cannot just simply extend from the cell surface. In contrast, the bent conformations of CNTN ectodomains conformation presented in this thesis are consistent with their localization within the limited space of paranodal junctions. Moreover, CNTN5 and CNTN6 were reported to localize at chemical synapses, where the distance between pre- and postsynaptic membranes is around 200 Å (Sakurai et al., 2010; Shimoda et al., 2012). Here, a bent conformation of a CNTN molecule localized on a presynaptic membrane might provide additional space to accommodate the possible CNTN interactors on a postsynaptic membrane. A similar arrangement has been observed for the ectodomain of the synaptic cell adhesion molecule NCAM2, which indicates that these folded protein conformations might be a common theme in the conformations of neural adhesion molecules (Kulahin et al., 2011).

It is tempting to speculate that *cis* and *trans* orientations of the PTPRG•CNTN complexes might be associated with the formation of functionally distinct co-receptors (Fig. 34). These complexes might have a differential effect on the phosphatase activity as it is in the case of type IIa RPTPs. For example, PTPRS is activated when binding to HSPGs in *cis* and inhibited when associating with CSPGs in *trans*. A similar effect has been uncovered with the phosphatase LAR in *Drosophila* (Johnson et al., 2006). The binding of Syndecan to LAR in *cis* activates the cytoplasmic phosphatase activity to promote the growth of synaptic boutons. In contrast, Dally-like protein, expressed on an opposing cell, displaces Syndecan in a competitive fashion to inhibit LAR, which results in the switch from the growth of synaptic boutons to the assembly of the synaptic active

zone (Johnson et al., 2006). The distinct effects that *cis* and *trans* might have on receptor activity is not limited to RPTPs, however, and have been described in Delta-Notch signaling. Here, the canonical *trans* binding results in the activation of the Notch pathway, whereas the formation of the same complex on the same cell surface in *cis* has an inhibitory effect (Matsugo et al., 2015). In this model, Delta-like protein 4 (DLL4) forms an antiparallel dimeric complex with Notch1 that is consistent both with the *trans* and *cis* orientations (Matsugo et al., 2015). For both scenarios, the Delta-Notch complex would be oriented in parallel to the cell surface, which is similar to our model of PTPRG•CNTN interaction. Importantly, CNTN6 and CNTN1 have been characterized as Notch ligands during the differentiation and maturation of oligodendrocytes (Hu et al., 2003; Cui et al., 2004). The L-shaped conformation of the CNTN ectodomain might thus be consistent with both *cis* and *trans* association with Notch. Although the mechanism of Delta/Notch signaling is completely different from that of RPTP signaling, we surmise that a similar scenario might take place for PTPRG and CNTN interactions.

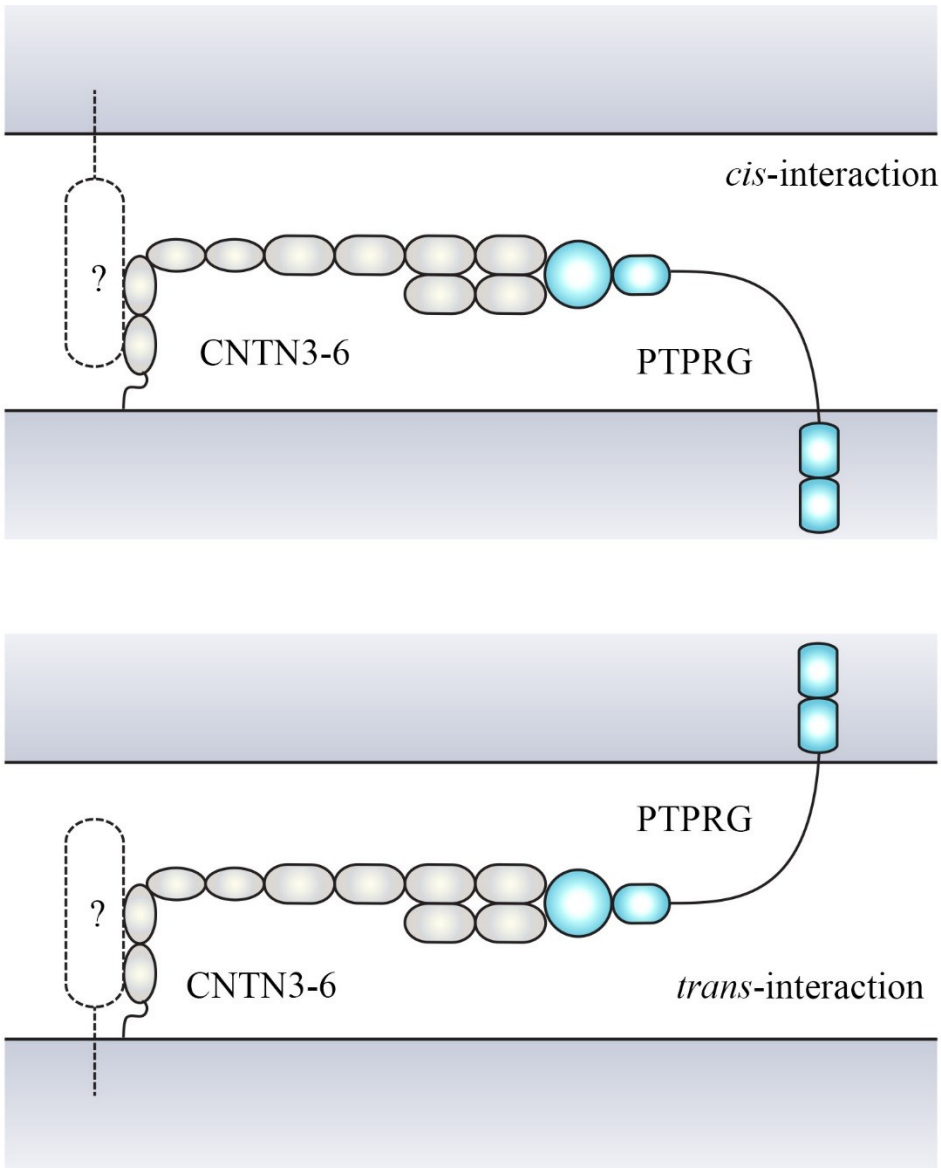

Figure 34. A possible model for the formation of PTPRG•CNTN co-receptor complexes in *cis* and *trans* orientations. PTPRG interacts with CNTN either in *cis* or *trans* orientation. By recruiting potential binding partners *cis* and *trans* PTPRG•CNTN co-receptors form tertiary complexes with alternative functionalities.

A possible role for PTPRG in photoreceptor outer segments

The discovery of the PTPRG•CNTN3 complex in the OS of photoreceptors raises a question about its physiological role in this region. We might speculate that this role is associated with the phosphatase activity of PTPRG. Given the fact that a PTPRG substrate has yet to be discovered, it is unclear what the substrates of PTPRG in photoreceptors could be. The OS is the region of a photoreceptor that is directly involved in phototransduction. The conversion of the light signal in a photoreceptor is performed by the G-protein-coupled receptor rhodopsin, which uses the G protein transducin to activate phosphodiesterase. This is turn leads to an increased cGMP hydrolysis and a closure of cyclic nucleotide-gated (CNG) channels, causing membrane hyperpolarization and further signal transduction. The activity of CNG channels is regulated in part by binding to Ca^{2+}/calmodulin, diacylglycerol and divalent ions (Kramer and Molokanova, 2001). One of the most important processes underlying the regulation of CNG channels is phosphorylation. The phosphorylation of Y498 on the CNG channel nucleotide-binding alpha domain results in the channel's closure due to its decreased affinity to cGMP (Molokanova et al., 1997, 1999). The presence of tyrosine phosphorylation as a regulatory factor would also indicate some tyrosine dephosphorylation activity that might be attributed to intracellular PTPs or RPTPs including PTPRG. It has been shown recently that the insulin receptor (IR) directly phosphorylates CNG channels either in a light- or insulin-dependent manner (Gupta et al., 2012). Conversely, IGF-1 secreted by retinal pigment epithelial cells increases the cGMP sensitivity of CNG channels, presumably by recruiting a phosphatase (Savchenko et al., 2001). Another link between the IGF-1 signaling and phosphatase activity in photoreceptors might be associated with

the STAT3 transcription factor. During the development of the retina, IGF-1 signaling mediates the downstream dephosphorylation of STAT3. This process has been shown to involve PKCβ1 and γ, and the non-receptor tyrosine phosphatases Shp1 and Shp2. This pathway is thought to be essential for the differentiation of the rod photoreceptors from the retinal progenitors (Pinzon-Guzman C, Xing T, Zhang SS, 2011). The increased expression of the tyrosine phosphorylated form of STAT3 (pSTAT3) has been also linked to photoreceptor survival in murine models of photoreceptor degeneration (Jiang et al., 2014). Several studies performed in cancer cell lines characterize pSTAT3 as a substrate for RPTPs, such as PTPRD, CD45, PTPRT, and PTPRJ (Zhang et al., 2007; Ortiz et al., 2014; Yan et al., 2015; Kumar et al., 2016). In fact, recent data suggest that STAT3 might be activated by PTPRG activity in monocytes (Mirenda et al., 2015). It is tempting to speculate that PTPRG might act cooperatively with other receptor phosphatases to ensure an adequate balance between the phosphorylated and non-phosphorylated STAT forms during the phototransduction or photoreceptor survival. In this regard, the OS of an adult mouse retina has been shown to be abundant in different receptor phosphatases, including PTPRS, PTPRE, PTPRJ, PTPRK, RPTPRR, as well as PTPRG (Horvat-Bröcker et al., 2008).

In the adult retina, the OS constantly renews itself through shedding of the apical disk, which is phagocytosed by the retinal pigmented epithelium (Kennedy and Malicki, 2009). The possible role of RPTPs in this area might include maintenance of proper substrate phosphorylation levels in the rapidly growing cell region. Interestingly, the OS of each photoreceptor is surrounded by an interphotoreceptor matrix (IPM) enriched with growth factors, enzymes and proteoglycans (Ishikawa et al., 2015). Here, the interaction

of PTPRG and CNTN3 on the OS membrane might provide an interface for the binding of molecules originated from the matrix. For example, similarly to what has been shown for PTPRS and LAR receptor phosphatases, proteoglycans of the IPM might be involved it the regulation of the phosphatase activity of PTPRG or other RPTPs. The primary physiological roles of the interaction between OS and IPM include the OS adhesion to RPE, retinoid, oxygen and nutrient transport to photoreceptors, and cytoskeletal rearrangements. It has been shown in murine models that components of IPM are significant in the etiology of retinal degeneration disorders (Ishikawa et al., 2015). Any of these processes might potentially involve the PTPRG/CNTN3 signaling.

Given a large number of receptor phosphatases in the OS, it is difficult to imagine an exact role for the PTPRG•CNTN complex in this region. *PTPRG*-null mice show no abnormality in retinal laminar organization or in the expression of specific retinal markers, suggesting only a minor role of PTPRG during the retinal development, if any. In contrast, the *PTPRZ*$^{-/-}$ mice exhibit decreased expression of vimentin, a marker for Müller glial cells, along with an altered morphology of Müller glial cell processes (Horvat-Bröcker et al., 2008). It should be noted that the current examinations of retinas were performed at a P1 stage and may not reflect the full role of PTPRG and PTPRZ during other developmental stages or well into adulthood.

Because of the lack of distinct anatomical phenotypes for mice deficient in PTPRG and CNTN3-6, further experiments should be focused on the detailed investigation of functional electrophysiological outputs. For example, removal of *CNTN4* in mice, which affects the ability of the specific subset of retinal ganglion cells to target the nucleus of the optic tract, results in a decreased ability to track the horizontal

movement of the image (Osterhout et al., 2015). *CNTN5* null mice have specific defects in the auditory system including abnormal responses to auditory stimuli and specific behavioral changes (Li et al., 2003). In summary, genetic removal of CNTN-encoding genes in sensory pathways does not lead to gross defects in sensory organ function, but rather appears to alter how the information is processed. These subtle changes might be significant at the level of the human brain by producing specific behavioral deviations. In fact, mutations in *CNTN3-6* genes have been shown to be associated with autism spectrum disorders (ASDs) and other neuropsychiatric diseases (Zuko et al., 2011). Thus, the role of the PTPRG•CNTN3 complex in the retina should be thoroughly investigated in knock-out animals during various developmental stages as well as in the adult animals with focus on the processing of specific visual inputs.

Future directions

The future directions of this work should be focused on both fundamental and clinically relevant research topics. Therefore, it is important to characterize the interactions between PTPRG and CNTN within the context of the existing disorders associated with PTPRG, CNTN3-6 or their binding partners, such as CNTNAPs, APP/APLP or L1-CAM family members.

Although we were able to show the formation of the PTPRG•CNTN complex *in vivo*, the exact function and the signaling pathway for this interaction has yet to be discovered. It is likely that both proteins act as parts of the larger membrane-associated protein complexes, and this should be further investigated. Characterizing these entities might shed a light on the functional difference between the *cis* and *trans* orientations of the PTPRG•CNTN complexes.

It is important to establish the relationship between the cell-adhesion created by PTPRG and CNTN and the phosphatase activity of PTPRG. For this reason, we need to identify substrates specific for PTPRG phosphatase function. It seems likely that that the activity of PTPRG in knock-out animals might be rescued by other RPTPs. Therefore, it is important to dissect possible overlap in RPTPs functionality by creating relevant experimental platforms. Finally, there are still questions related to the structural aspects of interactions of CAMs and RPTPs on the cell surface, such as the relationship between the phosphatase signaling and oligomerization.

APPENDIX

DETAILED PARAMETERS OBTAINED FROM DATA ANALYSIS CURVE-FITTING OF ALPHASCREEN BEAD-BASED COMPETITION ASSAYS.

Inhibitor	**Immobilized proteins**	**IC_{50} (nM)**	**R^2**	**Signal/Noise**	**Points analyzed**	**Outliers**	**95% confidence interval**
PTPRZ(CA)	PTPRZ(CA) CNTN1-Fc	353	0.99	1051	20	0	283 to 441 nM
PTPRZ(CA)	PTPRZ(CA) CNTN1-Fc	316	0.99	1307	19	0	242 to 413 nM
PTPRZ(CA)	PTPRZ(CA) CNTN1-Fc	328	0.98	417	19	0	224 to 481 nM
PTPRZ(CA)	PTPRZ(CA) CNTN1-Fc	332	0.93	445	17	2	157 to 705 nM
PTPRG(CA)	PTPRG(CA) CNTN3-Fc	306	0.98	994	18	1	224 to 418 nM
PTPRG(CA)	PTPRG(CA) CNTN3-Fc	437	0.98	997	19	0	324 to 589 nM
PTPRG(CA)	PTPRG(CA) CNTN3-Fc	465	0.99	1019	19	0	372 to 580 nM

"APPENDIX -- Continued."

DETAILED PARAMETERS OBTAINED FROM DATA ANALYSIS CURVE-FITTING OF ALPHASCREEN BEAD-BASED COMPETITION ASSAYS.

Inhibitor	**Immobilized proteins**	**IC_{50} (nM)**	**R^2**	**Signal/Noise**	**Points**	**Outliers**	**95% confidence interval**
PTPRG(CA)	PTPRG(CA) CNTN3-Fc	418	0.99	1206	18	1	365 to 479 nM
PTPRG(CA)	PTPRG(CA) CNTN3-Fc	564	0.98	932	19	0	408 to 780 nM
PTPRG(CA)	PTPRG(CA) CNTN3-Fc	412	0.99	780	19	0	315 to 538 nM
PTPRG(CA)	PTPRG(CA) CNTN3-Fc	397	0.98	621	19	0	282 to 559 nM
PTPRG(CA)	PTPRG(CA) CNTN4-Fc	146	0.98	303	19	0	103 to 205 nM
PTPRG(CA)	PTPRG(CA) CNTN4-Fc	192	0.98	364	19	0	142 to 259 nM
PTPRG(CA)	PTPRG(CA) CNTN4-Fc	207	0.99	605	19	0	173 to 248 nM

"APPENDIX -- Continued."

DETAILED PARAMETERS OBTAINED FROM DATA ANALYSIS CURVE-FITTING OF ALPHASCREEN BEAD-BASED COMPETITION ASSAYS.

Inhibitor	**Immobilized proteins**	**IC_{50} (nM)**	**R^2**	**Signal/Noise**	**Points**	**Outliers**	**95% confidence interval**
PTPRG(CA)	PTPRG(CA) CNTN4-Fc	235	0.99	579	19	0	193 to 287 nM
PTPRG(CA)	PTPRG(CA) CNTN4-Fc	153	0.96	303	19	0	92 to 254 nM
PTPRG(CA)	PTPRG(CA) CNTN4-Fc	236	0.99	729	17	2	202 to 274 nM
PTPRG(CA)	PTPRG(CA) CNTN4-Fc	297	0.99	460	19	0	239 to 367 nM
PTPRG(CA)	PTPRG(CA) CNTN4-Fc	343	0.98	183	19	0	261 to 451 nM
PTPRG(CA)	PTPRG(CA) CNTN4-Fc	236	0.97	350	19	0	187 to 296 nM
PTPRG(CA)	PTPRG(CA) CNTN4-Fc	305	0.98	193	19	0	230 to 401 nM

"APPENDIX -- Continued."

DETAILED PARAMETERS OBTAINED FROM DATA ANALYSIS CURVE-FITTING OF ALPHASCREEN BEAD-BASED COMPETITION ASSAYS.

Inhibitor	**Immobilized proteins**	**IC_{50} (nM)**	**R^2**	**Signal/Noise**	**Points**	**Outliers**	**95% confidence interval**
PTPRG(CA)	PTPRG(CA) CNTN5-Fc	311	0.99	802	19	0	257 to 377 nM
PTPRG(CA)	PTPRG(CA) CNTN5-Fc	298	0.99	1511	19	0	245 to 362 nM
PTPRG(CA)	PTPRG(CA) CNTN5-Fc	395	0.98	1334	18	1	288 to 541 nM
PTPRG(CA)	PTPRG(CA) CNTN5-Fc	315	0.99	678	19	0	243 to 409 nM
PTPRG(CA)	PTPRG(CA) CNTN5-Fc	317	0.98	606	18	1	236 to 426 nM
PTPRG(CA)	PTPRG(CA) CNTN6-Fc	397	0.98	289	19	0	287 to 550 nM
PTPRG(CA)	PTPRG(CA) CNTN6-Fc	636	0.99	431	17	2	490 to 824 nM

"APPENDIX -- Continued."

DETAILED PARAMETERS OBTAINED FROM DATA ANALYSIS CURVE-FITTING OF ALPHASCREEN BEAD-BASED COMPETITION ASSAYS.

Inhibitor	**Immobilized proteins**	**IC_{50} (nM)**	**R^2**	**Signal/Noise**	**Points**	**Outliers**	**95% confidence interval**
PTPRG(CA)	PTPRG(CA) CNTN6-Fc	406	0.98	390	17	2	284 to 579 nM
PTPRG(CA)	PTPRG(CA) CNTN6-Fc	563	0.96	332	17	2	327 to 967 nM
PTPRG(CA)	PTPRG(CA) CNTN6-Fc	579	0.96	324	17	2	344 to 975 nM
PTPRG(CA)	PTPRG(CA) CNTN6-Fc	586	0.99	254	18	1	445 to 771 nM
PTPRG(CA)	PTPRG(CA) CNTN6-Fc	465	0.97	43	17	2	315 to 686 nM
PTPRG(CA) H295A + V296A	PTPRG(CA) CNTN4-Fc	761	0.99	616	17	2	573 to 1,010 nM
PTPRG(CA) H295A + V296A	PTPRG(CA) CNTN4-Fc	940	0.99	378	19	0	724 to 1,220 nM

"APPENDIX -- Continued."

DETAILED PARAMETERS OBTAINED FROM DATA ANALYSIS CURVE-FITTING OF ALPHASCREEN BEAD-BASED COMPETITION ASSAYS.

Inhibitor	**Immobilized proteins**	**IC_{50} (nM)**	**R^2**	**Signal/Noise**	**Points**	**Outliers**	**95% confidence interval**
PTPRG(CA) H295A + V296A	PTPRG(CA) CNTN4-Fc	940	0.99	156	19	0	712 to 1,241 nM
PTPRG(CA) H295A + V296A	PTPRG(CA) CNTN4-Fc	1028	0.97	288	19	0	686 to 1,541 nM

REFERENCES

Adams, P. D.; Afonine, P. V.; Bunkóczi, G.; Chen, V. B.; Davis, I. W.; Echols, N.; Headd, J. J.; Hung, L. W.; Kapral, G. J.; Grosse-Kunstleve, R. W.; et al. PHENIX: A Comprehensive Python-Based System for Macromolecular Structure Solution. *Acta Crystallogr. Sect. D Biol. Crystallogr.* **2010**, *66* (2), 213–221.

Andersen, J. N.; Jansen, P. G.; Echwald, S. M.; Mortensen, O. H.; Fukada, T.; Del Vecchio, R.; Tonks, N. K.; Møller, N. P. H. A Genomic Perspective on Protein Tyrosine Phosphatases: Gene Structure, Pseudogenes, and Genetic Disease Linkage. *FASEB J.* **2004**, *18* (1), 8–30.

Arévalo, J. C.; Wu, S. H. Neurotrophin Signaling: Many Exciting Surprises! *Cell. Mol. Life Sci.* **2006**, *63* (13), 1523–1537.

Aricescu, A. R.; Lu, W.; Jones, E. Y. A Time- and Cost-Efficient System for High-Level Protein Production in Mammalian Cells. *Acta Crystallogr. Sect. D Biol. Crystallogr.* **2006**, *62* (10), 1243–1250.

Ashrafi, S.; Betley, J. N.; Comer, J.; Brenner-Morton, S.; Bar, V.; Shimoda, Y.; Watanabe, K.; Peles, E.; Jessell, T.; Kaltschmidt, J. Neuronal Ig/Caspr Recognition Promotes the Formation of Axoaxonic Synapses in Mouse Spinal Cord. *Neuron* **2014**, *81* (1), 120–129.

Barnea, G.; Silvennoinen, O.; Shaanan, B.; Honegger, a M.; Canoll, P. D.; D'Eustachio, P.; Morse, B.; Levy, J. B.; Laforgia, S.; Huebner, K. Identification of a Carbonic Anhydrase-like Domain in the Extracellular Region of RPTP Gamma Defines a New Subfamily of Receptor Tyrosine Phosphatases. *Mol. Cell. Biol.* **1993**, *13* (3), 1497–1506.

Barr, A. J.; Ugochukwu, E.; Lee, W. H.; King, O. N. F.; Filippakopoulos, P.; Alfano, I.; Savitsky, P.; Burgess-Brown, N. a; Müller, S.; Knapp, S. Large-Scale Structural Analysis of the Classical Human Protein Tyrosine Phosphatome. *Cell* **2009**, *136* (2), 352–363.

Bilwes, a M.; den Hertog, J.; Hunter, T.; Noel, J. P. Structural Basis for Inhibition of Receptor Protein-Tyrosine Phosphatase-Alpha by Dimerization. *Nature*. 1996, pp 555–559.

Blanchetot, C.; Tertoolen, L. G. J.; den Hertog, J. Regulation of Receptor Protein-Tyrosine Phosphatase Alpha by Oxidative Stress. *EMBO J.* **2002**, *21* (4), 493–503.

Bouyain, S.; Watkins, D. J. The Protein Tyrosine Phosphatases PTPRZ and PTPRG Bind to Distinct Members of the Contactin Family of Neural Recognition Molecules. *Proc. Natl. Acad. Sci. U. S. A.* **2010**, *107* (6), 2443–2448.

Boyle, M. E. T.; Berglund, E. O.; Murai, K. K.; Weber, L.; Peles, E.; Ranscht, B. Contactin Orchestrates Assembly of the Septate-like Junctions at the Paranode in Myelinated Peripheral Nerve. *Neuron* **2001**, *30* (2), 385–397.

Burridge, K.; Sastry, S. K.; Sallee, J. L. Regulation of Cell Adhesion by Protein-Tyrosine Phosphatases: I. Cell-Matrix Adhesion. *J. Biol. Chem.* **2006**, *281* (23), 15593–15596.

Canoll, P. D.; Petanceska, S.; Schlessinger, J.; Musacchio, J. M. Three Forms of RPTP-Beta Are Differentially Expressed during Gliogenesis in the Developing Rat Brain and during Glial Cell Differentiation in Culture. *J. Neurosci. Res.* **1996**, *44* (3), 199–215.

Chang, V. T.; Fernandes, R. A.; Ganzinger, K. A.; Lee, S. F.; Siebold, C.; McColl, J.; Jönsson, P.; Palayret, M.; Harlos, K.; Coles, C. H.; et al. Initiation of T Cell Signaling by CD45 Segregation at "Close Contacts." *Nat. Immunol.* **2016**, *17* (5).

Çolakoğlu, G.; Bergstrom-Tyrberg, U.; Berglund, E. O.; Ranscht, B. Contactin-1 Regulates Myelination and Nodal/paranodal Domain Organization in the Central Nervous System. *Proc. Natl. Acad. Sci. U. S. A.* **2014**, *111*, E394–E403.

Coles, C. H.; Shen, Y.; Tenney, A. P.; Siebold, C.; Sutton, G. C.; Lu, W.; Gallagher, J. T.; Jones, E. Y.; Flanagan, J. G.; Aricescu, a R. Proteoglycan-Specific Molecular Switch for RPTPσ Clustering and Neuronal Extension. *Science* **2011**, *332* (6028), 484–488.

Coles, C. H.; Mitakidis, N.; Zhang, P.; Elegheert, J.; Lu, W.; Stoker, A. W.; Nakagawa, T.; Craig, A. M.; Jones, E. Y.; Aricescu, a R. Structural Basis for Extracellular Cis and Trans RPTPσ Signal Competition in Synaptogenesis. *Nat. Commun.* **2014**, *5* (0615), 5209.

Cui, X.-Y.; Hu, Q.-D.; Tekaya, M.; Shimoda, Y.; Ang, B.-T.; Nie, D.-Y.; Sun, L.; Hu, W.-P.; Karsak, M.; Duka, T.; et al. NB-3/Notch1 Pathway via Deltex1 Promotes Neural Progenitor Cell Differentiation into Oligodendrocytes. *J. Biol. Chem.* **2004**, *279* (24), 25858–25865.

Desai, D. M.; Sap, J.; Schlessinger, J.; Weiss, a. Ligand-Mediated Negative Regulation of a Chimeric Transmembrane Receptor Tyrosine Phosphatase. *Cell* **1993**, *73* (3), 541–554.

Emsley, P.; Cowtan, K. Coot: Model-Building Tools for Molecular Graphics. *Acta Crystallogr. Sect. D Biol. Crystallogr.* **2004**, *60* (12 I), 2126–2132.

Franke, D.; Svergun, D. I. *DAMMIF* , a Program for Rapid *Ab-Initio* Shape Determination in Small-Angle Scattering. *J. Appl. Crystallogr.* **2009**, *42* (2), 342–346.

Fukada, M.; Fujikawa, A.; Chow, J. P. H.; Ikematsu, S.; Sakuma, S.; Noda, M. Protein Tyrosine Phosphatase Receptor Type Z Is Inactivated by Ligand-Induced Oligomerization. *FEBS Lett.* **2006**, *580* (17), 4051–4056.

Guinier, A.; Fournet, G. Small Angle Scattering of X-Rays. *Journal of Polymer Science*. 1956, pp 594–594.

Gupta, V. K.; Rajala, A.; Rajala, R. V. S. Insulin Receptor Regulates Photoreceptor CNG Channel Activity. *Am. J. Physiol. Endocrinol. Metab.* **2012**, *303* (11), E1363–E1372.

Hamaoka, B. Y.; Dann, C. E.; Geisbrecht, B. V; Leahy, D. J. Crystal Structure of Caenorhabditis Elegans HER-1 and Characterization of the Interaction between HER-1 and TRA-2A. *Proc. Natl. Acad. Sci. U. S. A.* **2004**, *101* (32), 11673–11678.

Harroch, S.; Furtado, G. C.; Brueck, W.; Rosenbluth, J.; Lafaille, J.; Chao, M.; Buxbaum, J. D.; Schlessinger, J. A Critical Role for the Protein Tyrosine Phosphatase Receptor

Type Z in Functional Recovery from Demyelinating Lesions. *Nat. Genet.* **2002**, *32* (3), 411–414.

Hasegawa, H.; Holm, L. Advances and Pitfalls of Protein Structural Alignment. *Curr. Opin. Struct. Biol.* **2009**, *19* (3), 341–348.

Hayashi, M.; Majumdar, A.; Li, X.; Adler, J.; Sun, Z.; Vertuani, S.; Hellberg, C.; Mellberg, S.; Koch, S.; Dimberg, A.; et al. VE-PTP Regulates VEGFR2 Activity in Stalk Cells to Establish Endothelial Cell Polarity and Lumen Formation. *Nat. Commun.* **2013**, *4*, 1672.

Hayashi, N.; Miyata, S.; Yamada, M.; Kamei, K.; Oohira, a. Neuronal Expression of the Chondroitin Sulfate Proteoglycans Receptor-Type Protein-Tyrosine Phosphatase β and Phosphacan. *Neuroscience* **2005**, *131* (2), 331–348.

Hermiston, M. L.; Xu, Z.; Weiss, A. CD45: A Critical Regulator of Signaling Thresholds in Immune Cells. *Annu. Rev. Immunol.* **2003**, *21*, 107–137.

Horvat-Bröcker, A.; Reinhard, J.; Illes, S.; Paech, T.; Zoidl, G.; Harroch, S.; Distler, C.; Knyazev, P.; Ullrich, A.; Faissner, A. Receptor Protein Tyrosine Phosphatases Are Expressed by Cycling Retinal Progenitor Cells and Involved in Neuronal Development of Mouse Retina. *Neuroscience* **2008**, *152* (3), 618–645.

Hu, Q.-D.; Ang, B.-T.; Karsak, M.; Hu, W.-P.; Cui, X.-Y.; Duka, T.; Takeda, Y.; Chia, W.; Sankar, N.; Ng, Y.-K.; et al. F3/contactin Acts as a Functional Ligand for Notch during Oligodendrocyte Maturation. *Cell* **2003**, *115* (2), 163–175.

Hura, G. L.; Menon, A. L.; Hammel, M.; Rambo, R. P.; Poole, F. L.; Tsutakawa, S. E.; Jr, F. E. J.; Classen, S.; Frankel, K. A.; Hopkins, R. C.; et al. NIH Public Access. **2011**, *6* (8), 606–612.

Ishikawa, M.; Sawada, Y.; Yoshitomi, T. Structure and Function of the Interphotoreceptor Matrix Surrounding Retinal Photoreceptor Cells. *Exp. Eye Res.* **2015**, *133*, 3–18.

Jiang, K.; Wright, K. L.; Zhu, P.; Szego, M. J.; Bramall, A. N.; Hauswirth, W. W.; Li, Q.; Egan, S. E.; McInnes, R. R. STAT3 Promotes Survival of Mutant Photoreceptors in Inherited Photoreceptor Degeneration Models. *Proc Natl Acad Sci USA* **2014**, *111* (52), E5716–E5723.

Johnson, K. G.; Tenney, A. P.; Ghose, A.; Duckworth, A. M.; Higashi, M. E.; Parfitt, K.; Marcu, O.; Heslip, T. R.; Marsh, J. L.; Schwarz, T. L.; et al. The HSPGs Syndecan and Dallylike Bind the Receptor Phosphatase LAR and Exert Distinct Effects on Synaptic Development. *Neuron* **2006**, *49* (4), 517–531.

Kaneko-Goto, T.; Yoshihara, S.-I.; Miyazaki, H.; Yoshihara, Y. BIG-2 Mediates Olfactory Axon Convergence to Target Glomeruli. *Neuron* **2008**, *57* (6), 834–846.

Kennedy, B.; Malicki, J. What Drives Cell Morphogenesis: A Look inside the Vertebrate Photoreceptor. *Dev. Dyn.* **2009**, *238* (9), 2115–2138.

Kramer, R. H.; Molokanova, E. Modulation of Cyclic-Nucleotide-Gated Channels and

Regulation of Vertebrate Phototransduction. *J. Exp. Biol.* **2001**, *204* (Pt 17), 2921–2931.

Krissinel, E.; Henrick, K. Inference of Macromolecular Assemblies from Crystalline State. *J. Mol. Biol.* **2007**, *372*, 774–797.

Krueger, N. X.; Saito, H. A Human Transmembrane Protein-Tyrosine-Phosphatase, PTP Zeta, Is Expressed in Brain and Has an N-Terminal Receptor Domain Homologous to Carbonic Anhydrases. *Proc. Natl. Acad. Sci. U. S. A.* **1992**, *89* (16), 7417–7421.

Kulahin, N.; Kristensen, O.; Rasmussen, K. K.; Olsen, L.; Rydberg, P.; Vestergaard, B.; Kastrup, J. S.; Berezin, V.; Bock, E.; Walmod, P. S.; et al. Structural Model and Trans-Interaction of the Entire Ectodomain of the Olfactory Cell Adhesion Molecule. *Structure* **2011**, *19* (2), 203–211.

Kumar, V.; Cheng, P.; Condamine, T.; Mony, S.; Languino, L. R.; McCaffrey, J. C.; Hockstein, N.; Guarino, M.; Masters, G.; Penman, E.; et al. CD45 Phosphatase Inhibits STAT3 Transcription Factor Activity in Myeloid Cells and Promotes Tumor-Associated Macrophage Differentiation. *Immunity* **2016**, *44* (2), 303–315.

Lamprianou, S.; Vacaresse, N.; Suzuki, Y.; Meziane, H.; Buxbaum, J. D.; Schlessinger, J.; Harroch, S. Receptor Protein Tyrosine Phosphatase Gamma Is a Marker for Pyramidal Cells and Sensory Neurons in the Nervous System and Is Not Necessary for Normal Development. *Mol. Cell. Biol.* **2006**, *26* (13), 5106–5119.

Lamprianou, S.; Chatzopoulou, E.; Thomas, J.-L.; Bouyain, S.; Harroch, S. A Complex between Contactin-1 and the Protein Tyrosine Phosphatase PTPRZ Controls the Development of Oligodendrocyte Precursor Cells. *Proc. Natl. Acad. Sci. U. S. A.* **2011**, *108* (42), 17498–17503.

Laskowski, R. A.; Swindells, M. B. LigPlot + : Multiple Ligand À Protein Interaction Diagrams for Drug Discovery. **2011**, 2778–2786.

Lawrence, M. C.; Colman, P. M. Shape Complementarity at Protein/protein Interfaces. *J. Mol. Biol.* **1993**, *234* (4), 946–950.

Lee, S.; Takeda, Y.; Kawano, H.; Hosoya, H.; Nomoto, M.; Fujimoto, D.; Takahashi, N.; Watanabe, K. Expression and Regulation of a Gene Encoding Neural Recognition Molecule NB-3 of the contactin/F3 Subgroup in Mouse Brain. *Gene* **2000**, *245* (2), 253–266.

Lein, E. S.; Hawrylycz, M. J.; Ao, N.; Ayres, M.; Bensinger, A.; Bernard, A.; Boe, A. F.; Boguski, M. S.; Brockway, K. S.; Byrnes, E. J.; et al. Genome-Wide Atlas of Gene Expression in the Adult Mouse Brain. *Nature* **2007**, *445* (7124), 168–176.

Leone, P.; Comoletti, D.; Ferracci, G.; Conrod, S.; Garcia, S. U.; Taylor, P.; Bourne, Y.; Marchot, P. Structural Insights into the Exquisite Selectivity of Neurexin/neuroligin Synaptic Interactions. *EMBO J.* **2010**, *29* (14), 2461–2471.

Levi-Montalcini, R. Effects of Mouse Tumor Transplantation on the Nervous System. *Ann. N. Y. Acad. Sci.* **1952**, *55* (2), 330–344.

Li, H.; Takeda, Y.; Niki, H.; Ogawa, J.; Kobayashi, S.; Kai, N.; Akasaka, K.; Asano, M.;

Sudo, K.; Iwakura, Y.; et al. Aberrant Responses to Acoustic Stimuli in Mice Deficient for Neural Recognition Molecule NB-2. *Eur. J. Neurosci.* **2003**, *17* (5), 929–936.

London, A.; Benhar, I.; Schwartz, M. The Retina as a Window to the Brain-from Eye Research to CNS Disorders. *Nat. Rev. Neurol.* **2013**, *9* (1), 44–53.

Longo, P. A.; Kavran, J. M.; Kim, M.-S.; Leahy, D. J. Transient Mammalian Cell Transfection with Polyethylenimine (PEI). *Methods Enzymol.* **2013**, *529*, 227–240.

Lorenzetto, E.; Moratti, E.; Vezzalini, M.; Harroch, S.; Sorio, C.; Buffelli, M. Distribution of Different Isoforms of Receptor Protein Tyrosine Phosphatase γ (Ptprg-RPTP γ) in Adult Mouse Brain: Upregulation during Neuroinflammation. *Brain Struct. Funct.* **2013**.

Mackerell, a D.; Jr; Bashford, D.; Bellott, M.; Dunbrack, R. L.; Evanseck, J. D.; Field, M. J.; Fischer, S.; Gao, J.; Guo, H.; et al. All-Atom Empirical Potential for Molecular Modeling and Dynamics Studies of Proteins. *J Phys Chem B* **1998**, *102* (97), 3586–3616.

Matsugo, S.; Matsuura, T.; Sarna, T.; Vargas, F.; Epe, B.; Schiffmann, D.; Wild, D.; Bommakanti, A.; Mitchell, D. Structural Basis for Notch1 Engagement of Delta-like 4. **2015**, *347* (6224), 847–854.

McCoy, A. J.; Grosse-Kunstleve, R. W.; Adams, P. D.; Winn, M. D.; Storoni, L. C.; Read, R. J. Phaser Crystallographic Software. *J. Appl. Crystallogr.* **2007**, *40* (4), 658–674.

Mirenda, M.; Toffali, L.; Montresor, A.; Scardoni, G.; Sorio, C.; Laudanna, C. Protein Tyrosine Phosphatase Receptor Type γ Is a JAK Phosphatase and Negatively Regulates Leukocyte Integrin Activation. *J. Immunol.* **2015**, *194* (5), 2168–2179.

Mohebiany, A. N.; Nikolaienko, R. M.; Bouyain, S.; Harroch, S. Receptor-Type Tyrosine Phosphatase Ligands: Looking for the Needle in the Haystack. *FEBS J.* **2013**, *280* (2), 388–400.

Molokanova, E.; Trivedi, B.; Savchenko, A.; Kramer, R. H. Modulation of Rod Photoreceptor Cyclic Nucleotide-Gated Channels by Tyrosine Phosphorylation. *J. Neurosci.* **1997**, *17* (23), 9068–9076.

Molokanova, E.; Maddox, F.; Luetje, C. W.; Kramer, R. H. Activity-Dependent Modulation of Rod Photoreceptor Cyclic Nucleotide- Gated Channels Mediated by Phosphorylation of a Specific Tyrosine Residue. *J Neurosci* **1999**, *19* (12), 4786–4795.

Nam, H. J.; Poy, F.; Krueger, N. X.; Saito, H.; Frederick, C. a. Crystal Structure of the Tandem Phosphatase Domains of RPTP LAR. *Cell* **1999**, *97* (4), 449–457.

Nam, H.-J. Structural Basis for the Function and Regulation of the Receptor Protein Tyrosine Phosphatase CD45. *J. Exp. Med.* **2005**, *201* (3), 441–452.

Nans, A.; Einheber, S.; Salzer, J. L.; Stokes, D. L. Electron Tomography of Paranodal Septate-like Junctions and the Associated Axonal and Glial Cytoskeletons in the Central Nervous System. *J. Neurosci. Res.* **2011**, *89* (3), 310–319.

Ortiz, B.; Fabius, A. W. M.; Wu, W. H.; Pedraza, A.; Brennan, C. W.; Schultz, N.; Pitter, K. L.; Bromberg, J. F.; Huse, J. T.; Holland, E. C.; et al. Loss of the Tyrosine Phosphatase PTPRD Leads to Aberrant STAT3 Activation and Promotes Gliomagenesis. *Proc. Natl. Acad. Sci. U. S. A.* **2014**, *111* (22), 8149–8154.

Osterfield, M.; Egelund, R.; Young, L. M.; Flanagan, J. G. Interaction of Amyloid Precursor Protein with Contactins and NgCAM in the Retinotectal System. *Development* **2008**, *135* (6), 1189–1199.

Osterhout, J. A.; Stafford, B. K.; Nguyen, P. L.; Yoshihara, Y.; Huberman, A. D. Contactin-4 Mediates Axon-Target Specificity and Functional Development of the Accessory Optic System. *Neuron* **2015**, *86* (4), 985–999.

Otwinowski, Z.; Minor, W. *Macromolecular Crystallography Part A*; Methods in Enzymology; Elsevier, 1997; Vol. 276.

Özkan, E.; Chia, P. H.; Wang, R. R.; Goriatcheva, N.; Borek, D.; Otwinowski, Z.; Walz, T.; Shen, K.; Garcia, K. C. Extracellular Architecture of the SYG-1/SYG-2 Adhesion Complex Instructs Synaptogenesis. *Cell* **2014**, *156* (3), 482–494.

Peles, E.; Nativ, M.; Campbell, P. L.; Sakurai, T.; Martinez, R.; Lev, S.; Clary, D. O.; Schilling, J.; Barnea, G.; Plowman, G. D.; et al. The Carbonic Anhydrase Domain of Receptor Tyrosine Phosphatase Beta Is a Functional Ligand for the Axonal Cell Recognition Molecule Contactin. *Cell* **1995**, *82* (2), 251–260.

Pettersen, E. F.; Goddard, T. D.; Huang, C. C.; Couch, G. S.; Greenblatt, D. M.; Meng, E. C.; Ferrin, T. E. UCSF Chimera - A Visualization System for Exploratory Research and Analysis. *J. Comput. Chem.* **2004**, *25* (13), 1605–1612.

Pinzon-Guzman C, Xing T, Zhang SS, B. C. Regulation Of Rod Photoreceptor Differentiation By STAT3 Is Controlled By A Tyrosine Phosphatase. **2011**, *18* (11), 1492–1501.

Sakurai, K.; Toyoshima, M.; Ueda, H.; Matsubara, K.; Takeda, Y.; Karagogeos, D.; Shimoda, Y.; Watanabe, K. Contribution of the Neural Cell Recognition Molecule NB-3 to Synapse Formation between Parallel Fibers and Purkinje Cells in Mouse. *Dev. Neurobiol.* **2009**, *69* (12), 811–824.

Sakurai, K.; Toyoshima, M.; Takeda, Y.; Shimoda, Y.; Watanabe, K. Synaptic Formation in Subsets of Glutamatergic Terminals in the Mouse Hippocampal Formation Is Affected by a Deficiency in the Neural Cell Recognition Molecule NB-3. *Neurosci. Lett.* **2010**, *473* (2), 102–106.

Sakurai, T.; Lustig, M.; Nativ, M.; Hemperly, J. J.; Schlessinger, J.; Peles, E.; Grumet, M. Induction of Neurite Outgrowth through Contactin and Nr-CAM by Extracellular Regions of Glial Receptor Tyrosine Phosphatase β. *J. Cell Biol.* **1997**, *136* (4), 907–918.

Sali, A.; Blundell, T. L. Comparative Protein Modelling by Satisfaction of Spatial Restraints. *J. Mol. Biol.* **1993**, *234* (3), 779–815.

Sallee, J. L.; Wittchen, E. S.; Burridge, K. Regulation of Cell Adhesion by Protein-

Tyrosine Phosphatases II. Cell-Cell Adhesion. *J. Biol. Chem.* **2006**, *281* (24), 16189–16192.

Sarkar, G.; Sommer, S. S. The "Megaprimer" Method of Site-Directed Mutagenesis. *Biotechniques* **1990**, *8* (4), 404–407.

Savchenko, a; Kraft, T. W.; Molokanova, E.; Kramer, R. H. Growth Factors Regulate Phototransduction in Retinal Rods by Modulating Cyclic Nucleotide-Gated Channels through Dephosphorylation of a Specific Tyrosine Residue. *Proc. Natl. Acad. Sci. U. S. A.* **2001**, *98*, 5880–5885.

Schindelin J, Arganda-Carreras I, Frise E, Kaynig V, Longair M, Pietzsch T, et al. Fiji: An Open-Source Platform for Biological-Image Analysis. *Nat. Publ. Group.* **2003**, *9* (7), 187.

Schindelin, J.; Arganda-Carreras, I.; Frise, E.; Kaynig, V.; Longair, M.; Pietzsch, T.; Preibisch, S.; Rueden, C.; Saalfeld, S.; Schmid, B.; et al. Fiji: An Open Source Platform for Biological Image Analysis. *Nat. Methods* **2012**, *9* (7), 676–682.

Schlessinger, J. Receptor Tyrosine Kinases: Legacy of the First Two Decades. *Cold Spring Harb. Perspect. Biol.* **2014**, *6* (3), a008912–a008912.

Schneidman-Duhovny, D.; Hammel, M.; Tainer, J. A.; Sali, A. Accurate SAXS Profile Computation and Its Assessment by Contrast Variation Experiments. *Biophys. J.* **2013**, *105* (4), 962–974.

Shimoda, Y.; Watanabe, K. Contactins: Emerging Key Roles in the Development and Funciton of the Nervous System. *Cell Adh. Migr.* **2009**, *3* (1), 64–70.

Shimoda, Y.; Koseki, F.; Itoh, M.; Toyoshima, M.; Watanabe, K. A Cis-Complex of NB-2/contactin-5 with Amyloid Precursor-like Protein 1 Is Localized on the Presynaptic Membrane. *Neurosci. Lett.* **2012**, *510* (2), 148–153.

Söderberg, O.; Leuchowius, K. J.; Gullberg, M.; Jarvius, M.; Weibrecht, I.; Larsson, L. G.; Landegren, U. Characterizing Proteins and Their Interactions in Cells and Tissues Using the in Situ Proximity Ligation Assay. *Methods* **2008**, *45* (3), 227–232.

Sonnenburg, E. D.; Bilwes, A.; Hunter, T.; Noel, J. P. The Structure of the Membrane Distal Phosphatase Domain of RPTPalpha Reveals Interdomain Flexibility and an SH2 Domain Interaction Region. *Biochemistry* **2003**, *42* (26), 7904–7914.

Stella, S. L.; Vila, A.; Hung, A. Y.; Rome, M. E.; Huynh, U.; Sheng, M.; Kreienkamp, H.-J.; Brecha, N. C. Association of Shank 1A Scaffolding Protein with Cone Photoreceptor Terminals in the Mammalian Retina. *PLoS One* **2012**, *7* (9), e43463.

Takeda, Y.; Akasaka, K.; Lee, S.; Kobayashi, S.; Kawano, H.; Murayama, S.; Takahashi, N.; Hashimoto, K.; Kano, M.; Asano, M.; et al. Impaired Motor Coordination in Mice Lacking Neural Recognition Molecule NB-3 of the contactin/F3 Subgroup. *J. Neurobiol.* **2003**, *56* (3), 252–265.

Tonks, N. K. Protein Tyrosine Phosphatases: From Genes, to Function, to Disease. *Nat. Rev. Mol. Cell Biol.* **2006**, *7* (11), 833–846.

Toyoshima, M.; Sakurai, K.; Shimazaki, K.; Takeda, Y.; Nakamoto, M.; Serizawa, S.; Shimoda, Y.; Watanabe, K. Preferential Localization of Neural Cell Recognition Molecule NB-2 in Developing Glutamatergic Neurons in the Rat Auditory Brainstem. *J. Comp. Neurol.* **2009**, *513* (4), 349–362.

Traka, M.; Goutebroze, L.; Denisenko, N.; Bessa, M.; Nifli, A.; Havaki, S.; Iwakura, Y.; Fukamauchi, F.; Watanabe, K.; Soliven, B.; et al. Association of TAG-1 with Caspr2 Is Essential for the Molecular Organization of Juxtaparanodal Regions of Myelinated Fibers. *J. Cell Biol.* **2003**, *162* (6), 1161–1172.

Volkov, V. V.; Svergun, D. I. Uniqueness of Ab Initio Shape Determination in Small-Angle Scattering. *J. Appl. Crystallogr.* **2003**, *36* (3), 860–864.

Winn, M. D.; Ballard, C. C.; Cowtan, K. D.; Dodson, E. J.; Emsley, P.; Evans, P. R.; Keegan, R. M.; Krissinel, E. B.; Leslie, A. G. W.; McCoy, A.; et al. Overview of the *CCP* 4 Suite and Current Developments. *Acta Crystallogr. Sect. D Biol. Crystallogr.* **2011**, *67* (4), 235–242.

Yamagata, M.; Sanes, J. R. Expanding the Ig Superfamily Code for Laminar Specificity in Retina: Expression and Role of Contactins. *J. Neurosci.* **2012**, *32* (41), 14402–14414.

Yan, C.-M.; Zhao, Y.-L.; Cai, H.-Y.; Miao, G.-Y.; Ma, W. Blockage of PTPRJ Promotes Cell Growth and Resistance to 5-FU through Activation of JAK1/STAT3 in the Cervical Carcinoma Cell Line C33A. *Oncol. Rep.* **2015**, 1737–1744.

Ye, H.; Tan, Y. L. J.; Ponniah, S.; Takeda, Y.; Wang, S.-Q.; Schachner, M.; Watanabe, K.; Pallen, C. J.; Xiao, Z.-C. Neural Recognition Molecules CHL1 and NB-3 Regulate Apical Dendrite Orientation in the Neocortex via PTP Alpha. *EMBO J.* **2008**, *27* (1), 188–200.

Yoshihara, Y.; Kawasaki, M.; Tani, A.; Tamada, A.; Nagata, S.; Kagamiyama, H.; Mori, K. BIG-1: A New TAG-1/F3-Related Member of the Immunoglobulin Superfamily with Neurite Outgrowth-Promoting Activity. *Neuron* **1994**, *13* (2), 415–426.

Zayas-Santiago, A.; Kang Derwent, J. J. Preservation of Intact Adult Rat Photoreceptors in Vitro: Study of Dissociation Techniques and the Effect of Light. *Mol. Vis.* **2009**, *15* (December 2008), 1–9.

Zhang, W.; Savelieva, K. V; Tran, D. T.; Pogorelov, V. M.; Cullinan, E. B.; Baker, K. B.; Platt, K. a; Hu, S.; Rajan, I.; Xu, N.; et al. Characterization of PTPRG in Knockdown and Phosphatase-Inactive Mutant Mice and Substrate Trapping Analysis of PTPRG in Mammalian Cells. *PLoS One* **2012**, *7* (9), e45500.

Zhang, X.; Guo, A.; Yu, J.; Possemato, A.; Chen, Y.; Zheng, W.; Polakiewicz, R. D.; Kinzler, K. W.; Vogelstein, B.; Velculescu, V. E.; et al. Identification of STAT3 as a Substrate of Receptor Protein Tyrosine Phosphatase T. *Proc. Natl. Acad. Sci. U. S. A.* **2007**, *104* (10), 4060–4064.

Zuko, A.; Bouyain, S.; van der Zwaag, B.; Burbach, J. P. H. *Contactins: Structural Aspects in Relation to Developmental Functions in Brain Disease.*; 2011; Vol. 84.

VITA

Roman M. Nikolaienko was born on July 16, 1986, in Kyiv, Ukraine. In 2007, he obtained his Bachelor of Arts degree in Industrial Biotechnology from National Technical University of Ukraine "Kyiv Polytechnic Institute" and graduated from National Technical University of Ukraine "Kyiv Polytechnic Institute" with a Master of Science in Biotechnology in 2009. He worked as a research assistant at Bioinformatics division of Biotechnology Department in National Technical University of Ukraine "Kyiv Polytechnic Institute" from 2009 to 2010.

He began graduate school in 2010 at the School of Biological Sciences of the University of Missouri Kansas City and joined the laboratory of Dr. Samuel Bouyain in 2010. During his PhD program, he worked on the structural and functional investigation of Receptor Protein Tyrosine Phosphatase Gamma and its ligands Contactins.